International
Progress Report

IPR-01-33

Äspö Hard Rock Laboratory

True Block Scale Project

Tracer test stage
Tracer tests, Phase C

Peter Andersson
Johan Byegård
Magnus Holmqvist
Mats Skålberg
Eva Wass
Henrik Widestrand

GEOSIGMA AB

October 2001

Svensk Kärnbränslehantering AB
Swedish Nuclear Fuel
and Waste Management Co
Box 5864
SE-102 40 Stockholm Sweden
Tel +46 8 459 84 00
Fax +46 8 661 57 19

Äspö Hard Rock
Laboratory

Report no.	No.
IPR-01-33	F56K
Author	Date
Andersson, Byegård, Holmqvist, Skålberg, Wass,Widestrand	02-08-31
Checked by	Date
Anders Winberg	02-08-31
Approved	Date
Christer Svemar	02-10-16

Äspö Hard Rock Laboratory

True Block Scale Project

Tracer test stage
Tracer tests, Phase C

Peter Andersson
Johan Byegård
Magnus Holmqvist
Mats Skålberg
Eva Wass
Henrik Widestrand

GEOSIGMA AB

October 2001

Keywords: True Block Scale, modelling, network, radioactive, retention, sorbing, tracer test

Abstract

This report describes the performance and results of the third and final phase, Phase C, of the TRUE Block Scale Tracer Test Stage. Phase C included four tracer injections performed in three different flow paths. The flow paths were selected based on results from previous tracer test phases and included both single structure flow paths and flow paths involving several different structures ("network flow paths"). The tests were performed both in radially converging and unequal dipole flow geometry. The main objectives of the tests were to increase the understanding of radionuclide retention in the studied fracture network. This was done by injecting a carefully selected mix of different monovalent and divalent radioactive cations (Na^{+}, Ca^{2+}, Sr^{2+}, Ba^{2+}, Rb^{+}, Cs^{+}, Co^{2+}, Zn^{2+}) together with non-sorbing tracers (HTO, ReO_4^{-}). The tests produced a high quality data set where both injection curves and breakthrough curves could be used to evaluate effects of different transport mechanisms such as matrix diffusion and sorption.

Sammanfattning

Denna rapport beskriver utförandet och resultaten av den tredje och avslutande fasen, Fas C, av TRUE Block Scale Tracer Test Stage. Fas C inkluderade fyra spårämnesinjiceringar utförda i tre olika flödesvägar. Flödesvägarna valdes ut baserat på resultat från föregående spårförsöksomgångar och omfattade både enskilda flödesvägar och flödesvägar inkluderande flera olika strukturer. Testerna utfördes både i radiellt konvergerande flödesfält och i ojämn dipolgeometri. Huvudsyftet med testerna var att öka förståelsen för retention av radionuklider i det studerade spricknätverket. Detta gjordes genom att injicera en noga utvald mix av monovalenta och divalenta katjoner (Na^{+}, Ca^{2+}, Sr^{2+}, Ba^{2+}, Rb^{+}, Cs^{+}, Co^{2+}, Zn^{2+}) tillsammans med icke-sorberande spårämnen (HTO, ReO_4^{-}). Testerna producerade ett dataset där både injiceringskurvor och genombrottskurvor kunde användas för att utvärdera effekterna av olika transportmekanismer såsom matrisdiffusion och sorption.

Executive Summary

The fourth and last of the defined field test stages of the TRUE Block Scale Project, the Tracer Test Stage, has been finalised. The last phase, Phase C, presented in this report includes a series of tracer injections performed with the main objective to investigate transport and retention of sorbing tracers in fracture networks. The tests also aimed to investigate the possible effects of fracture intersection zones (FIZ) and finally, to demonstrate the importance of alternative sorption mechanisms such as partial radiolysis and surface complexation.

The Phase C tests involved a total of three different flow paths using the same sink for all three injections (section KI0023B:P6) which was selected based on results from the Phase A (Andersson et al., 2000a) and Phase B tests (Andersson et al., 2000b). The fastest flow path was utilised for two different tracer injections performed about three months apart. The tracer injections were performed by injecting with a constant flow throughout the entire duration of the test, thereby creating an uneven dipole flow field with injection flow rates in the order of 0.5-2% of the withdrawal rate. One of the flow paths was not forcedly injected (KI0025F02:P3) as the flow through this section induced by the pumping was deemed to be high enough to allow a "passive" injection.

The use of a number of different radioactive sorbing tracers made it necessary to carefully select which tracers to use in what flow path taking into account expected travel times, radioactive decay and interference between different nuclides. Another important criterion was that the retention characteristics should be able to compare between the different flow paths, and also with the results of the TRUE-1 tracer tests (Winberg et al., 2000).

The tracer injections resulted in tracer breakthrough from all three injection points with tracer first arrivals ranging between four hours for a conservative tracer in the fastest flow path, and up to more than 300 hours for the most sorbing tracer, Co. It should also be noted that no breakthrough of Cs could be detected from the second injection (C2) in KI0025F03:P7.

The interpretation included not only the analysis of breakthrough curves but also an attempt to analyse the injection curves, as the measured injection concentrations clearly indicated retention effects on the borehole walls. The latter analysis included both analysis of the surface sorption coefficient and possible effects of non-linear sorption and kinetics. The analysis of the breakthrough curves included effects of both sorption and matrix diffusion.

The results of the analysis are:

- Dispersivity varies between 2.1m for the short flow path (16 m) to 9.0 m for the long "single" flow path (33 m). The latter high value may be an indirect indication that this flow path actually is longer and more complicated than deduced from the hydro-structural model.

- The transport parameters derived shows a significant difference between the fast flow path KI0025F03:P5 – KI0023B:P6 and the two slower ones, about one order of magnitude higher hydraulic conductivity/fracture aperture and about one order of magnitude lower flow porosity.

- Tracer mass recovery is high for all tested flow paths (73-100%).

- The conservative tracer breakthrough curves cannot be fitted well with a simple one-dimensional transport model with advection-dispersion only. The addition of matrix diffusion significantly improves the fits.

- The magnitude of the estimated A-parameter (accounting for matrix diffusion and matrix porosity) for conservative tracers is significantly lower (about a factor 1000) than a value based on laboratory data on matrix porosity and diffusivity. This may be an indication that matrix diffusion and/or matrix porosity is larger than derived from laboratory investigations. However, it should also be noted that similar effects on the shape of the breakthrough curves might occur due to effects of multiple flow paths and/or diffusion into stagnant parts of the flow field. A more elaborate modelling effort is needed to clarify this issue.

- The order of retention between the different species is the same as in TRUE-1 and in the laboratory tests, i.e. $Na^{+}<Ca^{2+}<Sr^{2+}<Ba^{2+}<Rb^{+}<Cs^{+}$.

- The retardation, expressed as the ratio of time at which 50% of the tracer was recovered relative to the conservative tracer ($R_{50\%}$), is about the same for most species when comparing TRUE-1 to the results of injection C1 and C4 in structure #20. However, for the breakthroughs of sorbing tracers in C2 and C3 (Na^{+} and Sr^{2+} in C3 and Ca^{2+} in flow path C2) a 20-60% stronger retardation (expressed as $R_{50\%}$) is obtained.

The reasons for this enhanced retardation between the two fast single structure flow paths (same souce-sink pair, C1 and C4) and the two slower and more complicated flow paths (C2 and C3) may be several; i.a. presence of gouge material in the structures, presence of gouge material in fracture intersection zones, differences in the mineralogy, larger portions of stagnant water to interact with, or higher a porosity in the fracture rim zone.

A more elaborate evaluation effort, including various modelling concepts (fracture network, channel network, etc.), is ongoing as a part of the TRUE Block Scale Project and will be added to the initial "basic" evaluation presented in this report (Andersson et al., 2002 and Poteri et al., 2002) This also includes a special effort to study if fracture intersection zones (FIZ) are critical for the transport in fracture networks.

Contents

1 Introduction

1.1 Background

The TRUE Block Scale project is an international partnership funded by ANDRA, ENRESA, Nirex, POSIVA, PNC and SKB (Winberg, 1997). The Block Scale project is one part of the Tracer Retention Understanding Experiments (TRUE) conducted at the Äspö Hard Rock Laboratory. This report presents the final phase of the experimental tracer test work, Phase C of the Tracer Test Stage. Phase A of this stage included a large number of tracer dilution tests and two series of tracer tests in different flow regimes (A4 and A5) have been analysed and interpreted (Andersson et al., 2000a). Phase B, included a series of tracer tests with non-sorbing tracers at two different flow regimes (B1 and B2), has also been performed (Andersson et al., 2000b) where sufficiently high mass recoveries were demonstrated. The main results of Phase A and B are presented in Chapter 1.3.

1.2 Hypotheses

In Winberg, ed., (2000) four basic questions were put forward in relation to the planned tests of the Tracer Test Stage:

- What is the conductive geometry of the TRUE Block Scale rock volume? Does the March 1999 structural model (and the results of the subsequent hydraulic reconciliation) reflect the conductive geometry with sufficient accuracy to allow design and performance of well controlled tracer tests?
- What are the properties of the fractures and fracture zones that control transport in networks of fractures?
- How do the retention processes control transport in fracture networks, and how can they be measured in field tracer tests?

Hypotheses were proposed for each of these questions:

H1) "The major conducting structures of the target volume for tracer tests in the TRUE Block Scale rock volume trend north-west and are sub-vertical. Being sub-vertical, and sub-parallel, they do not form a conductive network in the designated target volume. For the purpose of testing fracture network flow and transport effects in the current borehole array, second-order NNW features are required to provide the necessary connectivity between the major conducting NW structures!"

H2a) ”Fracture intersections have distinctive properties and have a measurable influence on transport in fracture/feature networks. These distinctive properties may make the intersection a preferential conductor, a barrier, or a combination of both!”

H2b) ”In-plane heterogeneity and anisotropy have a measurable influence on transport of solutes in a block scale fracture network!”

H3) “It is not possible to discriminate between breakthrough curves of sorbing tracers in a single fracture from those obtained in a network of fractures”!

1.3 Results from Phase A and B

In preparation for the Phase C tests with radioactive sorbing tracers two preceding and preparatory phases have been conducted, Phase A and Phase B (Andersson et al. 2000a,b). The former served to provide complementary tracer dilution data to identify suitable injection points for tracer. Further, two alternative sink sections (KI0023B:P6 and KI0025F03:P5) were investigated through a series of injections with conservative dye tracers. On the basis of the performed results, the KI0023B:P6 section was put forward as the preferred sink for subsequent tracer tests.

The Phase B tests had multiple objectives, among them address of transport in fracture networks and possible fracture intersection zone effects. However, the tests were primarily used to verify high mass recovery in the identified suitable injection sections. The results showed that at least three flow paths produced high mass recovery. Injection section KI0025F03:P5 showed 100 % mass recovery and a relatively short travel time (20 hours) which made it suitable for injection of short-lived radioisotopes. Section KI0025F02:P3 also showed high mass recovery (>80%) but a much longer mean travel time (about 250 hours) and section KI0025F03:P7 also showed >80 % mass recovery and a mean travel time of about 100 hours.

1.4 Objectives

The general objective of the Tracer Test Stage was to provide the data from which we could "increase understanding, and the ability to predict" "transport in a fracture network" in a block scale, i.e. over a length scale of 10–50 m. In addition, to "assess the importance of tracer retention mechanisms (diffusion and sorption) in a fracture network" (Winberg (ed), 2000).

The specific objectives of the Phase C tracer tests were:

- To investigate transport and retention of sorbing tracers in block scale fracture networks,
- To investigate transport and retention of sorbing tracers in single fractures (Structures #20 and #21) to enable comparison with transport in fracture networks.,
- To investigate the effects of fracture intersections (FIZ) on transport of sorbing tracers,
- To demonstrate the importance of alternative sorption mechanisms (partial hydrolysis surface complexation) in a flow path earlier studied with tracers featured by ion exchange.

The specific objective for each tracer test (injection) and the coupling to the stated hypotheses are presented in Table 1-1.

Table 1-1. Objectives and hypotheses addressed with Phase C tracer tests. The structural interpretation and notation refers to the March 2000 model, cf. Figure 1-1 (Hermanson & Doe, 2000).

Test #	Source-Reciever pair	Structures involved	Objective	Hypotheses addressed
C1	KI0025F03:P5 – KI0023B:P6	20, 21	Network and FIZ effects on retention	2, 3
C2	KI0025F03:P7 – KI0023B:P6	22, 20, 21	Network and FIZ effects on retention	2, 3
C3	KI0025F02:P3 – KI0023B:P6	21	Retention in a single fracture	2, 3
C4	KI0025F03:P5 – KI0023B:P6	20, 21	To demonstrate the importance of alternative sorption mechanisms (partial hydrolysis surface complexation)	N/A.

* Test C5 cancelled

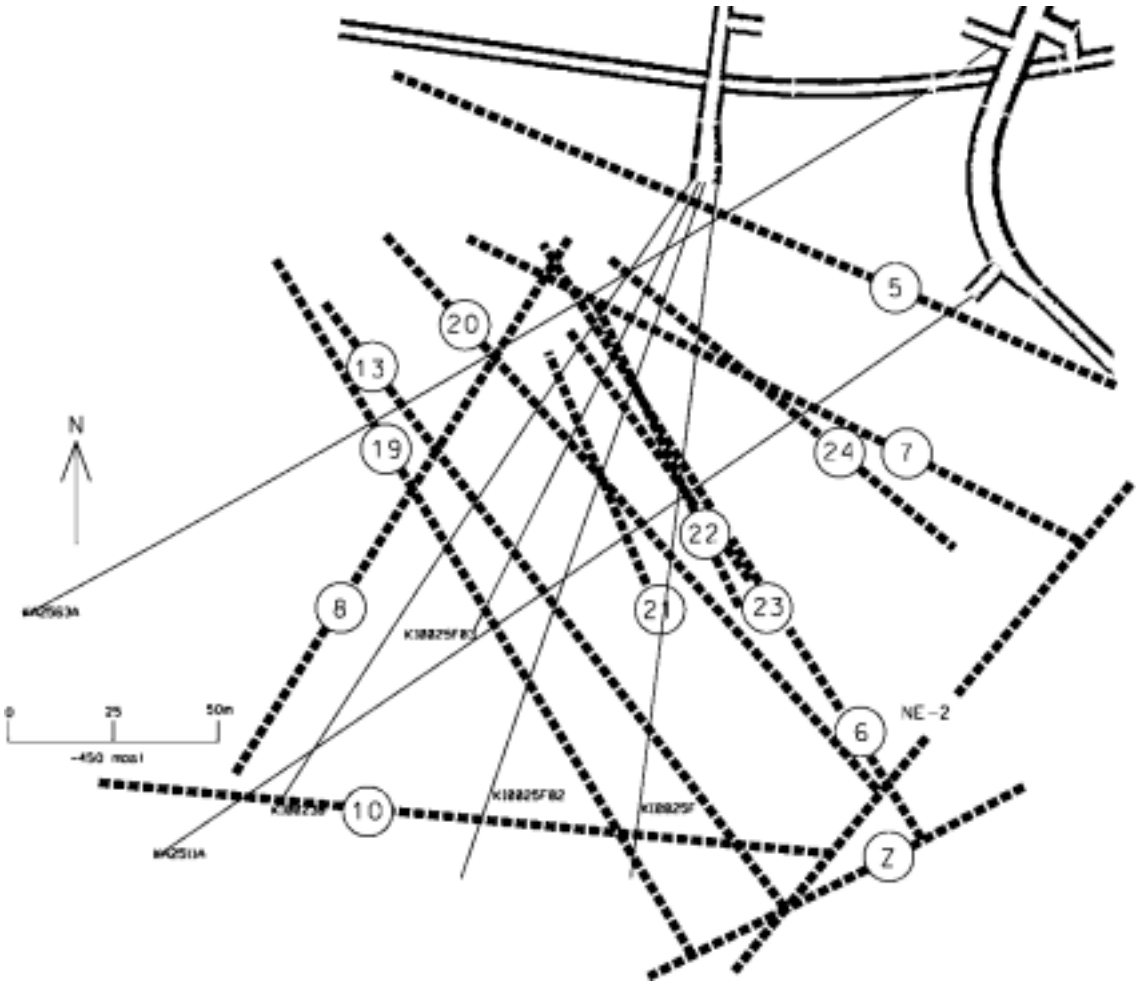

Figure 1-1 *Structural model March 2000 (Hermanson & Doe, 2000).*

2 Performance and evaluation procedure

2.1 Equipment use

2.1.1 Borehole equipment

The three characterisation boreholes involved in the tests are instrumented with 6-10 inflatable packers isolating 5-10 borehole sections. Each borehole section is connected to a pressure transducer which is connected the HMS-system. Each of the sections to be used for tracer tests are equipped with three nylon hoses, two with an inner diameter of 4 mm and one with an inner diameter of 2 mm. The two 4mm hoses are used for injection, sampling and circulation in the borehole section whereas the 2mm hose is used for pressure monitoring.

2.1.2 Injection equipment

A schematic drawing of the tracer test equipment is shown in Figure 2-1. The basic idea is to establish an internal circulation in the borehole section. The circulation makes it possible to obtain a homogeneous tracer concentration in the borehole and to sample the tracer concentration outside the borehole in order to monitor the injection rate of the tracer with time.

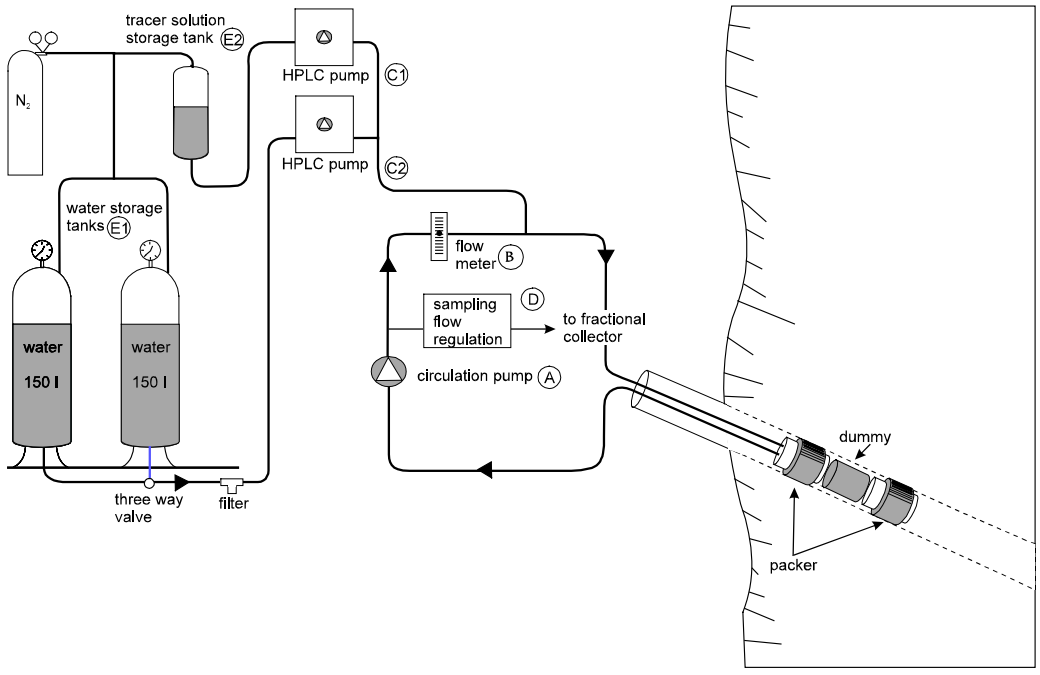

Figure 2-1 *Schematic drawing of the tracer injection/sampling system used in the TRUE Project.*

A pump with a variable speed controller (A) enables and controls circulation rates. The rates are measured by a flow meter (B). In sections with low flow rates, the tracer is forced into the flow path by applying a slight excess pressure using an external water injection pump (dipole flow geometry). Water and tracer injections are made with two different HPLC plunger pumps (C1 and C2). Water for injection is stored in a pressurised vessel (E1) under nitrogen atmosphere. The radioactive tracer solution was injected from a 1-litre plastic bottle placed behind lead shields to protect from radiation during the injection procedure. An optional tracer storage vessel is also available (E2) but was not used in Phase C.

The tracer concentration in the injection loop is measured both *in situ* and by sampling and subsequent analyses. The sampling is made by continuously extracting a small volume of water from the system through a flow controller (constant leak) to a fractional sampler (D). The in situ monitoring of tracer content in the injection system is made by using a HpGe-detector measuring on-line on the tubing (γ-emitting radionuclides). The tracer test equipment has earlier been used in the TRUE-1 tracer tests (e.g. Andersson, 1996). A thorough description of the equipment and procedures for measurements of the tracer activities/concentrations are given in Chapter 2.3.

2.1.3 Sampling and detection equipment

The tracer concentration in the detection loop is measured both in situ and by sampling and subsequent analyses. The sampling is made with two independent systems, a "constant leak" system producing 8 ml samples (same as the injection loop) integrated over some time (5-480 minutes) and a 24-valve sampling unit producing discrete 1 litre samples (sampling intervals between 5 minutes up to 100 hours). In order to continuously analyse the breakthrough of γ-emitting radionuclides (in-situ monitoring) a HpGe-detector was installed in the sampling loop measuring on-line on the tubing, see also Chapter 2.3.

After sampling, the withdrawal water was led through an in-line REDOX potential (Eh) probe and an electrical conductivity probe.

2.1.4 Tracers used

The radioactive tracers used in Phase C were isotopes of Bromide, tritiated water (HTO) and Iodide (non-reactive) and of Sr, Na, K, Ca, Ba, Cs, Rb (ion-exchange sorption) of the alkali and alkaline earth metals and Mn, Co and Zn (hydrolysis/surface complexation). Two non-sorbing fluorescent dye tracers were also used, Uranine (Sodium Fluorescein) from KEBO (purum quality) and Napthionate from Fluka (purum quality). Details on the production of the radionuclides and the preparation of the stock solutions are given in Appendix 1.

The radionuclides, all except HTO, were analysed by γ-spectrometry. HTO was analysed by liquid scintillation. The dye-tracers were analysed using fluorometry technique. The selection and measurement procedures are further discussed in Chapter 2.2 and 2.3.

2.2 Strategy for the choice of sorbing tracers

With regards to selection of sorbing tracers, the main set conquers with elements of the alkali and alkaline earth metals previously used in the TRUE-1 experiments (Winberg et al., 2000), which are all featured by ion exchange as the main sorption mechanism. A general trend could be observed in the *in situ* experiment in the TRUE-1 programme; Na^+, Ca^{2+} and Sr^{2+} were transported only very slightly retarded compared with the non-sorbing tracers, Rb^+ and Ba^{2+} moderately retarded, and Cs^+ strongly retarded. Using the concept of a retardation coefficient for each tracer, it was necessary to use tracers like Rb^+, Ba^{2+} and Cs^+ to be able to observe a significant retardation. However, it is possible that transport over longer distances (like in TRUE Block Scale) would result in increased retardation and that breakthrough would only be obtained from slightly sorbing tracers (like Na^+, Ca^{2+} and Sr^{2+}). It was therefore decided that at least one slightly sorbing tracer and one stronger sorbing tracer were to be used jointly in each injection.

It was also decided to perform an injection (C4) with tracers featured by other sorption mechanisms than cation exchange, (partial hydrolysis of cations and surface complexation). The rationale for this type of experiment is further discussed in Appendix 2.

The rationale for using radioactive tracers was similar to the one earlier used within the TRUE programme, i.e.;

1. In order to avoid increase of the concentrations, which may cause super-saturation and/or non-linear sorption effects, radioactive isotopes of each sorbing tracer were used. This makes it possible to obtain large dynamic (relative concentration) ranges without having to produce significant increase of the natural chemical concentrations of the cations.

2. Isotopes with decay associated with γ-radiation were preferred since they can be measured with γ-spectrometry; a technique which makes it possible to measure a large numbers of tracers simultaneously with only very small interference between the individual tracers.

3. The only tracer used without any measurable γ-radiation was tritiated water, HTO. This tracer was measured using liquid scintillation; a technique that has only limited possibilities to discriminate the β-decay from different radioisotopes. However, a combination of injection of comparably high activity of HTO with the fact of the low β-energy in the decay of tritium, makes it possible in most cases to measure HTO without having to make any separation procedures.

4. Optimisation of the radioactive tracers with respect to their half-lives had to be done; i.e., the most short-lived tracers could only be used for injection in the shortest flow path (injection in borehole section KI0025F03:P5).

5. The amount of injected activity for the tracers used was optimised using the following restrictions:

a. The total amount of each injected tracer should not exceed 10 ALI (1 ALI (Annual Limit of Intake) corresponds to the amount of a particular radioisotope that with an oral intake causes of dose equivalent of 12 mSv, ie. the maximum allowed dose per year)

b. The total amount of radioisotopes in one injection should not exceed 100 ALI.

c. The total amount of activity in the pumped outgoing water should not exceed 1 MBq/h. (using a pumping flow-rate of 2 litres per minute, this corresponds to maximum concentration of ~10 kBq/l).

d. The external dose-rate at the fence at the experimental site in the Äspö tunnel should not at any time exceed 2 μSv/h.

2.3 Measurements

2.3.1 *γ*-spectrometry

Samples

Both the samples taken from the injection side and the samples taken from the pump side were diluted to exactly 1000 g and were measured using a 1 litre Marinelli beaker geometry. In order to preserve the samples, 1 ml 65 % nitric acid was added to the solution. All samples were measured using a HpGe detector (35 % relative efficiency, EG&G Ortec) with an automatic sample exchanger (EG&G Ortec). Calibration of the detector was performed using a mixed radionuclide standard (Amersham QCY48) measured in the same 1 litre Marinelli geometry as the samples.

On-line measurements at injection side

On-line measurements of γ-emitting radionuclides were made on the injection side using a HpGe detector (25 % relative efficiency, EG&G Ortec) with a 10 cm thick lead shielding. The measurement cell (see Figure 2-2) consisted of nylon tubing (~1 ml) placed at a distance of ~2 cm from the detector. The nylon tube was a part of the loop used for circulation of the injection section. Four different circulation loops were connected to the detector, one for each injection section used during the test. Each position was calibrated individually with a geometrically identical measuring cell containing mixed radionuclide standard (Amersham QCY48).

On-line measurements at pump side

For the pump side, an on-line cell was constructed where all the pumped volume of groundwater could pass by the detector. A bobbin, cf. Figure 2-3, was constructed on which ~140 m of 6/8 mm nylon tubing were lined up, yielding a total volume of the flow cell of ~4 litre. The bobbin was placed on an HpGe-detector (18 % relative efficiency, EG&G Ortec) and a 4 cm thick lead shielding was placed around the measuring cell. A schematic drawing of the flow cell is given in Figure 2-3.

In order to prevent sorption of radioisotopes in the tubing of the flow cell, a small flow (~0.2 ml/min) of 65 % nitric acid was continuously injected in the water just before its passing through the detector at the pump side.

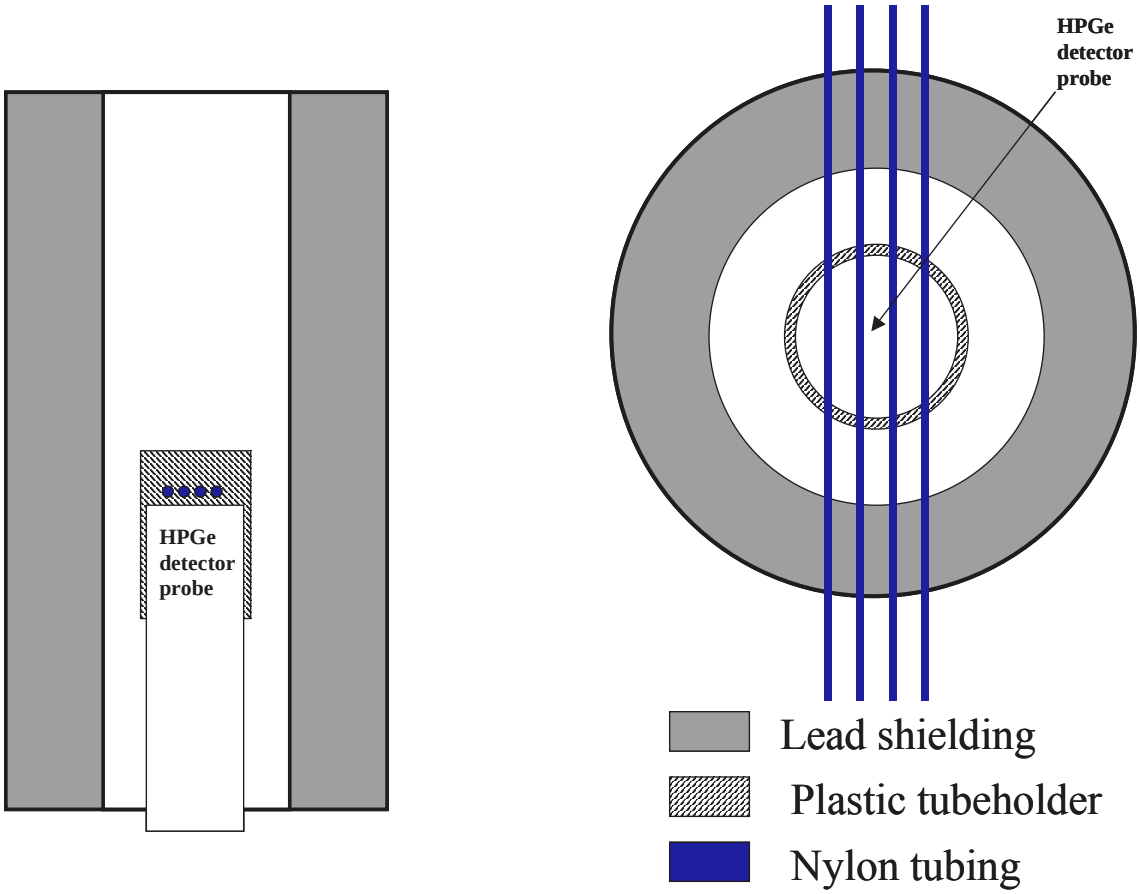

Figure 2-2. *Schematic drawing of the on-line measurement cell used for the injection side, seen from above (left) and from the side (right).*

The detector was calibrated by using one of the γ-spectrums obtained from the flow cell measurement after the C1 injection when ^{82}Br was the dominant radioisotope in the pumped groundwater. The individual count rates for all major ^{82}Br γ-ray peaks in the spectrum were registered and compared with a spectrum measured on a l litre sample measured in a Marinelli beaker geometry. The efficiency ($\Psi_{\gamma(f)}$) for each γ-energy studied was calculated according to:

$$\Psi_{\gamma(f)} = \frac{r_{(f)}}{r_{(M)}} \cdot \Psi_{\gamma(M)} \qquad (2\text{-}1)$$

where $r_{(f)}$ and $r_{(M)}$ are the counting rates on a particular γ-energy registered by the flow detector and the Marinelli beaker sample detector, respectively. $\Psi_{\gamma(M)}$ is the efficiency for the Marinelli beaker sample detector on that particular γ-energy, evaluated from the mixed radionuclide standard (Amersham QCY48) calibration using GammaVision (EG&G Ortec) efficiency calibration procedure. After injection C2, the same procedure was applied using spectra involving ^{186}Re. By including ^{186}Re, low γ-energies could be included in the calibration (112 and 137 keV). Since both $^{82}Br^-$ and $^{186}ReO_4^-$ are considered to act non-sorbing, it was assumed that there should not be any problem with sorption in the tubing in the flow cell, causing errors in the calibration.

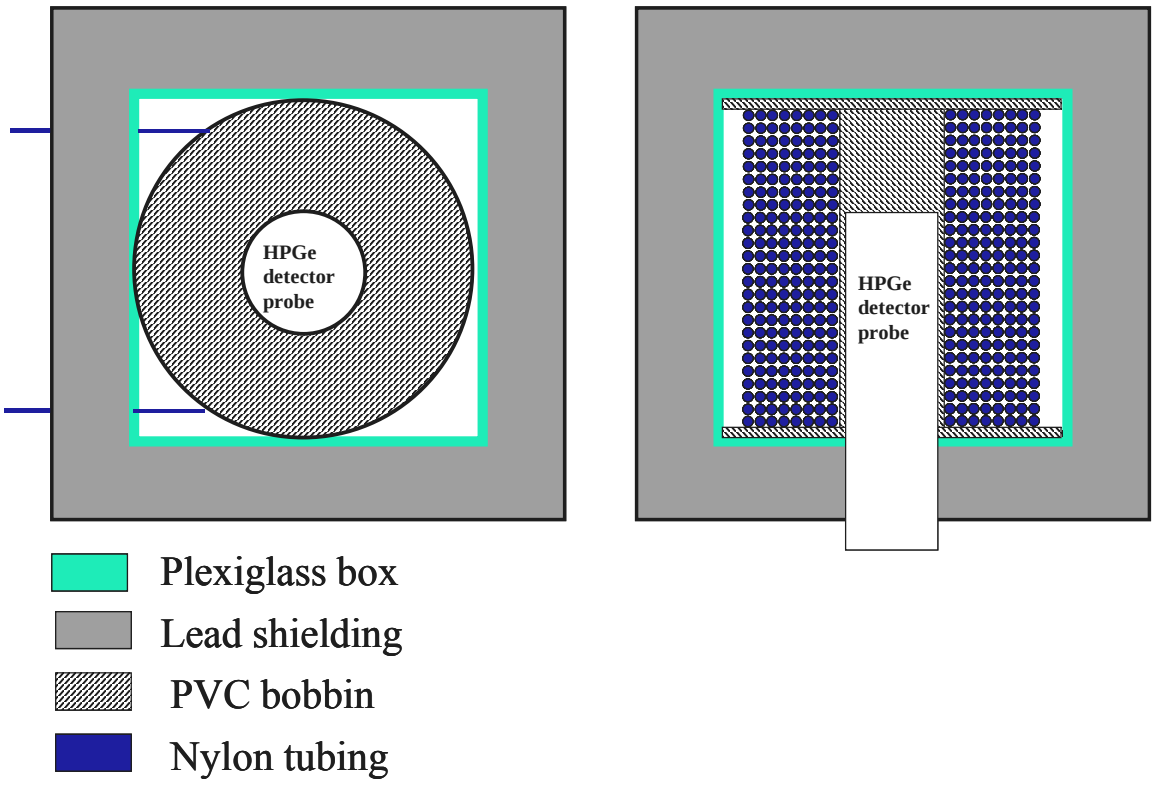

Figure 2-3. *Schematic drawing of the on-line measurement cell used for the pumping side, seen from above (left) and from the side (right).*

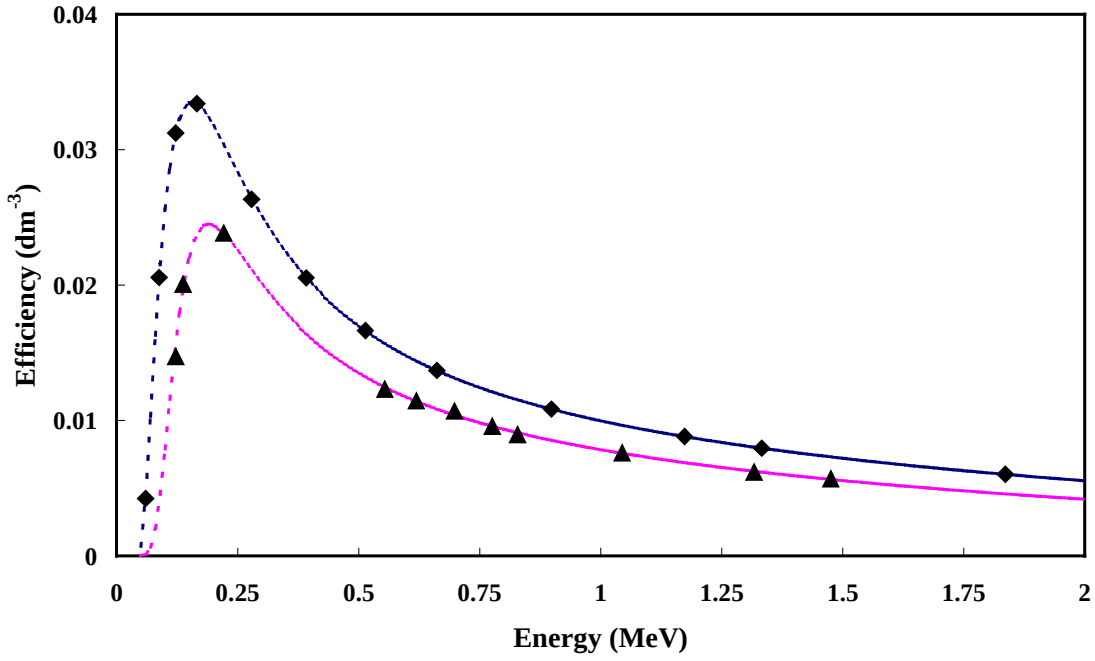

Figure 2-4. *Efficiency curve for the HpGe detector used for the on-line measurement on the pumping side (triangles) compared to the efficiency curve for the HpGe detector used for the sampling measurements in Marinelli Geometry (diamonds).*

When $\Psi_{\gamma(f)}$ had been calculated for all usable ^{82}Br γ-energies, these values were used as input to the efficiency calibration procedure in order to calculate the γ-energy dependent efficiency curve. This curve is shown in Figure 2-4 and is compared to the efficiency curve for the 1 litre Marinelli beaker sample detector. It can be observed that the efficiency is considerably lower for the flow cell detector equipment than for the sample detector equipment, despite the fact that the total volume of groundwater is four times as high in the flow cell detector compared to the sample detector. This can be explained by the higher HpGe detector efficiency in the sample detector equipment compared to the flow cell detector equipment (35 % versus 18 % relative efficiency, respectively). Furthermore, in the Marinelli sample detector equipment the water is distributed around the detector in a more efficient way than in the flow cell detector equipment.

Evaluation of γ-spectra

All γ-spectra measured were evaluated using the evaluation procedure in GammaVision ver 5.1 (EG&G Ortec). All measurements were evaluated using a decay correction to the time of injection.

2.3.2 Liquid scintillation

The tritiated water tracer (HTO) decays without emission of any measurable γ-energies. Liquid scintillation therefore had to be applied. Prior to the measurement, 3 ml of water sample was mixed with 15 ml of scintillation cocktail (Ultima Gold, Packard). The sample was measured using a liquid scintillation counter Wallac 1414 Guardian (EG&G Ortec). An energy discrimination was set in order to only obtain signals from the low energy part of the spectrum where the signal from tritium can be found. The efficiency calibration was performed using a HTO standard solution (Amersham TRY44).

For the samples extracted from the injection side, interferences in the liquid scintillation measurements of HTO were obtained from the simultaneously injected tracers $^{22}Na^{+}$, $^{83}Rb^{+}$ and $^{85}Sr^{2+}$. Liquid scintillation measurements of these tracers showed they had considerable "spill-over" to the low energy part of the spectrum that had been reserved for the tritium signal. These interferences were quantified by individual measurements of known amounts of the different isotopes, i.e., the amount of interferences per Bq of the different radioisotopes, R_i, (cpm/Bq) was determined. Since the exact amounts of interfering radioisotopes in the samples, A_i (Bq), were known from γ-spectrometric measurements, compensations during the evaluations of the HTO activity could be performed according to:

$$A_{HTO} = \frac{R_{tot} - \sum_i A_i R_i}{\Psi_{HTO}} \qquad 2\text{-}2$$

where A_{HTO} (Bq) is the activity of tritiated water in the sample, R_{tot} (cpm) is the total count of the sample in the low energy part of the spectrum and Ψ_{HTO} (cpm/Bq) is the detector efficiency for HTO (determined using the HTO calibration standard).

During the breakthrough of tritiated water in the pumped section, only very low activities of interfering radioisotopes were present. It was therefore decided that no compensations had to be performed for these samples.

2.3.3 Fluorometry

The content of the fluorescent dye Uranine was monitored by analyses on collected samples at the SKB BASLAB Laboratory using a Turner Laboratory Fluorometer.

2.3.4 Chemical Separations

Separation of $^{133}Ba^{2+}$ using $CaCO_3$(s) co-precipitation

In the injection C3, the injected amount of $^{133}Ba^{2+}$ was considerably lower than the other tracers injected simultaneously; 0.55 MBq $^{133}Ba^{2+}$ to be compared with 20-50 MBq of the tracers $^{22}Na^{+}$, $^{83}Rb^{+}$ and $^{85}Sr^{2+}$. Although the highly selective γ-spectrometry technique was used, interference caused a general increased background level that made it difficult to measure the small amounts of $^{133}Ba^{2+}$. For the C3 injection samples, a separation procedure with co-precipitation of $^{133}Ba^{2+}$ in $CaCO_3$(s) was therefore outlined, according to:

1. A solution of 1M Na_2CO_3 was prepared which was added to the samples (1 ml per 10-ml samples), yielding a precipitate of $CaCO_3$(s).

2. The mixture was passed through a 0.45 μm syringe filter.

3. 10 ml of concentrated HCl was thereafter passed through the filter, in order to dissolve the $CaCO_3$(s). The solution which passed through the filter was collected and measured with γ-spectrometry.

A test was performed in which an injection sample was treated with the method described. The solutions obtained above, together with the syringe filter, were all measured with γ-spectrometry and the concentrations of the tracers were compared. The relative distribution of the different tracers is given in Table 2-1.

Table 2-1. Data for the test of the Ba/Sr separation method used, i.e. co-precipitation in $CaCO_3$.

Tracer	% Not co-precipitated in the $CaCO_3$(s)	% Co-precipitated in $CaCO_3$(s), dissolved by HCl	% Remaining in the filter, not dissolved by HCl
$^{22}Na^{+}$	99	1	<1
$^{83}Rb^{+}$	97	3	<1
$^{85}Sr^{2+}$	<8	>91	<2

Quantification of the distribution of $^{133}Ba^{2+}$ could not be performed since the high activities of $^{22}Na^{+}$ and $^{85}Sr^{2+}$ in the first elute totally mask out the possibilities to detect any non-precipitated $^{133}Ba^{2+}$. Regarding the fact that $^{85}Sr^{2+}$ (Ca^{2+}, Sr^{2+} and Ba^{2+} all form very insoluble carbonate precipitates) is almost totally precipitated, one may assume that the precipitation procedure worked well.

12 samples from the C3 injection were treated with this $CaCO_3$ co-precipitation method. The results gave measurements with much lower uncertainty than both the untreated samples and the on-line measurements. There are some indications in the results that C/A_{tot} values are lower for $^{133}Ba^{2+}$ than for $^{85}Sr^{2+}$ that were also used in the C3

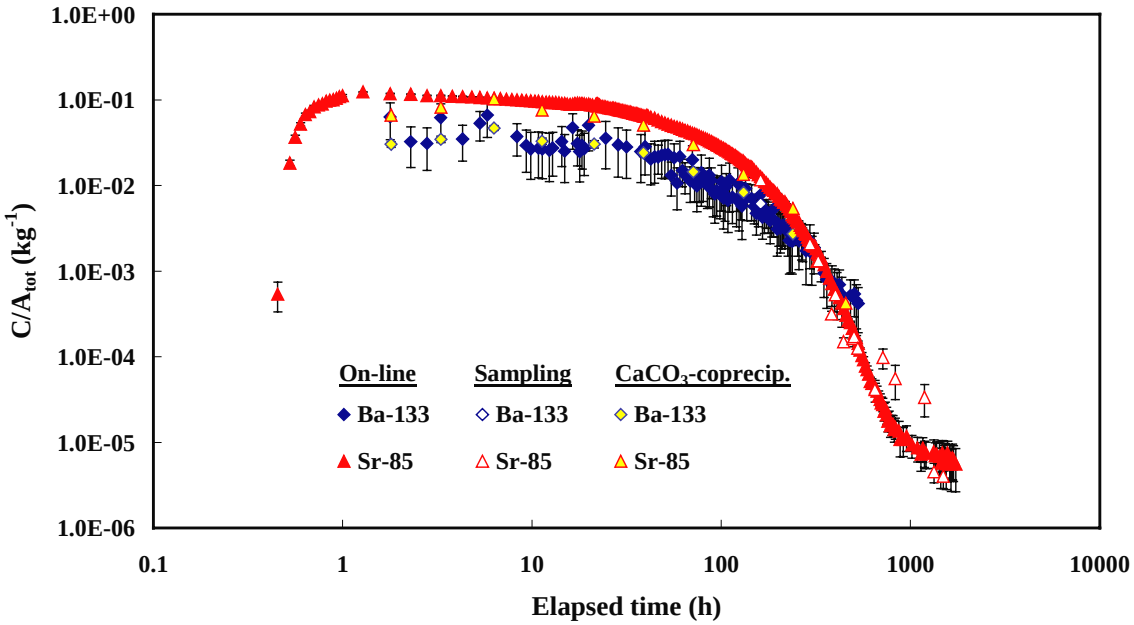

Figure 2-5. *Comparison of the injection curves obtained for $^{133}Ba^{2+}$ and $^{85}Sr^{2+}$ in the C3 injection. Data are given for the on-line measurements, sampling measurements and sampling/co-precipitation measurements. Error bars represent one standard deviation.*

injection, cf. Figure 2-5. The possibility that $^{133}Ba^{2+}$ would be lost in the separation procedure is, however, contradicted by the observation that also the $^{133}Ba^{2+}$ measurements show lower C/A_{tot} values without any co-precipitation (i.e., on-line measurements and sampling measurements). This indicates that a loss of $^{133}Ba^{2+}$ occurred directly after the injection.

2.4 Performance of the Phase C tracer tests (C1 – C4)

Phase C was divided in four sub-tests, C1 through C4. Injections C1 through C3 was performed in three selected source-sink pairs (cf. Table 2-2) using maximum possible pump flow rate (Q=2.0 l/min) in the selected sink section KI0023B: P6. Test C4 was performed in the same flow path as test C1, again using maximum possible pump flow rate in KI0023B: P6. The pumping and injection points are shown superimposed on the hydro-structural model in Figure 2-6.

Table 2-2 provides a description of the tracer inventory used for each injection.

The injections were made in a radially converging flow geometry in flow paths with high flow rates, according to the Phase A tracer dilution tests and tracer test results from Phase A and Phase B (Andersson et al., 2000a, b). In sections having low flow rates, the tracer was forced into the flow path by applying a slight excess pressure using an external injection pump.

Table 2-2. Performance of Phase C tracer tests (C1 through C4). The structural interpretation and notation refers to the March 2000 model (Hermanson & Doe, 2000). Distances within brackets are calculated along the structures.

Test #	Flow path	Struc-tures	Flow geometry	Inj. flow (ml/min)	Pump flow (ml/min)	Tracer	Distance
C1	KI0025F03:P5 – KI0023B:P6	20, 21	Forced injection	45	1950	$^{82}Br^-$, $^{24}Na^+$, $^{42}K^+$, $^{47}Ca^{2+}$, $^{86}Rb^+$, $^{134}Cs^+$, Uranine	14 (16)
C2	KI0025F03:P7 – KI0023B:P6	23, 20, 21	Forced injection	10	1950	$^{186}ReO_4^-$, $^{47}Ca^{2+}$, $^{131}Ba^{2+}$, $^{137}Cs^+$ Naphtionate	17 (97)
C3	KI0025F02:P3 – KI0023B:P6	21	Passive injection	1.8	1950	HTO, $^{22}Na^+$, $^{85}Sr^{2+}$, $^{83}Rb^+$, $^{133}Ba^{2+}$	33 (33)
C4	KI0025F03:P5 – KI0023B:P6	20, 21	Forced injection	45	1950	$^{82}Br^-$, $^{131}I^-$, $^{47}Ca^{2+}$, $^{131}Ba^{2+}$, $^{54}Mn^{2+}$, $^{57}Co^{2+}$, $^{65}Zn^{2+}$	14 (16)

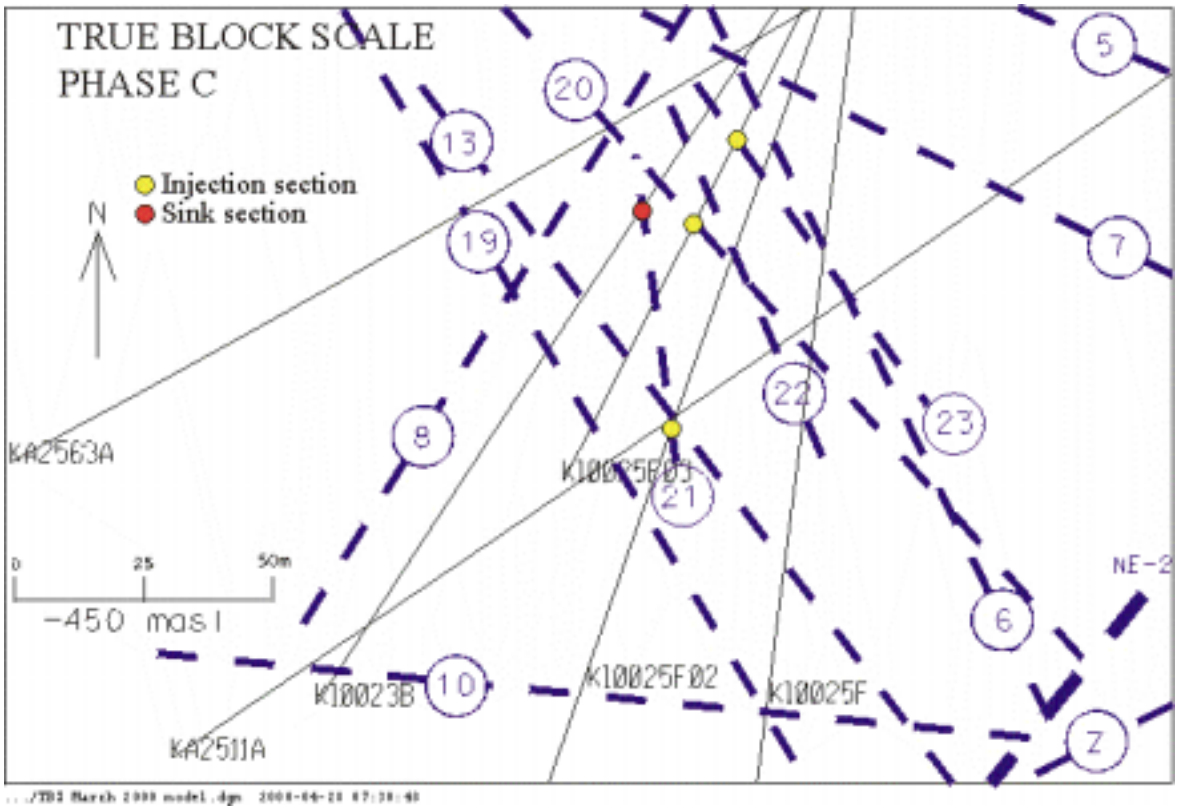

Figure 2-6. *Plan view of sink and source sections superimposed on the March 2000 structural model, see also Figure 1-1.*

The water used for injection was taken from borehole section KA3385A:P1 which has a very similar water chemistry to that found in the target structures in the TRUE Block Scale array. The borehole is also located at such distance from the TRUE Block Scale array (about 200 m) that no pressure disturbance is expected due to the pressure release during filling of the water storage vessels. The water from KA3385A was led through nylon tubing directly to the storage vessels without contact with air. The storage vessels were equipped to enable simultaneous refilling and operation without disturbance.

The electrical conductivity and Redox potential (Eh) of the withdrawal water were measured continuously in-line during the pumping and stored on a field logger (Borre 21) together with the injection flow rate in section KI0025F03:P5 measured continuously with a flow meter.

The positions of the sink and sections used for tracer injections in the TRUE Block Scale Phase C tests are shown in Figure 2-6.

2.5 Evaluation

2.5.1 Evaluation of breakthrough curves

The evaluation of the Phase C tracer tests has involved computer modelling using a one-dimensional advection-dispersion model with matrix diffusion and sorption. Unlike earlier modelling approaches within the TRUE-project the evaluation this time also included sorption and diffusion parameters by fitting the so-called A-parameter which is a lumped parameter including both matrix diffusion and sorption. The governing equations may be written as (Moreno et al, 1983):

$$R_a \frac{\partial C_f}{\partial t} - D_L \frac{\partial^2 C_f}{\partial x^2} + v \frac{\partial C_f}{\partial x} - \frac{2}{\delta} D_e \frac{\partial C_p}{\partial z}\Big|_{z=0} = 0 \qquad (2\text{-}3)$$

for the fracture, and:

$$\frac{\partial C_p}{\partial t} - \frac{D_e}{K_d \rho_p} \frac{\partial^2 C_p}{\partial z^2} = 0 \qquad (2\text{-}4)$$

for the matrix. C_f and C_p are the solute concentrations in the fracture and rock matrix, respectively, D_L is the longitudinal dispersion coefficient (m^2/s), v is the average water velocity (m/s), R_a is the linear retardation coefficient in the fracture, D_e is the effective diffusion coefficient, δ is the fracture aperture (m), K_d is the linear sorption bulk distribution coefficient for the rock matrix (m^3/kg), and ρ_b is the bulk density of the rock matrix (kg/m^3).

For zero initial concentration, constant concentration at the inlet during the tracer injection, a solution to the above equations is (Tang et al, 1981):

$$\frac{C_f}{C_0} = \left(\frac{2}{\sqrt{\pi}}\right) \exp\left(\frac{Pe}{2}\right) \int_l^\infty \exp\left(-\frac{\zeta^2 - Pe^2}{16\zeta^2}\right) \bullet erfc\left(\frac{(Pe\ t_{0'} / 8A\zeta^2)}{\sqrt{t - (Pe\ t_{0'} / 4\zeta^2)}}\right) d\zeta \qquad (2\text{-}5)$$

where

$$l = \sqrt{\frac{Pe\, t_{0'}}{4t}} \qquad (2\text{-}6)$$

$$Pe = \frac{vx}{D_L} \tag{2-7}$$

where $t_{0'}$ is the water residence time, C_0 is the tracer injection concentration, ε_p is the matrix porosity and R_d is the matrix retardation factor.

For a finite rectangular pulse tracer injection, solutions are superimposed by:

$$C(t) = C_f(t) - C_f(t - \Delta t) \qquad C_f(t - \Delta t) = 0 \text{ for } t - \Delta t < 0 \tag{2-8}$$

Finally, a proportionality factor, *pf*, is introduced in order to obtain the actual concentration in the sampling borehole, C_{bh},

$$C_{bh} = pf \cdot C(t) \tag{2-9}$$

where *pf* represents the dilution in the sampling borehole and other proportional losses. In an ideal radially converging flow field, *pf* equals the ratio of the injection flow rate to the pumping flow rate. However, under non-ideal conditions *pf* may also be used to account for incomplete recovery. In addition, since flow rates and tracer injection concentration (i.e. injected tracer mass) likely can not be used with absolute certainty, *pf* may be used as an estimation parameter to also account for such uncertainties.

The model applied was used to estimate parameters using an automated parameter estimation program, PAREST (Nordqvist, 1994). PAREST uses a non-linear least squares regression where regression statistics (correlation, standard errors and correlation between parameters) also is obtained.

The residence time of the tracer, the dispersion (Peclet number), a proportionality factor (basically the ratio of the flow rate in the injection borehole and pumping rate in the withdrawal borehole) and a lumped sorption/matrix diffusion parameter, A, were used as fitting parameters. In the model, it is thus assumed that a non-time dependent surface retardation is occurring for the transport in the fracture and that the surface retardation is dependent on the fracture aperture, δ (m); all according to:

$$R_a = \left(1 + \frac{2K_a}{\delta}\right) \tag{2-10}$$

$$t_0' = R_a t_0 \tag{2-11}$$

where R_a is the surface retardation coefficient, t'_0 (h) is the residence time of a sorbing tracer and t_0 (h) is the residence time of a conservative tracer. Furthermore, a contact time dependent retardation process is occurring and can be described by the parameter A, i.e.;

$$A = \frac{\delta R_a}{2\sqrt{D_e(\varepsilon + K_d \rho)}} = \frac{\delta + 2K_a}{2\sqrt{D_e(\varepsilon_p + K_d \rho)}} \tag{2-12}$$

By assuming that the transport takes place in a single parallel plate fracture, the fracture aperture can be calculated directly from the residence time of the conservative tracer; according to:

$$\delta = \frac{Qt_0}{\left(r^2 - r_w^2\right)\pi} \tag{2-13}$$

where Q(m^3/h) is the mean pumping rate, r(m)is the travel distance and r_w(m) is the borehole radius. Using these calculations, the surface retardation coefficients K_a and a product of the matrix diffusion determining parameters, $D_e(\varepsilon+K_d\rho)$ can be calculated directly from the results of the breakthrough curves and thus be compared to the corresponding data obtained from laboratory experiment. The result of the evaluation is presented in Chapter 3.4.

Based on the mean travel times, t_m, determined from the parameter estimation, the hydraulic fracture conductivity, K_{fr} (m/s), was calculated assuming radial flow and validity of Darcy's law (Gustafsson & Klockars, 1981);

$$K_{fr} = \ln (r/r_w) (r^2-r_w^2) / 2\cdot t_m \cdot \Delta h \qquad (2\text{-}14)$$

where: r = travel distance (m)

r_w= borehole radius (m)

t_m= mean travel time of tracer (s)

Δh= head difference (m)

Flow porosity, θ_k, was calculated using:

$$\theta_k = K/K_{fr} \qquad (2\text{-}15)$$

where K is the hydraulic conductivity of the packed-off section of the borehole determined from steady state evaluation of the interference test (Moye, 1967):

$$K = (Q/\Delta h \cdot L) \cdot ((1+\ln L/2r_w)/2\pi) \qquad (2\text{-}16)$$

where L (m) is the length of the packed-off section. It should be noted that the term flow porosity might be misleading to use in a fractured heterogeneous rock as it is defined for a porous media. However, it is often used in fractured media as a scaling factor for transport, but then defined over a finite thickness which, in his case, is defined as the length of the packed-off borehole section (L = 1.0 m).

The values calculated are presented together with parameters determined from the numerical modelling of the tracer breakthrough in Table 3-14.

2.5.2 Evaluation of tracer injection curves

Linear surface sorption model

For the case of an isolated borehole section with a fracture of flowing water transecting the section, the mass balance of a non-sorbing aqueous tracer introduced to the section gives:

$$Q_{\text{in}} \cdot C_{\text{in}} \cdot dt - Q_{\text{out}} \cdot C_{\text{out}} \cdot dt = d\left(C_{\text{aq}} V\right) \qquad (2\text{-}17)$$

where Q (m^3/s) is the dilution flow rate, V (m^3) is the system volume, C_{aq} (mole/m^3) is the aqueous tracer concentration and t (s) is the time.

If the tracer can sorb on the borehole walls and a linear sorption approach can be used, (i.e.,

$$C_{\text{ads}} = K_a \cdot C_{\text{aq}} \tag{2-18}$$

where C_{ads} (mole/m^2) is the concentration of tracer on the borehole walls, K_a (m) is the surface sorption coefficient) the mass balance is instead written:

$$Q_{\text{in}} \cdot C_{\text{in}} \cdot dt - Q_{\text{out}} \cdot C_{\text{out}} \cdot dt = d\left(C_{\text{aq}} V\right) + d\left(C_{\text{ads}} A\right) \tag{2-19}$$

where A (m^2)is the geometric surface area of the borehole walls. Rearranging and inserting (2-18) in (2-19) yields

$$Q_{\text{in}} \cdot C_{\text{in}} \cdot dt - Q_{\text{out}} \cdot C_{\text{out}} \cdot dt = d\left(C_{\text{aq}} V\right) + d\left(C_{\text{aq}} K_a A\right) \tag{2-20}$$

Normally, the following conditions are applicable:

$$\begin{aligned} &Q_{\text{in}} = Q_{\text{out}} = Q \\ &C_{\text{in}} = 0 \\ &dV = 0, dK_a = 0, dA = 0 \\ &C_{\text{out}} = C_{\text{aq}} \end{aligned} \tag{2-21}$$

and (2-20) can therefore be written as:

$$-Q \cdot C_{\text{aq}} \cdot dt = dC_{\text{aq}} \left(V + K_a A\right) \tag{2-22}$$

With the boundary condition of C_{aq}=$C_{\text{aq,0}}$ at t=0, equation (2-22) has the analytical solution:

$$\ln C_{aq} = \ln C_{aq,0} - \frac{Q}{(V + K_a A)} t \tag{2-23}$$

In this model, it is assumed that the injection section can be approximated with an ideal tank behaviour. For the validity of the model, it is therefore important that the dilution flow rate across the borehole section is low compared to the circulation flow rate. The model also implies that no diffusion and sorption into the rock matrix occurs, i.e., the only mass transfer process is the surface sorption.

From the straight-line decrease in concentration in logarithmic-linear scales of the non-sorbing tracers (i.e., K_a=0), the dilution flow rate can be calculated. A deviation in the slope makes it possible to calculate K_a-values. These sorption coefficients could be of interest to compare with sorption coefficients obtained in laboratory experiment and with retention data obtained from the modelling of the breakthrough results in the pumping borehole. Attempts were therefore made to fit equation (2-23) to some of the experimental results from TRUE-1 (Winberg et al., 2000) and TRUE Block Scale Phase C.

It should be noted that during this evaluation of the injection curves from the TRUE-1 and TRUE Block Scale experiments, the C_{aq} refers solely to the concentration of the injected radioactive tracer of the element used. The impact of any changes in the total chemical concentrations of the different element used as tracers are discussed below.

Results of the analysis using the surface sorption model are presented in Section 3.3.1.

Non-linear sorption approach

Sorption on crystalline rocks has in many works been interpreted using a Freundlich isotherm, i.e.;

$$C_{ads} = K_a \cdot C_{aq}^{\ n} \tag{2-24}$$

where K_a and n are empirical constants and C_{ads} and C_{aq} are referring to the chemical concentration of the element studied. With n=1 the sorption is linear and equivalent to equation (2-18). Using n<1 implies that the relative sorption (C_{ads} / C_{aq}) will increase as the total concentration of the element decreases, i.e., an example of non-linear sorption. The latter has often been observed for e.g., Cs in laboratory experiments (e.g., Skagius et al., 1982, Andersson, 1983) and n≈0.5 is often observed.

However, in the TRUE experiments chemical concentration gradients are avoided by the use of radioactive tracers, always injected in the concentrations found naturally in the groundwater. For the total chemical concentration of the elements used as tracers, it seems therefore reasonable to assume that C_{in}=C_{out} in equation (2-19). This will imply that dC_{ads}=0 and dC_{aq}=0, i.e., no total concentration changes will occur in the system and a linear sorption approach should be applicable.

Nevertheless, a non-linear approach has been tested in this modelling in order to investigate the effects non-linear sorption could possibly have on the injection curves of the TRUE Block Scale experiments. In contradiction to the discussion above, an assumption is made that the non-linear effect is caused by the decrease of the concentration of the radioactive tracers solely, i.e., the effect of naturally abundant stable tracers of the elements are not considered. Equation (2-24) is therefore inserted in (2-19) under the assumption that C_{ads} and C_{aq} are the concentration of the radioactive tracer in the adsorbed phase and in the aqueous phase, respectively. By also applying the conditions in (2-21), the following expression for the dilution of a non-linearly sorbing tracer is obtained:

$$-Q \cdot C_{aq} \cdot dt = d\left(C_{aq} V\right) + d\left(C_{aq}^{\ n} K_a A\right) = V \cdot dC_{aq} + K_a A \cdot d\left(C_{aq}^{\ n}\right) \tag{2-25}$$

Equation (2-25) can be solved by Euler integration technique and by using the boundary condition C_{aq}=$C_{aq,0}$ at t=0.

Results of the analysis using the non-linear sorption approach are presented in Section 3.3.2.

First order kinetics approach

It is possible that the shape of the injection curves is influenced by kinetically hindered sorption and de-sorption. Attempts have therefore been made in order to interpret the sorption from a first order kinetics perspective, i.e.;

$$C_{aq} \underset{k_{des}}{\overset{k_s}{\rightleftharpoons}} C_{ads} \tag{2-26}$$

where k_s (s^{-1}) is the rate constant for the sorption reaction and k_{des} ($m^{-1}s^{-1}$) is the rate constant for the de-sorption reaction. A system consisting of an isolated borehole section where the tracer injected sorb and de-sorb with a kinetically hindered mechanism, can thus be described by the following equations:

$$\frac{dC_{aq}}{dt} = -\frac{Q}{V}C_{aq} - \frac{A}{V}\frac{dC_{ads}}{dt} \tag{2-27}$$

and

$$\frac{dC_{ads}}{dt} = k_s C_{aq} - k_{des} C_{ads} \tag{2-28}$$

where the following boundary conditions are applicable:

$$t = 0, \quad C_{aq} = C_{aq,0} \quad C_{ads} = C_{ads,i} \tag{2-29}$$

$$t = \infty, \quad C_{aq} = 0 \qquad C_{ads} = 0 \tag{2-30}$$

An analytical solution this system has been obtained by Laplace-transformation, giving the following equation:

$$C_{aq} = \frac{\left(C_{aq,0}s_0 + k_{des}C_{aq,0} + k_{des}k_2 C_{ads,0}\right)\cdot e^{(s_0 t)} - \left(C_{aq,0}s_1 + k_{des}C_{aq,0} + k_{des}k_2 C_{ads,0}\right)\cdot e^{(s_1 t)}}{s_0 - s_1} \tag{2-31}$$

where:

$$s_0 = \frac{Q/V + k_{des} + k_s A/V}{2} + \sqrt{\left(\frac{Q/V + k_{des} + k_s A/V}{2}\right)^2 - \frac{Ak_{des}}{V}} \tag{2-32}$$

and

$$s_1 = \frac{Q/V + k_{des} + k_s A/V}{2} - \sqrt{\left(\frac{Q/V + k_{des} + k_s A/V}{2}\right)^2 - \frac{Ak_{des}}{V}} \tag{2-33}$$

Results of the analysis using the first order kinetics approach are presented in Section 3.3.3.

2.6 Environmental monitoring programme

Samples have been taken from a number of positions in the Prototype Repository tunnel, the intersection of the A-tunnel by the I-tunnel and in the I-tunnel, in total six sampling locations, cf. Figure 2-7. These points were sampled during the course of the experiment to detect any uncontrolled spill or transport of radionuclides to the tunnel. Results show no enhanced concentrations of radionuclides or dye tracer, indicating that tracer is not ending up in the low points made up by the southwestern parts of the tunnel system.

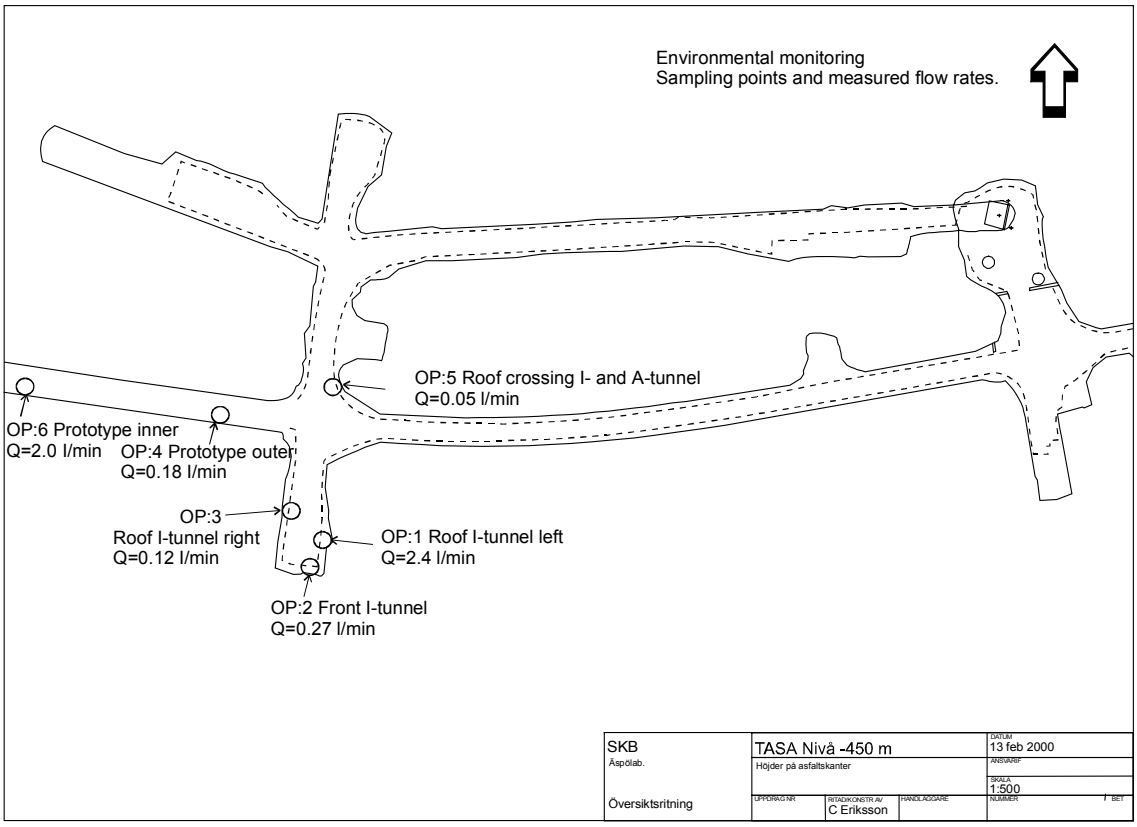

Figure 2-7. *Environmental monitoring sampling points with measured flow rates, cf. Figure 1-1.*

3 Results and interpretation

3.1 General

The test period described in this report lasted between June 15th, 2000 and November 1st, 2000. In general, the equipment used in the Phase C tracer tests worked well. However, some disturbances occurred caused by malfunction of the injection pumps used for creating the dipole flow fields. Long-term injection of water or tracer solution seems to be difficult to perform without pump failure using HPLC plunger pumps. The time sequence for injection and the problems related to the tests are listed in the Log of Events in Appendix 3.

3.2 Tracer injections

Tests C1, C2 and C4 were performed in an unequal strength dipole flow geometry where the tracer was forced into the flow path by applying a slight excess pressure using an external water injection pump. Test C3 was performed as a radially converging tracer test (passive injection) since the induced flow rate in the injection section was considered high enough. Tracer injection data for each test are given in Tables 3-1 through 3-4. The injection concentrations are the actually measured ones. In Figure 3-1 the different tracers in each test are plotted in the same diagram (log-log scale) as injection concentration (normalised to the total injected activity) versus time.

The flow rate in tests C1 and C4 determined from the tracer dilution is only around 25 ml/min while the injection flow measured with a very accurate flow meter is 45 ml/min. The reason for this mismatch is most probably due to inadequate mixing in the injection interval. The unlabelled water added to the system (45 ml/min) is not mixed with the entire volume of the circulation loop, which gives a lower mass flux from the system. Thus, when calculating the tracer mass flux, a flow rate of 25 ml/min should be used instead of the measured flow rate, 45 ml/min. Similar mismatches have been noticed earlier on (Phase B) and it can also bee seen that the mismatch decreases with decreasing flow rate, e.g. if the flow meter shows 10 ml/min as in test C2, the tracer dilution gives 9 ml/min.

Injection data for the conservative dye tracers Uranine injected in test C1 and Naphtionate injected in test C2 are not presented in the tables or figures. Uranine was found to be considerably delayed compared to the other non-sorbing tracer $^{82}Br^-$ (cf. Chapter 3.4) and the results have therefore been omitted. Naphtionate could not be analysed at BASLAB with high enough resolution. However, the breakthrough data of the other non-sorbing tracer $^{186}ReO_4^-$ was judged to be good enough for the evaluation of the test without adding the Naphtionate data.

Table 3-1. Tracer injection data for test C1. Borehole section notation is shortened by removing the prefix "KI00-" from the borehole label.

Borehole section	Section Volume (ml)	Inj. rate flow meter (ml/min)	Inj. rate dil.curve (ml/min)	Tracer	$t_{1/2}$	Max inj. conc. (Bq/kg)	Total Inj. amount (MBq)
F03:P5	7214	45	25	$^{82}Br^-$	35.3 h	$1.82 \cdot 10^7$	138
				$^{24}Na^+$	15.0 h	$2.14 \cdot 10^6$	15.6
				$^{42}K^+$	12.4 h	$2.79 \cdot 10^7$	229
				$^{47}Ca^{2+}$	4.5 d	$1.64 \cdot 10^6$	10.7
				$^{86}Rb^+$	18.7 d	$2.12 \cdot 10^6$	13.3
				$^{134}Cs^+$	2.1 y	$6.21 \cdot 10^5$	7.79

Table 3-2. Tracer injection data for test C2. Borehole section notation is shortened by removing the prefix "KI00-" from the borehole label.

Borehole section	Section Volume (ml)	Inj. rate flow meter (ml/min)	Inj. rate dil.curve (ml/min)	Tracer	$t_{1/2}$ (d)	Max inj. conc. (Bq/kg)	Total Inj. amount (MBq)
F03:P7	4978	10	8.5	$^{186}ReO_4^-$	3.8 d	$3.80 \cdot 10^7$	171
				$^{47}Ca^{2+}$	4.5 d	$1.45 \cdot 10^7$	56.4
				$^{131}Ba^{2+}$	11.5 d	$5.74 \cdot 10^6$	25.7
				$^{137}Cs^+$	30.2 y	$4.46 \cdot 10^6$	23.5

Table 3-3. Tracer injection data for test C3. Borehole section notation is shortened by removing the prefix "KI00-" from the borehole label.

Borehole section	Section Volume (ml)	Inj. rate flow meter (ml/min)	Inj. rate dil.curve (ml/min)	Tracer	$t_{1/2}$ (d)	Max inj. conc. (Bq/kg)	Total Inj. amount (MBq)
F02:P3	8424	-	1.8	HTO	12.3 y	$2.12 \cdot 10^7$	244
				$^{22}Na^+$	2.6 y	$2.68 \cdot 10^6$	21.6
				$^{85}Sr^{2+}$	64.9 d	$2.74 \cdot 10^6$	22.1
				$^{83}Rb^+$	86.2 d	$5.12 \cdot 10^6$	45.9
				$^{133}Ba^{2+}$	10.5 y	$2.61 \cdot 10^4$	0.55

Table 3-4. Tracer injection data for test C4. Borehole section notation is shortened by removing the prefix "KI00-" from the borehole label.

Borehole section	Section Volume (ml)	Inj. Rate flow meter (ml/min)	Inj. rate dil.curve (ml/min)	Tracer	$t_{1/2}$	Max inj. conc. (Bq/kg)	Total Inj. amount (MBq)
F03:P5	7214	45	25-27	$^{82}Br^-$	35.3 h	$6.70 \cdot 10^5$	11.4
				$^{131}I^-$	8 d	$6.21 \cdot 10^5$	9.84
				$^{47}Ca^{2+}$	4.5 d	$1.18 \cdot 10^5$	1.94
				$^{131}Ba^{2+}$	11.5 d	$2.95 \cdot 10^6$	65.1
				$^{54}Mn^{2+}$	312 d	$3.58 \cdot 10^6$	71.1
				$^{57}Co^{2+}$	271 d	$1.63 \cdot 10^5$	28.9
				$^{65}Zn^{2+}$	244 d	$2.02 \cdot 10^4$	20.0

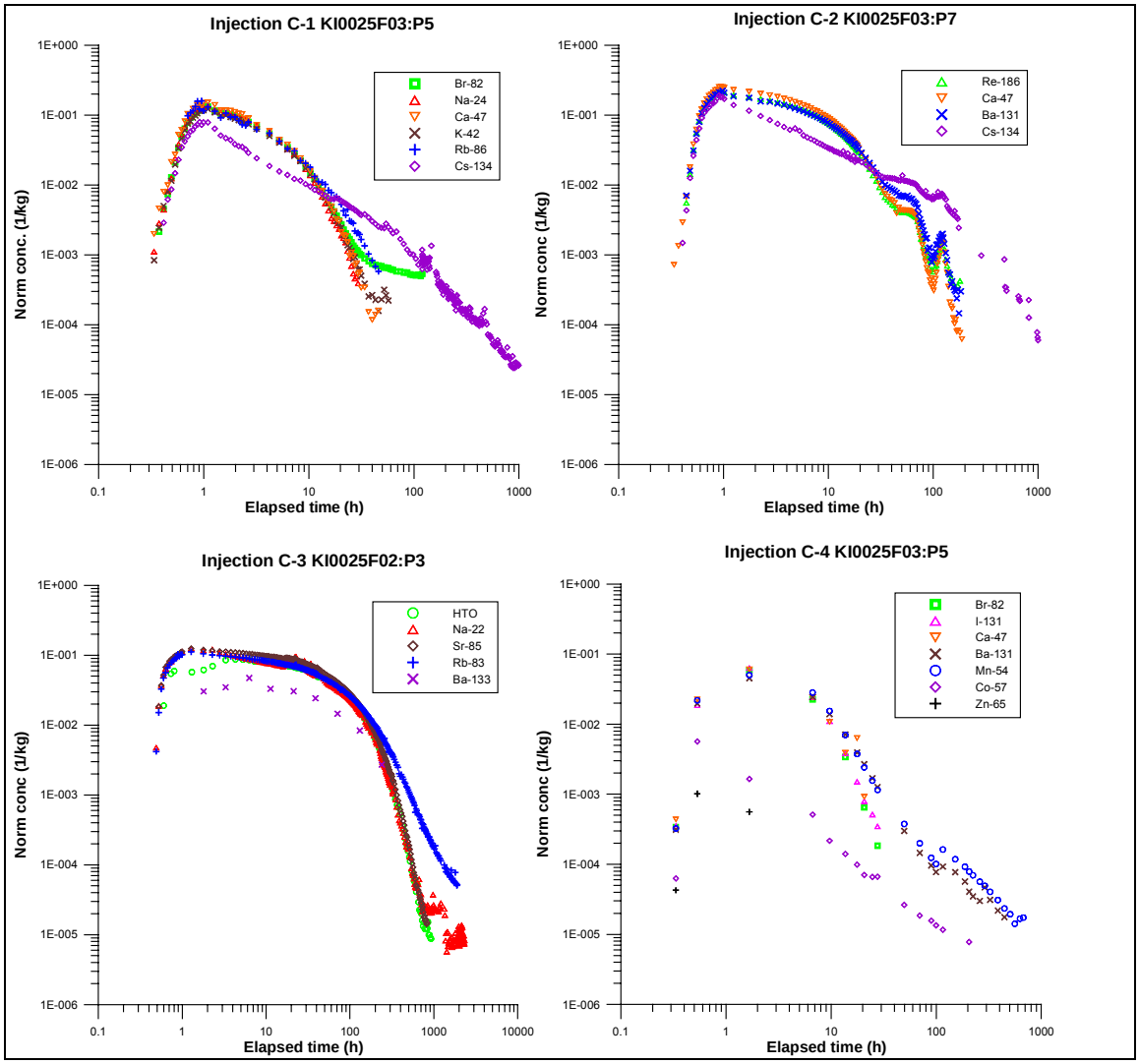

Figure 3-1. *Injection concentrations (normalised to the total injected activity) versus time for the different tracers injected in tests C1 - C4 (logarithmic scales).*

3.3 Sorption coefficients obtained from the injection data

Within the framework of TRUE Block Scale – Phase C, it was decided to use the data from the injection procedure to make an interpretation of sorption behaviour. The general aim was to see if the observed slower dilution rates of the sorbing tracers compared to the conservative tracers could be used for obtaining information of the sorption characteristics. In these calculations, injection data both for the TRUE Block Scale experiment Phase C and the different injections of sorbing tracers in the TRUE-1 experiments (Winberg et al., 2000) were used. Three different sorption models, cf. Section 2.5.2, were used, namely;

- Interpretation of the data using a linear surface sorption model, i.e., considering the borehole section as a well mixed tank with linear sorption occurring only on the borehole walls
- A matrix diffusion approach, i.e., a small part of the tracers would diffuse in to the microfractures closest to the borehole walls.
- A surface sorption model including non-linear surface sorption.
- A linear surface sorption model including first order kinetics, i.e., involving an assumption that the rate of sorption and desorption processes would be kinetically hindered.

The aim of the study was to see if the different sorption models used would be able to describe the characteristics of the dilution curves and if thereby verify any of the processes. Furthermore, process might possibly produce data that could be used in the modelling of the breakthrough data. It would also be interesting to observe if this injection curve produced sorption data would in any way be consistent with the laboratory data.

3.3.1 Linear surface sorption model

Data from TRUE-1

Fitting of equation (2-21) to the experimental data for STT-1 and STT-2 are shown in Figure 3-2 and 3-3, respectively. The obtained surface distribution coefficients for Rb^+, Cs^+ and Ba^{2+} are given in Table 3-5. The sorption for the Na^+, Ca^{2+} and Sr^{2+} is very weak and was not evaluated since the slope of the dilution curves of those tracers did not deviate significantly from the dilution curve of the non-sorbing tracers. A slightly increased sorption is observed in STT-2 compared to STT-1, which may be explained by the observed decreased salinity in the STT-2 experiment compared to the STT-1 experiment. It should be noted that K_a values were estimated by this method although the tracers, due to probable reasons discussed in the following sections, did not show an ideal straight line for the whole time interval studied. The evaluated values of K_a agree reasonably well to the values obtained in the TRUE-1 laboratory experiments (Byegård et al. 1998).

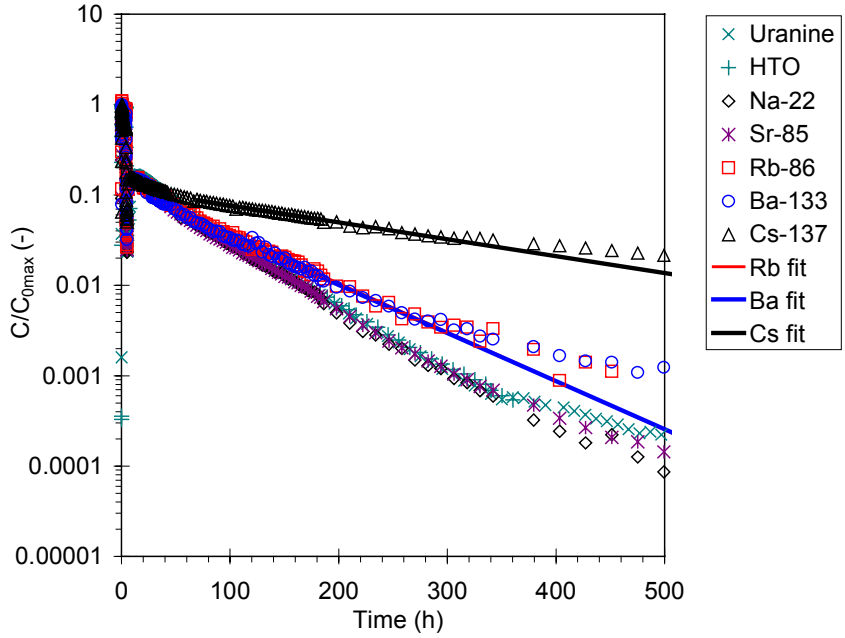

Figure 3-2 *Results of the fitting of Equation (2-21) to the injection data of the STT-1 experiment. The data for the time interval 70-200 h were used for the calculations.*

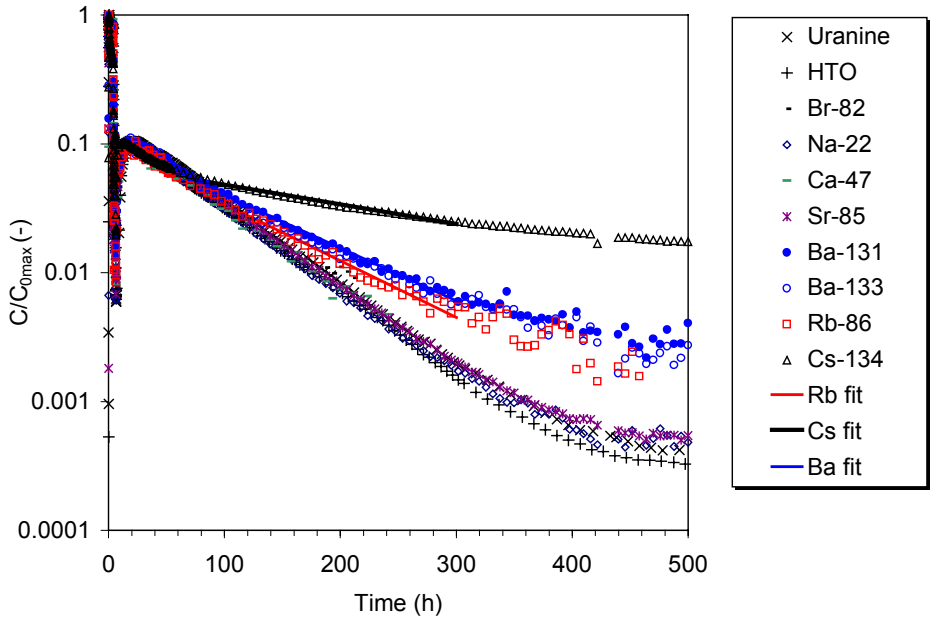

Figure 3-3*. Results of the fitting of Equation (2-23) to the injection data of the STT-2* ***.****experiment. The data for the time interval 70-300 h were used for the calculations.*

Table 3-5. Surface distribution coefficients, K_a, obtained from the fitting of injection data from the STT-1 and STT-2 experiments (TRUE-1) and the C3 injection (TRUE Block Scale). As a comparison, the K_a values obtained in the TRUE-1 laboratory experiments are also presented (Byegård et al. 1998).

	TRUE-1		*TRUE Block Scale*	*TRUE-1 Laboratory*
Tracer	K_a STT-1 (Eq. 2-21)	K_a STT-2 (Eq. 2-21)	K_a C3 (Eq. 2-21)	K_a Lab
$^{83,86}Rb^+$	1.4E-3	2.0E-3	2.3E-3	5E-4 – 4E-3
$^{133}Ba^{2+}$	1.5E-3	2.6E-3	-	2E-4 – 6E-4
$^{134,137}Cs^+$	1.6E-2	1.7E-2	-	8E-3 – 1E-2

Data from TRUE Block Scale

A forced injection flow was used in two of the injections performed in the Phase C experiments. As a result, a significant increase in the injection flow was obtained compared to the TRUE-1 experiment. In the injections C1/C4 and C2 the flow rate was 2600 ml/h and 600 ml/h respectively which can be compared to the injection flow of the TRUE-1 experiment (~30 ml/h). The consequence of this is that the sorption has less time for equilibration, and that the injection flows no longer are negligible compared to the circulation flow (12 000 ml/h). The residence time in the injection section becomes shorter and doubts can be raised about the assumption of the borehole section as an ”ideal tank”. It is therefore a certain risk that non-homogeneously mixed tracer solution might have been directly injected into the fracture system during the initial phase of the injection. The calculation of the mass balance within the borehole section therefore becomes uncertain.

The concept of fitting of Equation (2-23) to the injection experimental data has for TRUE Block Scale only been applied to injection C3 (cf. Figure 3-4). This injection was performed without applying any extra injection flow, i.e.; the observed dilution was only a result of the pumping performed in the pump borehole. As for the TRUE-1 injections, the deviations in the behaviour of the slightly sorbing tracers used in C3 (Na^+ and Sr^{2+}) from the non-sorbing tracer (HTO) were not sufficient to allow a calculation of the K_a. Furthermore, the general uncertainty of the $^{133}Ba^{2+}$ tracer used (mainly because of the low activity used for that tracer) also excluded any meaningful analysis of that particular tracer. The fitting calculation was therefore only done for Rb^+ where data for the 70-300 h was used for a K_a-calculation according to Equation (2-23). The result is given in Table 3-5 and is in good agreement both with the results based on TRUE-1 data and the laboratory data. It should, however, be noted that the declining Rb^+ concentration is not linear over a longer time scale, which somewhat contradict the assumption of a sorption model consisting of a fast reversible sorption only on the borehole walls.

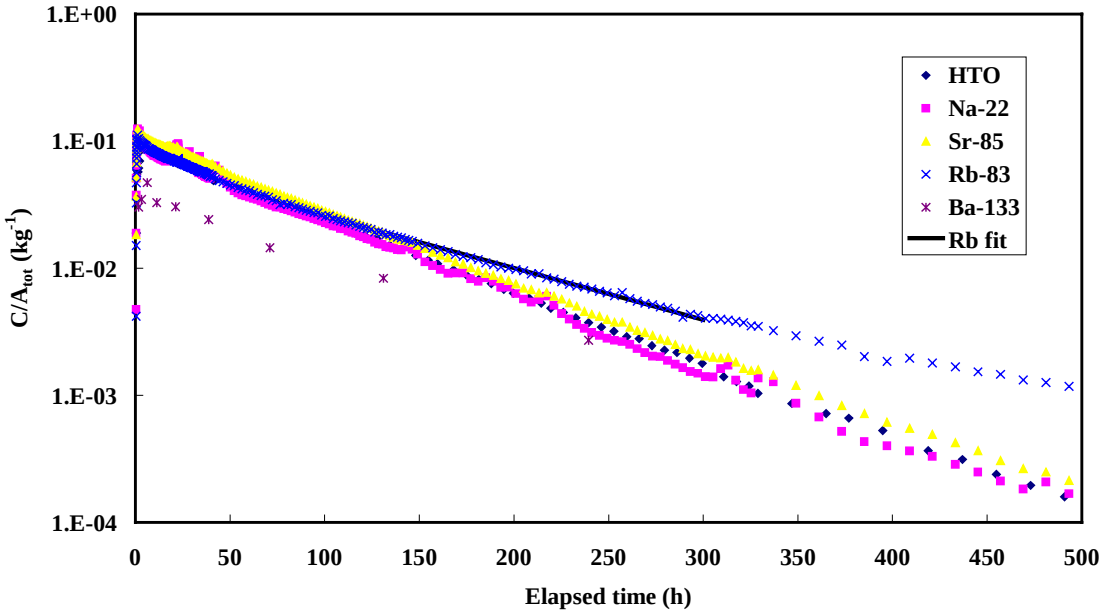

Figure 3-4 *Dilution curves for TRUE Block Scale injection C3 including the fit of Equation (2-23) to the Rb data in the time interval 70-300 h.*

Matrix diffusion approach

As been shown in the previous section, deviations are observed in the experimental data from the model including only dilution and surface sorption. A possible explanation could be that the tracers diffuse into the pores of the rock matrix where sorption may take place. Observing the dilution curves for STT-2 in log-log scale (cf. Figure 3-5) a tendency of a slope of –3/2 is indicated after 500 h, which could be indicative of diffusion out of the rock matrix is the rate limiting process (described by e.g., Heer and Hadermann 1994).

An interesting observation in the TRUE Block Scale injections C1 and C2 (cf. Figure 3-5), is that the slopes for the injection curves for Cs after 200 h in log-log scale approach -3/2. This time-dependence in the concentration may indicate that diffusion is the rate limiting process for the de-sorption of Cs. Furthermore, the same tendency of a late time slope of -3/2 in the log-log scale can be observed in injection C3 for Rb and in injection C4 for Ba and Mn.

For the non- or very weakly sorbing tracers used (e.g., HTO, Na, Sr) a change in the slope in the log-log scale can be observed after 500 h, both for STT2, TRUE-1 and for injection C3, TRUE Block Scale, all data in Figure 3-5.

However, one should be aware of that impact of sorption/de-sorption kinetics might give deviations in the injection curves similar to those attributed to matrix diffusion processes. Laboratory experiments (e.g., Byegård et al., 1998) have indicated limited sorption reversibility, especially for Cs, but also to some extent for Rb and Ba. The impact of sorption kinetics is analysed below.

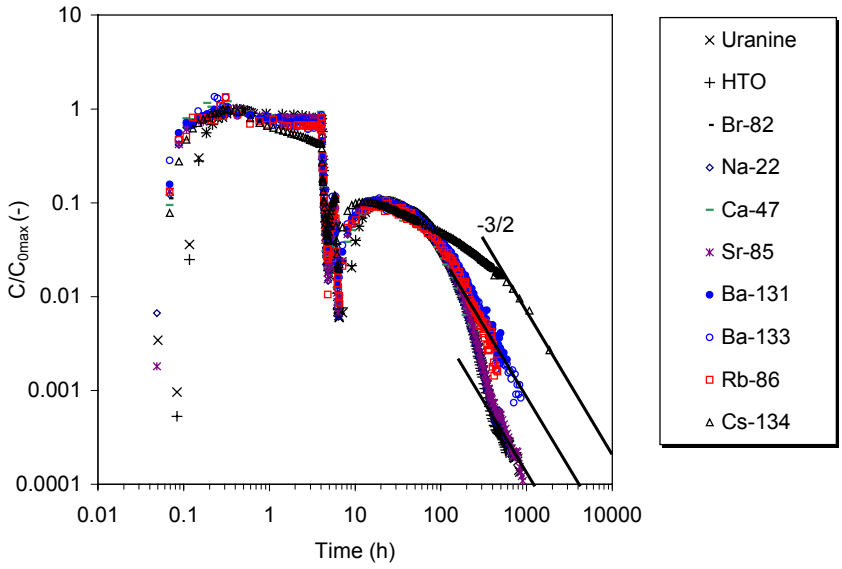

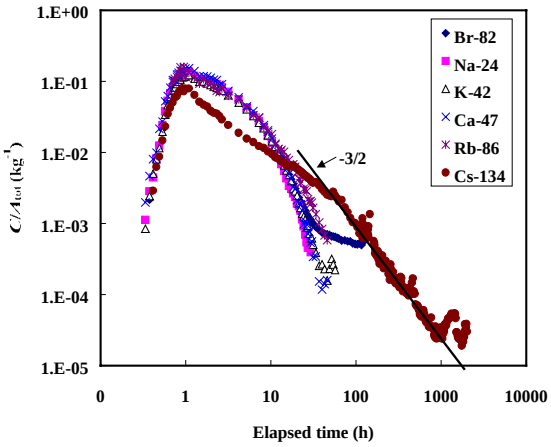

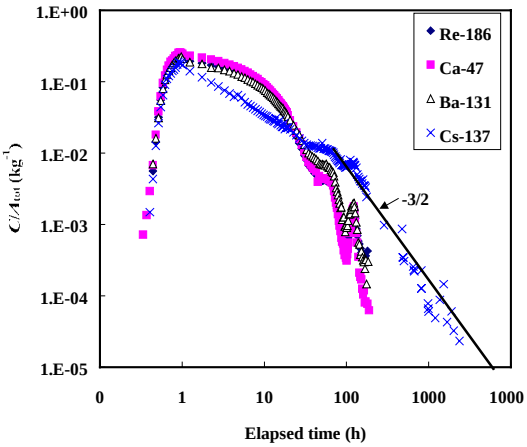

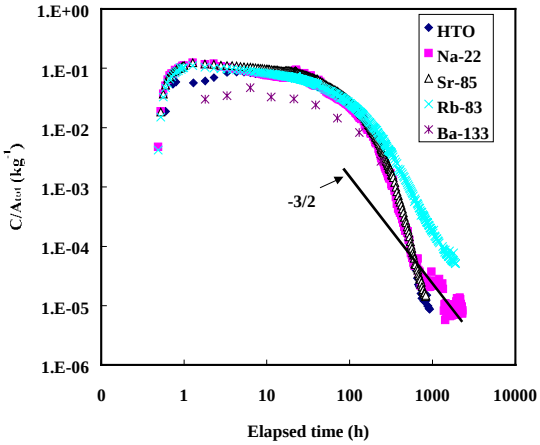

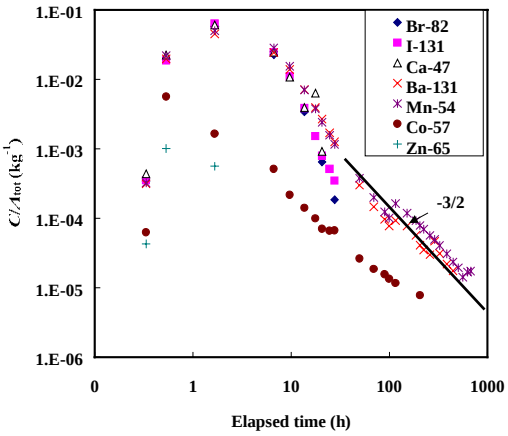

Figure 3-5 *Injection curves for STT2 experiment in TRUE-1 (top), injection C1 (middle, left), injection C2 (middle, right), injection C3 (bottom, left) and injection C4 (bottom, right).*

3.3.2 Non-linear sorption approach

The dilution curves for $^{134}Cs^{+}$ in injection C1 and for $^{83}Rb^{+}$ in injection C3 have been used to exemplify the impact of this non-linear sorption approach. K_a and n (Eq. 2-23) have been used as the fitting parameter; with support from the literature data n=0.5. The results (Figure 3-6 and Table 3-6) indicate that the non-linear approach gives rather good fit to the experimental results. For Cs the initial loss is not satisfactorily explained by the non-linear approach. However, the straight line behaviour in log-log scale of the experimental data at the late time can be fitted by the non-linear sorption model. Concerning Rb, the whole dilution curve can be satisfactorily explained by a non-linear sorption model, except for the behaviour after 500 h where the slope in the experimental results deviates from the tested model. For both tracers, it is indicated that the experimental results give slopes that are lower than the fitted slope obtained from the non-linear sorption model.

It is an interesting fact that the non-linear approach with a Freundlich isotherm can reproduce the form of the injection curves of Cs and Rb quite well. However, it is difficult to find any mechanistic explanation for non-linear sorption behaviour. The concentrations of the injected radioactive tracers are ~1E-10 M (Rb) and ~1E-8 M (Cs) which can be compared to the natural background concentration of 6E-7 M and 4E-8 M for Rb and Cs, respectively. It is therefore difficult to explain a change in the total concentration, leading to a variation of the relative sorption, as stated by equation 2-22.

One could speculate in the background concentration of these elements being present in another chemical form (e.g., colloidal from, microscopic rock fragments) compared to the ionic form that the radioactive tracers are injected in. The loss observed for the radioactive tracer would then be equivalent to the concentration decrease of the ionic species of the elements and the Freundlich isotherm (Eq. 2-22) would be valid. However, explaining the behaviour of Rb and Cs with non-linear effects in the injection curves for TRUE Block Scale would imply that some type of saturation of sorption sites would occur at concentrations below 1E-10 M. It is generally agreed that sorption should be more or less linear when the concentrations are decreased. However, Andersson (1983) reports that a Freundlich isotherm with n=0.5 could explain the sorption of Cs on Stripa granite down to a total concentration of 1E-8 M, the lowest concentration studied in that experiment.

It must also be mentioned that other possible retention processes taking place in the injection borehole (e.g., heterogeneous matrix diffusion, kinetically hindered sorption/de-sorption) may give rise to a behaviour of the tracers that erroneously can be interpreted by a non-linear sorption model. Further investigations are probably necessary to obtain a clearer picture of this problem.

Table 3-6. Numerical values of the parameters obtained from the fitting of a non-linear sorption approach to the injection curves.

Injection	Tracer	K_a (m)	n
Block Scale (C1)	$^{134}Cs^{+}$	1.33E-1	0.379
Block Scale (C3)	$^{83}Rb^{+}$	3.07E-2	0.497
TRUE-1 (STT2)	$^{134}Cs^{+}$	2.85E-1	0.450

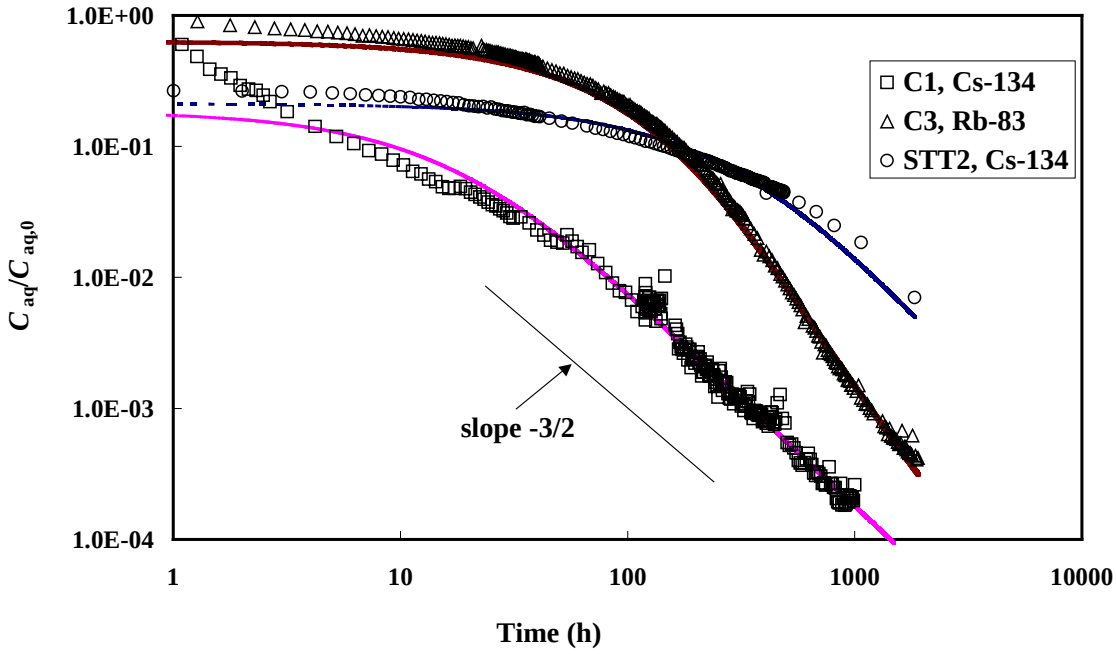

***Figure 3-6**. Fit of a non-linear (Freundlich isotherm) sorption model to the injection .curves for $^{134}Cs^{+}$ (injection C1, injection STT2 in TRUE-1) and $^{83}Rb^{+}$ (injection C3).*

3.3.3 First order kinetics approach

This model has been used for interpretation of the injection curves of $^{134}Cs^{+}$ (injection C1) and of $^{83}Rb^{+}$ (injection C3). The rate constants for the sorption and de-sorption reactions (k_s and k_{des}, respectively) were varied in order to fit Equation (2-31) to the experimental results. The results are presented in Figure 3-7 and Table 3-7 and it is indicated that systematic deviations from the model are obtained, especially for Cs^{+} in the C1 injection. On the contrary, for the TRUE-1 STT2 injection the first order kinetics approach can very well explain the shape of the injection curve. However, one should be aware of the fact that the injection curve of Cs^{+} in the TRUE Block Scale experiment has a dynamic range of >3.5 orders of magnitudes compared to the injection curve of Cs^{+} in the TRUE-1 STT2 injection (1.5 orders of magnitudes). Limitations of the possibility to use the first order kinetics sorption model to explain the characteristics of the dilution curves are therefore likely to be more obvious in the former case than in the latter.

An additional consideration in succeeding to fit the first order kinetics sorption model to the data of the Cs^{+} injection in the TRUE-1 STT2 injection is that only the data obtained after the exchange of the water in the injection section has been used in the interpretation. (See Winberg et al., 2000) for description of injection procedure for the TRUE-1 tracer experiments). As a test, the sorption parameters obtained were used for calculating the sorption before the exchange of the groundwater in the injection section. The results of that calculation indicated that the sorbed amount during the initial phase was underestimated by a factor 5 compared to the actual experimental results.

Table 3-7. Numerical values of the parameters obtained from the fitting of a first order kinetics sorption approach to the injection curves.

Injection	Tracer	k_s (s^{-1})	k_{des} ($m^{-1}s^{-1}$)	K_a (m) (=k_s/ k_{des})
Block Scale C1	$^{134}Cs^+$	9.1E-8	1.8E-6	5.1E-2
Block Scale C3	$^{83}Rb^+$	1.8E-9	7.3E-7	2.4E-3
TRUE-1 (STT2)	$^{134}Cs^+$	2.6E-9	4.7E-7	5.4E-3

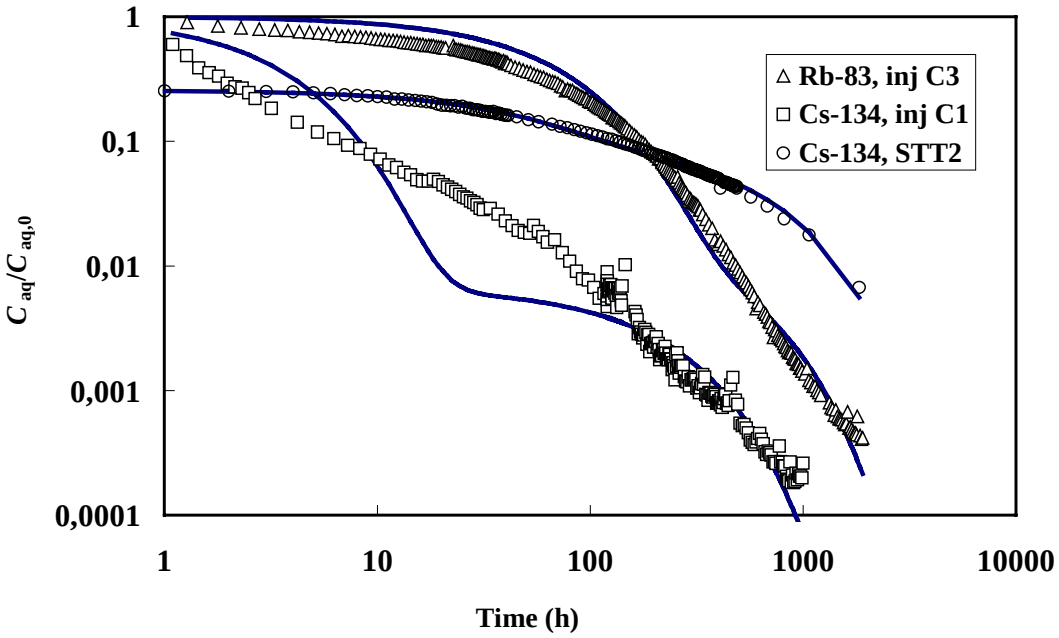

Figure 3-7 *Results of the fitting of a first order kinetics sorption approach to the injection curves .for $^{134}Cs^+$ (injection C1 in TRUE Block Scale and injection STT2 in TRUE-1) and $^{83}Rb^+$ (injection C3 in TRUE Block Scale).*

3.4 Tracer breakthrough

Tracer breakthrough in the pumping section KI0023B:P6 was monitored for all tracers injected in test C1 (injection section KI0025F03:P5 Structure #20). The tracer mass recovery was very high for the conservative and weakly sorbing tracers, cf. Table 3-8. Test C4 was conducted in the same flow path as test C1 and breakthrough was observed for all tracers injected except Zn.

As can be seen in Figure 3-8, the breakthrough of Uranine from injection C1 is considerably delayed compared to the non-sorbing tracer $^{82}Br^-$. Earlier performed injections of Uranine in that flow-path did not indicate any sorbing behaviour of the tracer so the observation is difficult to explain. The only circumstance that in any way can be correlated to this observation is the different preparation procedure applied for the stock solution used in the C1 injection.

Normally when a Uranine stock solution is prepared, the sodium salt of Uranine is dissolved directly in distilled water. However, in the C1 injection some of the tracers were delivered as irradiated chemicals (see Table 1 in Appendix 1) that needed to be dissolved using hydrochloric acid. The sodium salt of Uranine was therefore dissolved

and mixed with the strongly acidic solution, in which a yellow precipitate of the protonated form of Uranine was formed. However, when the NaOH was added, the precipitate was dissolved and the solution returned to its characteristic green colour again. It may be possible that the contact with the strongly acidic solution caused irreversible chemical alteration of the Uranine molecule; although, no description of such behaviour has been found in the literature.

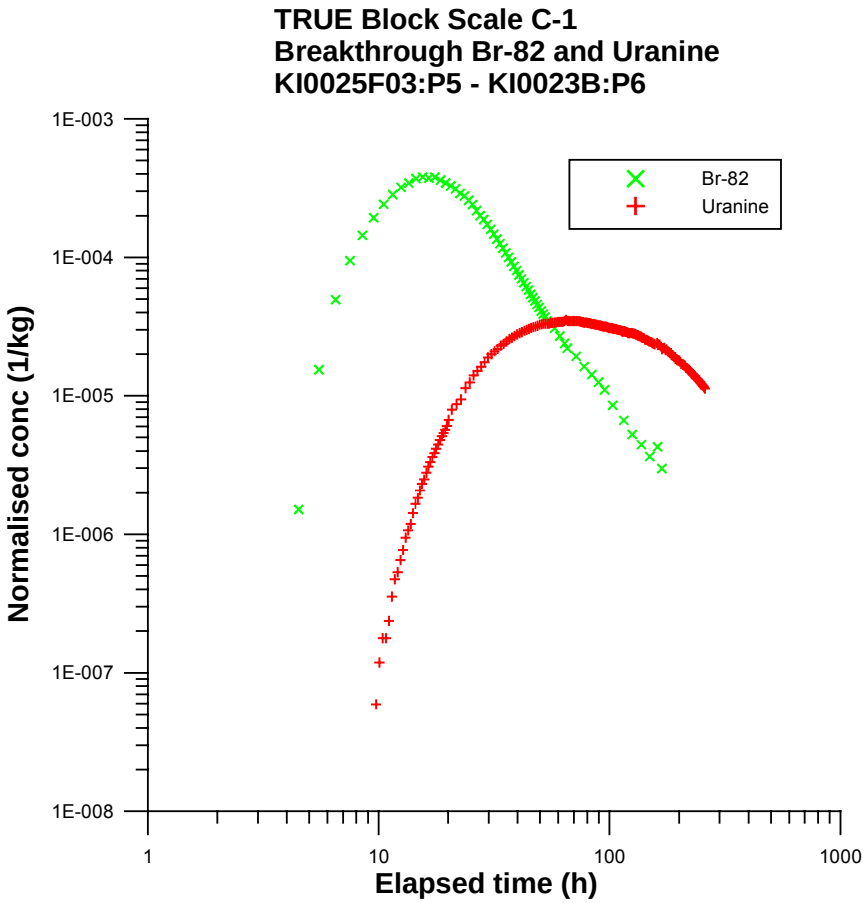

Figure 3-8. *Comparison of breakthrough of the conservative tracers $^{82}Br^-$ and Uranine in Test C1.*

From the injection in section KI0025F03:P7 in test C2, tracer breakthrough was observed from the non-sorbing and weakly sorbing tracers Re and Ca while no breakthrough could be detected in the pumping section from the moderately and strongly sorbing tracers Ba and Cs, cf. Table 3-9.

Also in test C3 with injection in KI0025F02:P3 tracer breakthrough in pumping section was only monitored for the conservative and weakly sorbing tracers HTO, Na and Sr, cf. Table 3-10.

Tracer mass recovery was calculated in the same way for all tracers detected in the pumping section. Before the injection a sample of the stock solution was taken and the tracer solution vessel was weighed. After the injection the vessel was weighed again and the tracer concentrations of the stock solution sample were measured to determine the injected mass of the different tracers, cf. Tables 3-1 through 3-4. The tracer mass

recovered in the pumping borehole section was determined by integration of the breakthrough curves for mass flux (Bq/h) versus time (h).

Tracer travel times, t_5, t_{50} and t_{95} (defined as times when 5, 50 and 95 % of the recovered mass has arrived in the pumping section at the stop time of sampling, t_t) were calculated and are presented together with the total mass recovery (calculated at the stop time of sampling, t_t) in Tables 3-8 through 3-10.

Figure 3-9 shows the tracer breakthrough for the different tracers in each test as normalised concentration versus time. In Figure 3-10 tracer breakthrough for all tracers injected in tests C1 and C4, conducted in the same flow path (KI0025F03:P5 - KI0023B:P6), are plotted together for comparison.

Table 3-8. TRUE Block Scale Tests C1 and C4, flow path KI0025F03:P5 - KI0023B:P6. Tracer travel times, t_5, t_{50} and t_{95} and tracer mass recovery at t_t based on total injected amount (t_t is the time for the last sample taken).

Tracer	t_5 (h)	t_{50} (h)	t_{95} (h)	t_t (h)	Recovery (%)
C1					
$^{82}Br^-$	9	20.5	49.5	165	100
$^{24}Na^+$	10.5	27.5	107	111	96
$^{47}Ca^{2+}$	14.5	46	264	297	98
$^{42}K^+$	21.5	103	-	111	53
$^{86}Rb^+$	66	405	-	734	67
$^{134}Cs^+$	530	-	-	3255	39
C4					
$^{82}Br^-$	9	23	-	38	69
$^{131}I^-$	9	22	-	222	90
$^{47}Ca^{2+}$	16.5	-	-	69	49
$^{131}Ba^{2+}$	28	290	-	885	67
$^{54}Mn^{2+}$	145	1110	-	1221	52
$^{57}Co^{2+}$	-	-	-	1221	0.6
$^{65}Zn^{2+}$	-	-	-		no breakthrough

Table 3-9. TRUE Block Scale Test C2, flow path KI0025F03:P7 - KI0023B:P6. Tracer travel times, t_5, t_{50} and t_{95} and tracer mass recovery at t_t based on total injected amount (t_t is the time for the last sample taken).

Tracer	t_5 (h)	t_{50} (h)	t_{95} (h)	t_t (h)	Recovery (%)
$^{186}ReO_4^-$	94	258	-	495	80
$^{47}Ca^{2+}$	296	-	-	798	29
$^{131}Ba^{2+}$	-	-	-		no breakthrough
$^{137}Cs^+$	-	-	-		no breakthrough

Table 3-10. TRUE Block Scale Test C3, flow path KI0025F02:P3 - KI0023B:P6. Tracer travel times, t_5, t_{50} and t_{95} and tracer mass recovery at t_t based on total injected amount (t_t is the time for the last sample taken).

Tracer	t_5 (h)	t_{50} (h)	t_{95} (h)	t_t (h)	Recovery (%)
HTO	227	818	-	3051	73
$^{22}Na^{+}$	336	1450	-	3135	70
$^{85}Sr^{2+}$	640	2960	-	3135	52
$^{83}Rb^{+}$	-	-	-		no breakthrough
$^{133}Ba^{2+}$	-	-	-		no breakthrough

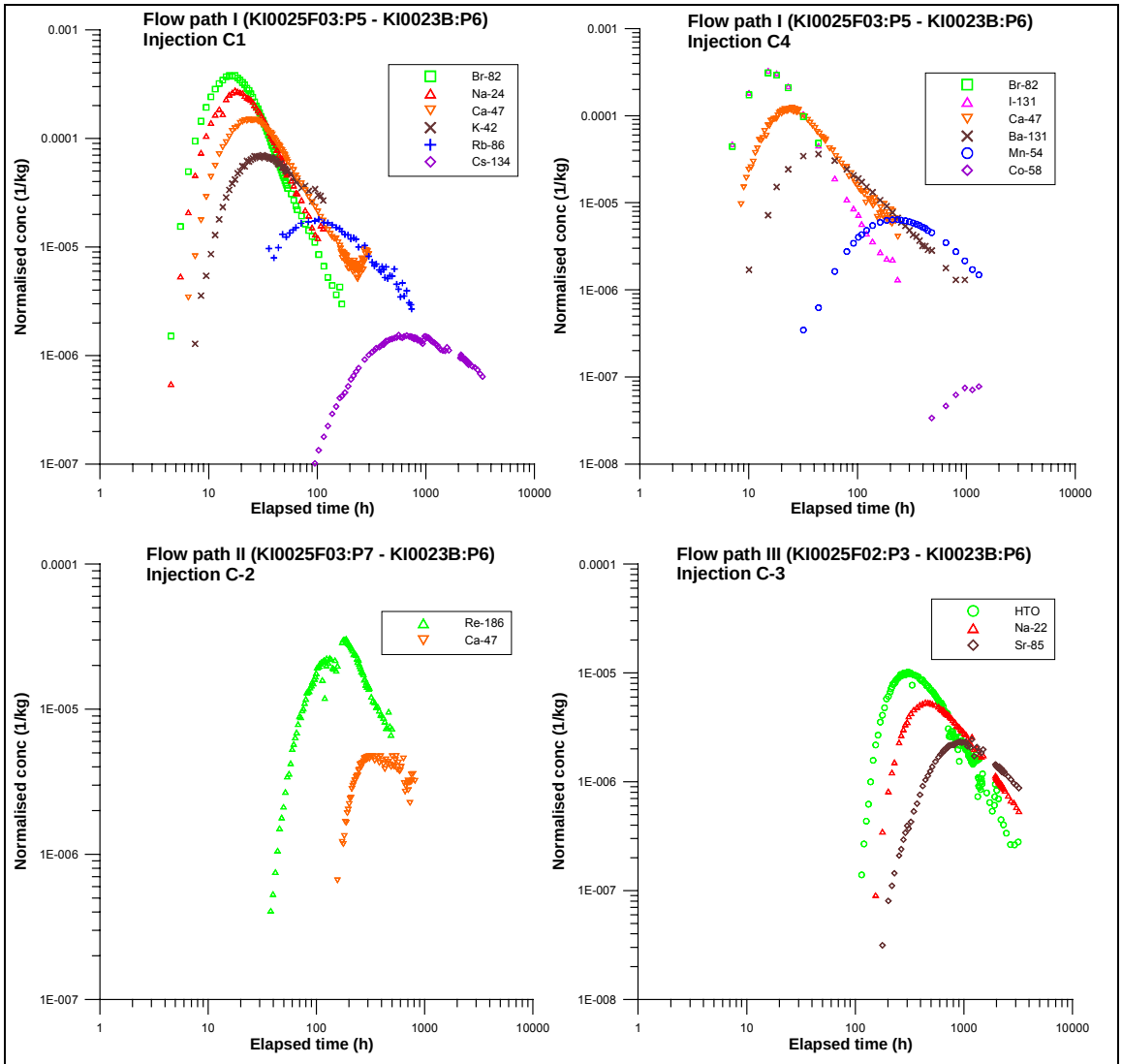

Figure 3-9. *Tracer breakthrough concentrations (normalised to the total injected activity) versus time for the different tracers injected in Tests C1 - C4 (logarithmic scales).*

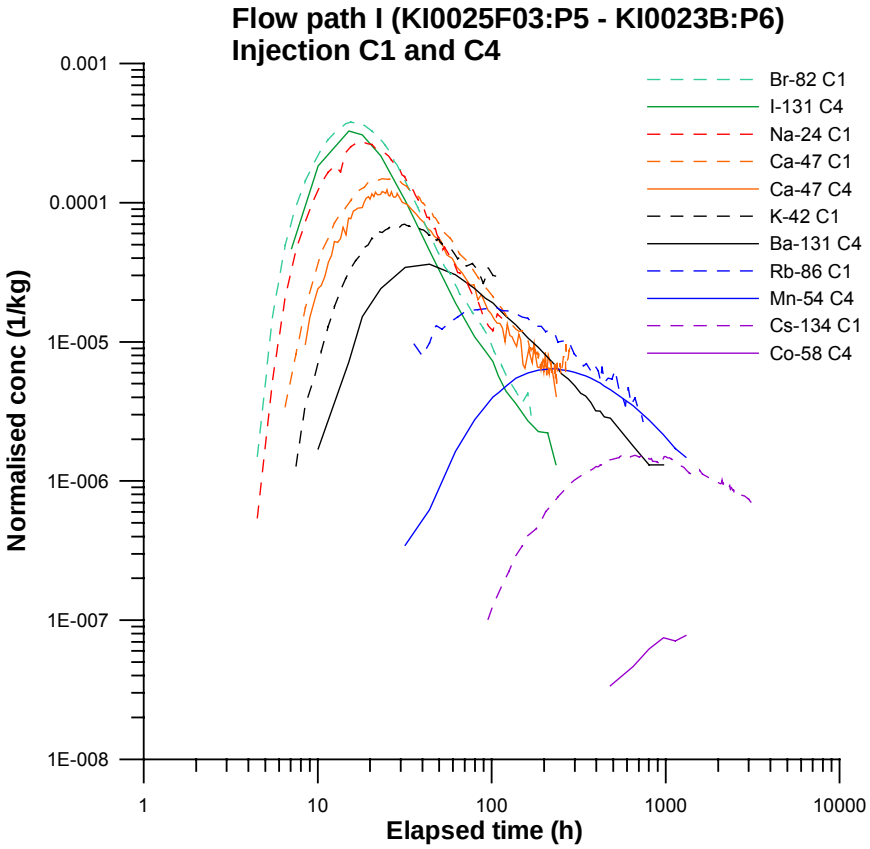

Figure 3-10. *Normalised tracer breakthrough for all tracers injected in Tests C1 and C4.*

3.5 Comparison of sample measurements and on-line measurements

In this experiment, γ-spectrometric measurements were performed on-line and by sampling; comparisons were thus obtained both for the pump side measurements and for the injection side measurements. Some interesting observations can be made from the comparisons:

- For all anionic species used (i.e., $^{82}Br^-$, $^{131}I^-$ and $^{186}ReO_4^-$) the on-line measurements give a "smoothing out" at the late part of the tracer injection and breakthrough curves. This behaviour is not in any case supported by the measurements on samples. Furthermore, the sampling results of $^{131}I^-$ (both the injection side and the pump side) and $^{82}Br^-$ (pump side, injection C1) contradict this "smoothing out". The behaviour is therefore likely to be explained by a weak anion-sorption on the polyamide tubing in the on-line cells. Diffusion of the tracers into the polyamide tubing is also possible, but it is somewhat contradicted by the observation that no similar behaviour can be observed for the very weakly sorbing cations, e.g., $^{22}Na^+$, $^{24}Na^+$, $^{47}Ca^{2+}$ and $^{85}Sr^{2+}$, cf. Figure 3-11.

- Among the slightly and moderately sorbing cationic tracers, e.g., $^{22}Na^+$, $^{24}Na^+$, $^{47}Ca^{2+}$, $^{85}Sr^{2+}$, $^{83}Rb^+$, $^{86}Rb^+$, $^{131}Ba^{2+}$ and $^{133}Ba^{2+}$ there are no observations of systematic deviations of the results obtained from on-line measurements from the results obtained from measurements on samples. The injection curves for

these tracers are in most cases very similar to the injection curves for the non-sorbing tracers, i.e., no or very little sorption occurs in the injection section, cf. Figure 3-11.

- For $^{134}Cs^{+}$ and $^{137}Cs^{+}$ no general systematic differences between the on-line measurements and the measurements on samples can be observed, cf. Figure 3-11. However, there is an indication that with longer contact time, the online measurements on the injection side give higher concentrations than the corresponding measurements on samples. This is an indication that sorption of Cs^{+} is occurring on the polyamide tubing. In the TRUE-1 experiment (non-published results, Byegård et al. 2001), it was observed that deviations of the on-line measurements from the measurements on samples could be correlated to an observation of a build-up of a dark precipitate on the inside walls of the polyamide tubing. Leaching of the tubing in concentrated nitric acid followed by ICP-MS measurement of the leaching solution showed that Zn was the major element leached from the precipitate.

- For the strongest sorbing tracers in injection C4, i.e., $^{57}Co^{2+}$ and $^{65}Zn^{2+}$ pronounced differences between the on-line measurements and the sample measurements can be observed at the injection side. In fact, $^{65}Zn^{2+}$ is only observed in the first three measurements on samples while the concentrations derived from the on-line measurements stabilises at a C/A_{tot} of ~1.4E-2, cf. Figure 3-12. This can be explained by a severe sorption of particularly $^{65}Zn^{2+}$ but also $^{57}Co^{2+}$ already in the injection borehole section. Additionally, a significant part of the injected amount is sorbed on the polyamide tubing in the flow cell and probably also on the stainless steel tubing used in the major part of the circulation circuit. The situation is complicated by the fact that a stainless steel filter is mounted in the sampling line before the sampling equipment. It is therefore not unlikely that the sampling measurements also give a misrepresentation of the actual tracer concentration in the groundwater injection section. The outcome of this comparison highlights that an optimisation of the borehole equipment (i.e. other materials and procedures) is necessary when stronger sorbing tracers are to be used in this type of field tracer experiments.

- There are additional indications of differences between the on-line measurements and the measurements on samples at the injection side in the C4 injection. For $^{131}Ba^{2+}$ and $^{54}Mn^{2+}$, it is indicated that the measurements on samples give higher concentrations than the corresponding on-line measurements, cf. Figure 3-12. This observation is difficult to explain. However, one possible source of uncertainty is the general high level of γ-ray counting rate in the on-line measurement in injection because of the sorption of $^{65}Zn^{2+}$ in the measurement cell. This high level gives measurement conditions that are different from the conditions used during the calibration of the detector, i.e., measurements of the low amounts $^{131}Ba^{2+}$ and $^{54}Mn^{2+}$ was performed under severe interference of the Compton part of the $^{65}Zn^{2+}$ spectrum.

- All measurements using the flow-cell at the pump side corresponded well to the measurements on samples (except for the anionic tracers used, this topic is discussed above). No build-up of sorbing tracers (due to sorption of tracers in the tubing in the flow cell) could be verified. An explanation to why this occurred at the injection side but not at the pump side is probably that a small flow of nitric acid continuously was injected in the water just before its passing of the detector at the pump side but not at the injection side.

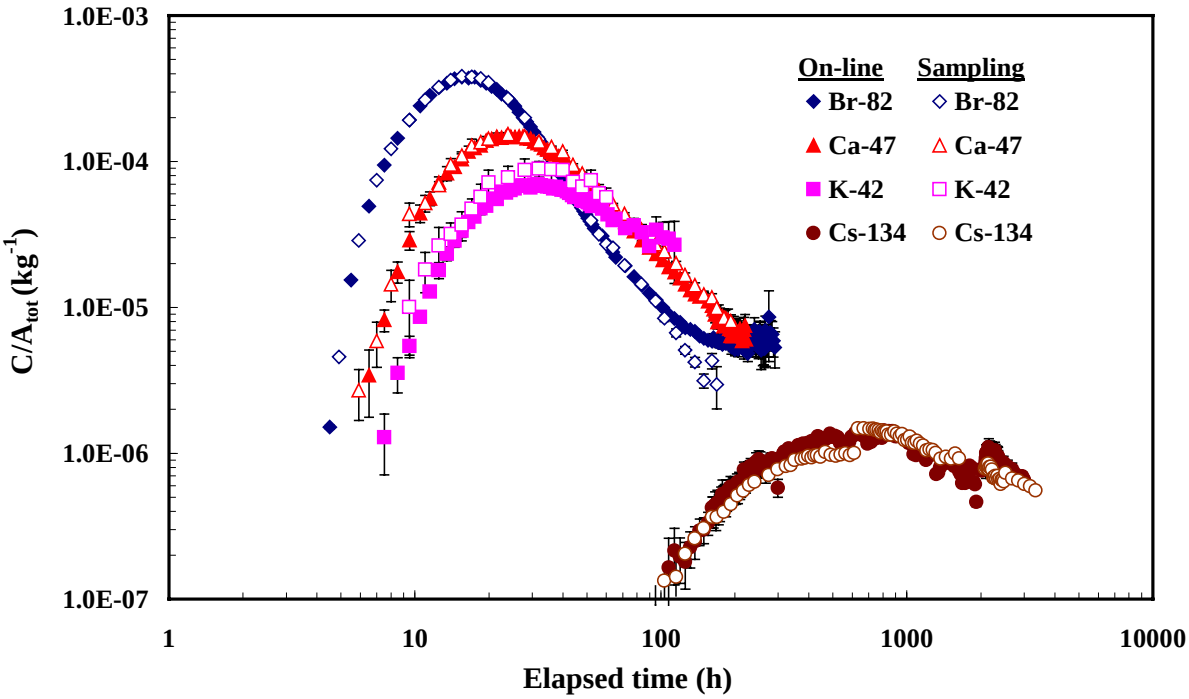

Figure 3-11. *Breakthrough curves for selected tracers used in the flowpath KI0025F03:P5-KI0023B:P6, injection C1. Comparison between on-line measurements and measurements on samples are performed. Error bars represent one standard deviation.*

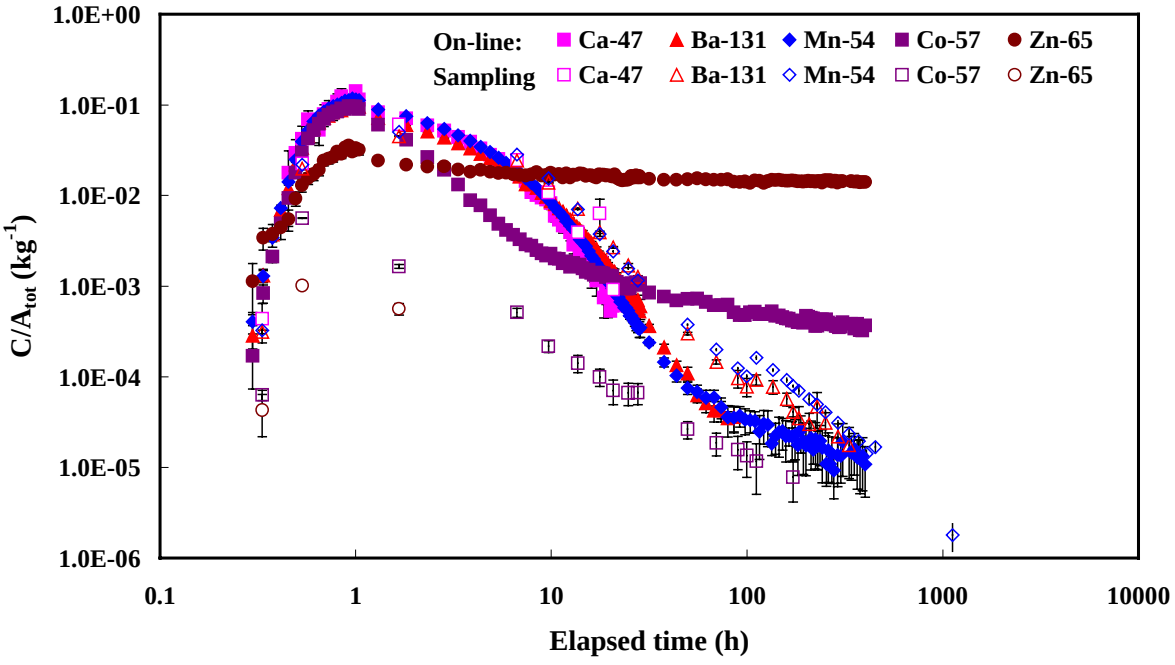

Figure 3-12. *Injection curves for the divalent cationic tracers used in the flowpath KI0025F03:P5-KI0023B:P6, injection C4. Comparison between on-line measurements and measurements on samples are performed. Error bars represent one standard deviation.*

3.6 Numerical modelling and analytical interpretation

The breakthrough curves from test C1 - C4 were evaluated using the model described in Chapter 2.4. The results of the modelling are presented in Tables 3-11 through 3-14. In the modelling, each sorbing tracer breakthrough curve has been fitted together with the results of simultaneously injected conservative tracer, two by two but also up to four tracers simultaneously. Additionally, calibration calculations have also been performed using only the data for the conservative tracers. The model fits are shown in Figures 3-13 through 3-15 (one example for each flow path) and also in Appendix 4.

The simulations included two basic cases. In the first case the A-parameter was fixed to the laboratory data for the conservative tracer, i.e., the diffusivity and the porosity was fixed. A value on the A-parameter of 82400 was chosen based on laboratory experiment using Äspö diorite (Byegård et al. 1998), giving a formation factor, F, equal to $6 \cdot 10^{-5}$ ($D_e = D_w \cdot F$, where D_e is the effective diffusivity and D_w is the diffusivity in water), ε=0.004, and an equivalent fracture aperture, δ, arbitrarily set to 4 mm. Accordingly with the definition of a conservative tracer, the retardation coefficient, R_a, was set to 1. In the fittings, The following parameters were thus used for the fitting procedure:

- the A-parameter for the sorbing tracer
- the retardation coefficient, R_a for the sorbing tracer
- the mean transport time (t_m), same value for both tracers
- the dispersivity, Peclet number (Pe), same value for both tracers
- the proportionality factor (pf), same value for both tracers

A special case was also run where pf was estimated to study the variation of this parameter.

A total number of 5 to 13 fitting parameters were used for the fitting of two to four data sets. In the case where only the data for the conservative tracer was used, only the three latter parameters were varied in order to fit the data, i.e., three free parameters for one data set.

The second basic case was performed as described above, with the exception that the A-parameter for the conservative tracer was also used as a fitting parameter. This implied that the diffusivity and the porosity were not fixed by the laboratory data as was done in the first case. Estimation of the A-parameter was only done for a selection (1-3) of the sorbing tracers in each test.

A comparison between the two different modelling procedures shows that when both A-parameters are estimated, significant matrix diffusion can be applied to the conservative tracer quite contrary to what is assumed when the modelling is performed with a fixed and very high A-parameter for the conservative tracer. The fits are also generally better. This indicates the influence of a diffusion-like process which is further discussed in Chapter 4.

When comparing the different flow paths a difference can be seen, not only in mean travel time and dispersivity, but also in the A-parameter. The flow path KI0025F03:P5 - KI0023B:P6 (Tests C1 and C4) is fast with a low dispersivity and quite low A-parameter values, which implies high matrix diffusion. The flow path used in Test C2, KI0025F03:P7 - KI0023B:P6, is slower, has a higher dispersivity and also higher

A-parameters which implies lower matrix diffusion. The third flow path, KI0025F02:P3 - KI0023B:P6 (the only passive injection), is the slowest one with the highest dispersivity and also the highest A-parameters resulting in the lowest matrix diffusion of the three flow paths tested during Phase C. It should be noted that the C3 flow path only was modelled with a fixed A-parameter.

The mean travel times and Peclet numbers are derived from the modelling of the non-sorbing tracer and should in principle be the same for all simulations of a particular flow path. However, as can be seen in Tables 3-11 through 3-13, some variations occur as each simulation run includes different data sets. The difference is especially obvious when comparing the different runs of the conservative tracers Br and I in Table 3-11. Including the A parameter for the conservative tracers means that matrix diffusion accounts for some of the spreading and delay of the curve that was accounted for by advection/dispersion in the fixed case, i.e. the mean travel time gets shorter and the Peclet number increases.

The standard errors (uncertainties) for the mean travel times and Peclet numbers are in general low (except for Test C2 when estimating both A-parameters) while the errors for the retardation factors (*R*) and the A-parameters are considerably higher. In general, the fits were the A-parameter is fitted for both sorbing and non-sorbing tracers are better in terms of correlation coefficient but more uncertain (non-unique) as the number of fitting parameters are increased by one (six instead of five).

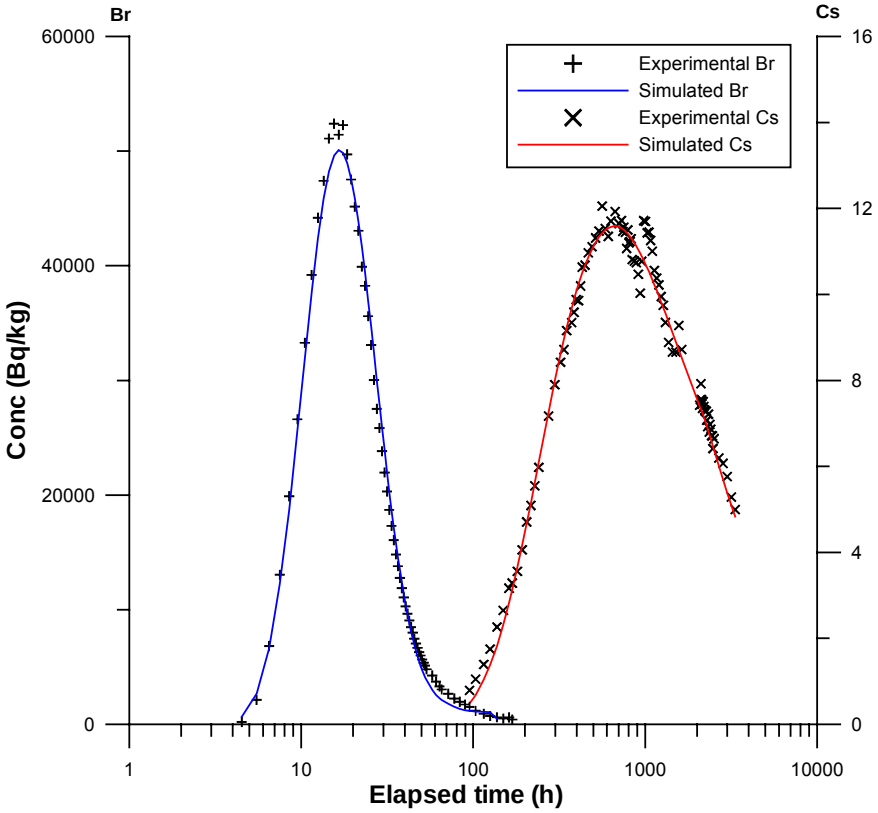

Figure 3-13. *Simultaneous model fit of Br and Cs in test C1 (flow path KI0025F03:P5 - KI0023B:P6).*

Table 3-11. Evaluated parameters for the tracers in Tests C1 and C4 (KI0025F03:P5 - KI0023B:P6 using PAREST (advection-dispersion-sorption-matrix diffusion model). Simultaneous fits of one conservative and one to four sorbing tracers. Values within brackets are standard errors in percent.

Run no.	Tracers	t_m (h)	Pe	D/v* (m)	D/v** (m)	Pf ($\cdot 10^{-3}$)	R_a	A ($s^{1/2}$)
C1								
1:1	$^{82}Br^-$	18.0 (1)	6.0 (3)	2.3	2.7	14.5	1 (fixed)	82400 (fixed)
1:2	$^{82}Br^-$	18.0 (1)	6.0 (2)	2.3	2.7	14.5	1 (fixed)	82400 (fixed)
	$^{24}Na^+$						1.1 (5)	820 (38)
1:3	$^{82}Br^-$	18.0 (1)	6.0 (2)	2.3	2.7	14.5	1 (fixed)	82400 (fixed)
	$^{86}Rb^+$						5.3 (48)	280 (61)
1:4	$^{82}Br^-$	18.0 (1)	6.0 (2)	2.3	2.7	14.5	1 (fixed)	82400 (fixed)
	$^{134}Cs^+$						15.6 (22)	200 (25)
1:5	$^{82}Br^-$	14.6 (1)	8.5 (2)	1.6	1.9	16.2	1 (fixed)	760 (4)
	$^{134}Cs^+$						6.4 (27)	65 (28)
1:6	^{82}Br	14.6 (1)	8.5 (2)	1.6	1.9	16	1 (fixed)	744 (3)
	$^{24}Na^+$						1.08 (2)	349 (7)
	$^{86}Rb^+$						3.8 (22)	144 (25)
	$^{134}Cs^+$						6.4 (22)	65 (22)
1:7	^{82}Br	14.6 (1)	8.6 (1)	1.6	1.9	16 (0.4)	1 (fixed)	735 (3)
	$^{24}Na^+$					17 (3)	1.05 (2)	292 (10)
	$^{86}Rb^+$					17 (13)	3.3 (45)	118 (57)
	$^{134}Cs^+$					14 (5)	10 (18)	115 (21)
C4								
4:1	$^{131}I^-$	20.4 (5)	4.1 (12)	3.4	3.9	18.9	1(fixed)	82400 (fixed)
4:2	$^{131}I^-$	20.4 (2)	4.1 (5)	3.4	3.9	18.8	1(fixed)	82400 (fixed)
	$^{47}Ca^{2+}$						1.4 (12)	380 (28)
4:3	$^{131}I^-$	20.4 (3)	4.1 (8)	3.4	3.9	18.4	1(fixed)	82400 (fixed)
	$^{131}Ba^{2+}$						2.1 (9)	210 (13)
4:4	$^{131}I^-$	18.7 (4)	5.1 (10)	2.7	3.1	20.6	1(fixed)	82400 (fixed)
	$^{54}Mn^{2+}$						10.2 (10)	300 (13)
4:5	$^{131}I^-$	13.9 (7)	8.2 (13)	1.7	2.0	19.8	1(fixed)	500 (20)
	$^{131}Ba^{2+}$						1.4 (12)	85 (18)
4:6	$^{131}I^-$	16.5 (5)	7.5 (11)	1.9	2.1	20	1 (fixed)	905 (26)
	$^{47}Ca^{2+}$						1.2 (19)	205 (33)
	$^{131}Ba^{2+}$						1.8 (9)	139 (13)
	$^{54}Mn^{2+}$						7.1 (9)	187 (13)
4:7	$^{131}I^-$	16.6 (4)	7.5 (9)	1.9	2.1	21 (3)	1 (fixed)	870 (22)
	$^{47}Ca^{2+}$					19 (12)	1.2 (18)	236 (39)
	$^{131}Ba^{2+}$					16 (3)	2.1 (7)	205 (13)
	$^{54}Mn^{2+}$					21 (2)	7.1 (7)	187 (10)

* D/v calculated using the Euclidean distance, 14 m.
** D/v calculated using the distance along interpreted deterministic structures, 16 m.

Table 3-12. Evaluated parameters for the tracers in test C2 (KI0025F03:P7 - KI0023B:P6) using PAREST (advection-dispersion-sorption-matrix diffusion model). Simultaneous fit of Re and Ca, with and without a fixed A-parameter. Values within brackets are standard errors in percent.

Run no.	Tracers	t_m (h)	Pe	D/v* (m)	D/v** (m)	Pf ($\cdot 10^{-3}$)	R_a	A ($s^{1/2}$)
C2 2:1	$^{186}ReO_4^-$	282 (4)	4.1 (6)	4.2	24	3.8	1 (fixed)	82400 (fixed)
2:2	$^{186}ReO_4^-$	280 (3)	4.1 (5)	4.1	23	3.8	1 (fixed)	82400 (fixed)
	$^{47}Ca^{2+}$						2.4 (4)	1200 (9)
2:3	$^{186}ReO_4^-$	274 (49)	3.9 (52)	4.3	25	6.4	1 (fixed)	1320 (146)
	$^{47}Ca^{2+}$						1.7 (25)	390 (84)

* D/v calculated using the Euclidean distance, 17 m.
** D/v calculated using the distance along interpreted deterministic structures, 97 m.

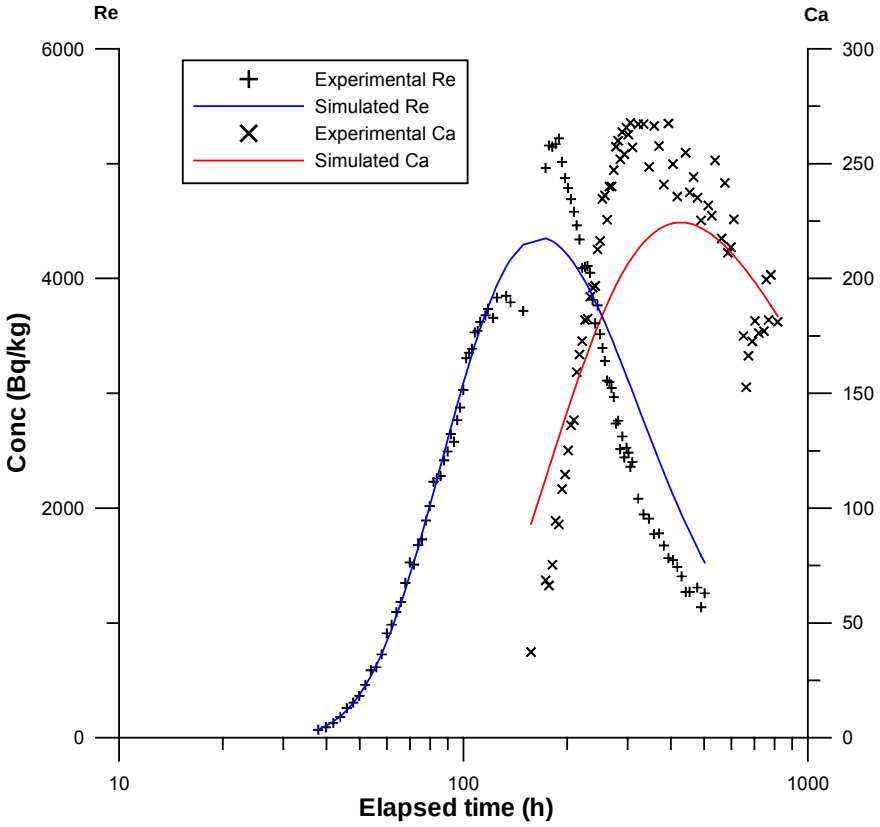

Figure 3-14. *Comparison of measured and simulated breakthrough of $^{186}ReO_4^-$ and $^{47}Ca^{2+}$ from test C2, flow path KI0025F03:P7 - KI0023B:P6. Simultaneous run of Re and Ca, A-parameters estimated for both tracers*

Table 3-13. Evaluated parameters for the tracers in test C3 (KI0025F02:P3 - KI0023B:P6) using PAREST (advection-dispersion-sorption-matrix diffusion model). Simultaneous fit HTO and one to two sorbing tracers. Values within brackets are standard errors in percent.

Run no.	Tracers	t_m (h)	Pe	D/v (m)	pf ($\cdot 10^{-3}$)	R_a	A ($s^{1/2}$)
C3 3:1	HTO	514 (2)	3.7 (5)	9.0	0.85	1 (fixed)	82400 (fixed)
3:2	HTO $^{22}Na^+$	562 (2)	3.1 (4)	10.6	0.90	1 (fixed) 1.7 (2)	82400 (fixed) 7510 (18)
3:3	HTO $^{85}Sr^{2+}$	521 (2)	3.6 (4)	9.2	0.85	1 (fixed) 3.2 (3)	82400 (fixed 3530 (11)
3:4	HTO $^{22}Na^+$ $^{85}Sr^{2+}$	432 (11)	4.1 (15)	8.0	1.11	1 (fixed) 1.8 (2) 3.5 (4)	2413 (36) 2320 (31) 2051 (25)

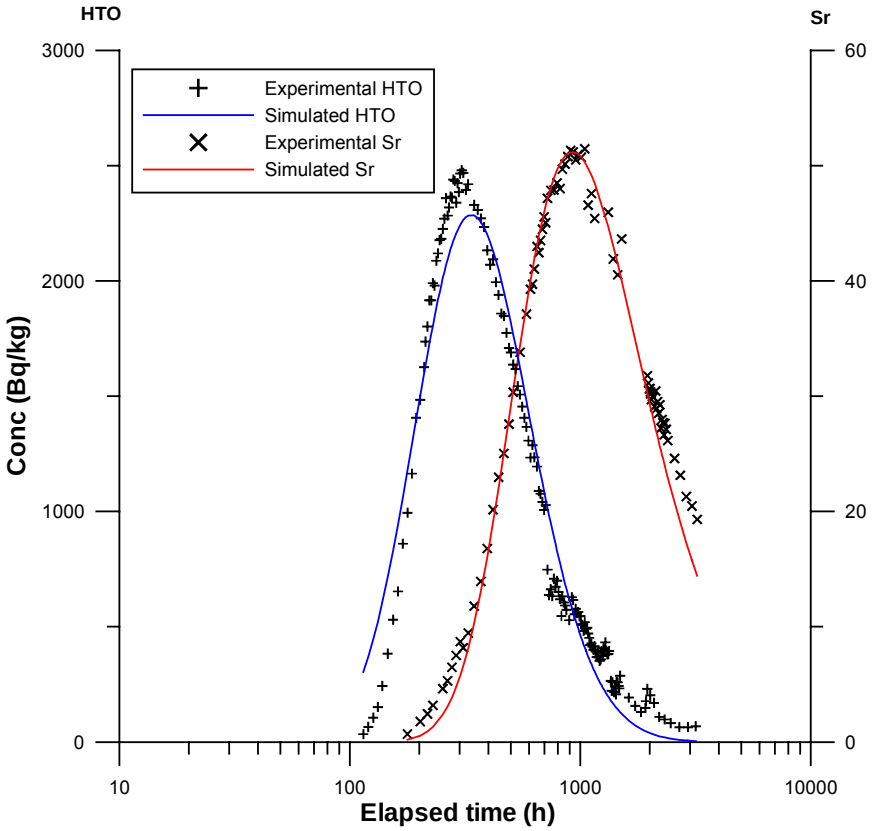

Figure 3-15. *Comparison of measured and simulated breakthrough of HTO (Tritiated water) and $^{85}Sr^{2+}$ from test C3. Simultaneous run of HTO and Sr, A-parameter fixed for HTO.*

The transport parameters derived from the numerical modelling and the analytical expressions described in Chapter 2.4 are presented in Table 3-14. There are two different distances for each flow path presented, the Euclidean distance, which is the shortest geometrical distance, and the distance calculated along the interpreted deterministic structures of the hydrostructural model, which in general is longer. Both distances are quite similar for flow paths KI0025F03:P5 - KI0023B:P6 (C1) and KI0025F02:P3 - KI0023B:P6 (C3). For flow path KI0025F03:P7 - KI0023B:P6 (C2) on the other hand, the difference is rather large, the Euclidean distance is 17 m and the distance along structures is 97 m, cf. Figure 1-1. Since the distance is used in calculations of some of the parameters presented in Table 3-14, these parameters also differ quite a lot depending on the distance used. In accordance with earlier performed tests and evaluations within the TRUE-project the distance used in the calculations is the Euclidean distance.

The transport parameters derived from a combination of numeric modelling and using analytical expressions (Table 3-14) are generally consistent with values determined in earlier stages of the project (Pre-Tests and Phases A and B). The only striking difference is the mean travel time obtained in C3 (514 hours) being significantly longer than the one obtained in PT-4 (140 hours) although the difference in pumping rate is only about 30% (Andersson et al., 2001). The explanation for this is that the mean travel time is a model parameter determined on the basis of existing data. In the case of PT-4 only a very short part of the tail of the breakthrough curve was available resulting in an underestimation of the mean travel time.

Table 3-14. Summary of hydraulic and transport parameters for the flow paths tested in Tests C1 - C4 using KI0023B:P6 as sink. The length used in the calculations is the Euclidean distance. Values within brackets are standard errors in percent.

Parameter	C1 KI0025F03:P5	C2 KI0025F03:P7	C3 KI0025F02:P3	C4 KI0025F03:P5	Source
Distance along structures (m)	16	97	33	16	Geometry
Euclidean distance, *L* (m)	14	17	33	14	Geometry
Mean head difference, Δh (m)	159	171	181	163	HMS
Inj. flow rate (ml/min)	45*	10*	1.8	45*	Injection curve
Mean travel time, t_m (h)	18.0 (1)	282 (4)	514 (2)	16.1 (3)	PAREST
Mean velocity, *v* (m/s)	$2.16 \cdot 10^{-4}$ (1)	$1.68 \cdot 10^{-5}$ (4)	$1.78 \cdot 10^{-5}$ (2)	$2.41 \cdot 10^{-4}$ (3)	PAREST
First arrival, t_a (h)	4.5	38	114	7	Break-through curve
Peclet number, *Pe*	6.0 (3)	4.1 (6)	3.7 (5)	6.7 (7)	PAREST
Dispersivity, *D/v* (m)	2.3 (3)	4.2 (6)	9.0 (5)	2.1 (7)	PAREST
Fracture conductivity, K_{fr} (m/s)	$5.6 \cdot 10^{-5}$	$5.1 \cdot 10^{-6}$	$1.1 \cdot 10^{-5}$	$6.1 \cdot 10^{-5}$	Eq. 2-12
Equivalent fracture aperture, *b* (m)	$3.4 \cdot 10^{-3}$	$3.6 \cdot 10^{-2}$	$1.8 \cdot 10^{-2}$	$3.1 \cdot 10^{-3}$	Eq. 2-13
Flow porosity (1 m thickness)	$1.8 \cdot 10^{-3}$	$2.0 \cdot 10^{-2}$	$9.2 \cdot 10^{-3}$	$1.7 \cdot 10^{-3}$	Eq. 2-14
Mass recovery, *R* (%)	100	80	73	90	Break-through curve

*= induced

A comparison was made between the A-parameters obtained from the modelling and A-parameters calculated from equation 2-12. In the calculation laboratory data on intact unaltered Äspö diorite (Byegård et al., 1998) has been used for the D_e, ε_p and ρ (density of the rock)and these data has been combined with the modelled R_a to yield the A-parameter. The results are presented in Table 3-15. The calculated values of the A-parameter are in general about two orders of magnitude higher than the ones obtained from modelling, which means a significantly enhanced retardation in the flow paths tested compared to what is seen in the laboratory data.

When calculating the A-parameter (Eq. 2-12) the fracture aperture, δ, is used, which in turn is a parameter dependent on the distance (Eq. 2-13). As discussed earlier there are two distances determined for each flow path, the Euclidean distance and the distance along structures. The distance used in the calculations of the parameters presented is the Euclidean distance. For flow path KI0025F03:P7 - KI0023B:P6 in test C2 the length of these two distances differ considerably. Hence, there is also a large difference in the calculated value of the A-parameter for Ca in test C2 depending on the distance used. When using the Euclidean distance the A-parameter is calculated to about 1 823 000 $s^{1/2}$ while it is about 56 000 $s^{1/2}$ if the distance along structures (L=97 m) is used (a factor 32 difference in A-parameter).

Table 3-15. Comparison between A-parameters calculated using a combination of model data (this work) and laboratory data (Byegård et al., 1998), A_{calc}, and A-parameters obtained from the modelling, A_{model}.

Tracer	Test	K_d (m^3/kg)	D_e (m^2/s)	R_{model}	A_{calc} ($s^{1/2}$)	A_{model} ($s^{1/2}$)
HTO	C3	-	$1.2 \cdot 10^{-13}$	1	36 700	82400 (fixed)
Na^+	C1	$1.4 \cdot 10^{-6}$	$6.7 \cdot 10^{-14}$	1.1	119 600	820
	C3			1.7	972 700	7 510
Rb^+	C1	$4 \cdot 10^{-4}$	$1.0 \cdot 10^{-13}$	5.3	27 400	280
Cs^+	C1	$8 \cdot 10^{-4}$	$1.0 \cdot 10^{-13}$	15.6*	57 000	200
				6.4**	19 100	65
Ca^{2+}	C2	$5.2 \cdot 10^{-6}$	$4.0 \cdot 10^{-14}$	2.4*	1 823 000	1 200
				1.7**	1 266 000	390
	C4			1.4	92 200	380
Sr^{2+}	C3	$4.7 \cdot 10^{-6}$	$4.0 \cdot 10^{-14}$	3.2	1 278 000	3 530
Ba^{2+}	C4	$2 \cdot 10^{-4}$	$4.2 \cdot 10^{-14}$	2.1*	21 500	210
				1.4**	10 300	85

* fixed A-parameter for the conservative tracer
** estimated A-parameter for the conservative tracer

Another way of comparing the field and laboratory data are by dividing the A parameter obtained from the modelling into a surface retention parameter (K_a) and a matrix diffusion/retention ($D_e(\varepsilon+K_d \rho)$) part (Equations 2-10 and 2-12). This was first done for the modelling where the A- parameter was fixed to 82400 (i.e., $F=6 \cdot 10^{-5}$, $D_e=D_w \cdot F$, $\varepsilon=0.004$, $\delta=4$ mm). Using the tabulated water diffusivities for the different tracers (D_w), Li and Gregory (1974), the matrix sorption coefficient, K_d, can thus be determined. The results from this concept are given in Table 3-16. The second concept (using the A-parameter for the conservative tracer as a fitting parameters) implies that only a lumped matrix diffusion parameter, $D_e(\varepsilon+K_d \rho)$ is obtained is obtained for each tracers. In this concept, the experimentally obtained fracture aperture (Table 3-14) was used. The results are given in Table 3-17.

It is indicated that the magnitude of the *in situ* retardation (both concerning the matrix diffusion parameters and the surface sorption parameters) is significantly higher than could be expected from the laboratory results based on intact unaltered Äspö diorite. A possible explanation is that the model used in this work, i.e., one that assumes transport taking place in a single parallel plate fracture surrounded by low porous rock, is too simple for describing the real situation of the *in situ* transport. Fracture filling materials (Fault breccia/fault gouge) may be present in and around the structures, and hence an increased amount of rock material for the tracer to interact with. Porosity measurements using water saturation performed within the project (Andersson et al., 2002) have shown higher porosity values for altered wall rock, fault breccia pieces and fault gouge fragments than for fresh rock samples. Heterogeneously distributed porosity, discussed by Byegård et al. (2001), may add heterogeneity to the in situ transport which can not be addressed by the simple model used in this work.

Table 3-16. Retention parameters obtained from preliminary modelling using a fixed A parameter for the conservative tracer. The results compared to corresponding values determined from laboratory experiment (Byegård et al. 1998)

Injection	Tracer	Surface retention parameter, K_a (m)		Matrix sorption coefficient, K_d(m^3/kg)	
		In situ [1]	Lab	*In situ* [2]	Lab
C1	$^{24}Na^+$	$2.0 \cdot 10^{-4}$	$5 \cdot 10^{-6}$	$3.4 \cdot 10^{-2}$	$1.4 \cdot 10^{-6}$
	$^{86}Rb^+$	$8.6 \cdot 10^{-3}$	$1 \cdot 10^{-3}$	4.4	$4 \cdot 10^{-4}$
	$^{134}Cs^+$	$2.9 \cdot 10^{-2}$	$8 \cdot 10^{-3}$	75	$8 \cdot 10^{-4}$
C4	$^{47}Ca^{2+}$	$8.0 \cdot 10^{-4}$	$3 \cdot 10^{-5}$	0.4	$5.2 \cdot 10^{-6}$
	$^{131}Ba^{2+}$	$2.2 \cdot 10^{-3}$	$6 \cdot 10^{-4}$	2.9	$2 \cdot 10^{-4}$
	$^{54}Mn^{2+}$	$1.8 \cdot 10^{-2}$	-	41	-
C2	$^{47}Ca^{2+}$	$2.8 \cdot 10^{-3}$	$3 \cdot 10^{-5}$	0.12	$5.2 \cdot 10^{-6}$
C3	$^{22}Na^+$	$1.4 \cdot 10^{-3}$	$5 \cdot 10^{-6}$	$1.2 \cdot 10^{-2}$	$1.4 \cdot 10^{-6}$
	$^{85}Sr^{2+}$	$4.4 \cdot 10^{-3}$	$2 \cdot 10^{-5}$	$3.1 \cdot 10^{-2}$	$4.7 \cdot 10^{-6}$

1) From Equation (2-10) and (2-11)
2) From Equation (2-12)

Table 3-17. Retention parameters obtained from preliminary modelling using the A-parameter of the conservative tracer as a fitting parameter. The results are compared to corresponding values determined from laboratory experiment (Byegård et al. 1998)

Injection	Fracture aperture [1] (m)	Tracer	Surface retention parameter, K_a (m)		Matrix diffusion retention parameter, $D_e(\varepsilon+K_d\rho)$ (s^{-2})	
			In situ [2]	Lab	*In situ* [3]	Lab
C1	$3.4 \cdot 10^{-3}$	$^{82}Br^-$	-	-	$5.0 \cdot 10^{-12}$	$4.0 \cdot 10^{-16}$
		$^{134}Cs^+$	$9.2 \cdot 10^{-3}$	$8 \cdot 10^{-3}$	$2.8 \cdot 10^{-8}$	$2.2 \cdot 10^{-13}$
C4	$3.1 \cdot 10^{-3}$	$^{131}I^-$	-	-	$9.6 \cdot 10^{-12}$	$4.0 \cdot 10^{-16}$
		$^{131}Ba^{2+}$	$8.4 \cdot 10^{-3}$	$6 \cdot 10^{-4}$	$1.4 \cdot 10^{-8}$	$2.3 \cdot 10^{-14}$
C2	$3.6 \cdot 10^{-2}$	$^{186}ReO_4^-$	-	-	$1.9 \cdot 10^{-10}$	$3.9 \cdot 10^{-16}$
		$^{47}Ca^{2+}$	$1.3 \cdot 10^{-2}$	$3 \cdot 10^{-5}$	$6.2 \cdot 10^{-9}$	$1.8 \cdot 10^{-15}$

1) From Equation (2-13)
2) From Equation (2-10) and (2-11)
3) From Equation (2-12)

3.7 Supporting data

In addition to tracer concentration measurements, some other parameters were also monitored during the Phase C experiment. These parameters were injection and pump flow rates, electrical conductivity and redox potential of the withdrawal water and hydraulic head in both injection and sink boreholes.

The injection flow rate in section KI0025F03:P5 (test C1 and C4) was measured continuously with a flow meter during the test period and the result is shown in Figure 3-16. A lot of disturbances due to problems with the water injection pump occurred during the test period, see also the Log of Events in Appendix 3.

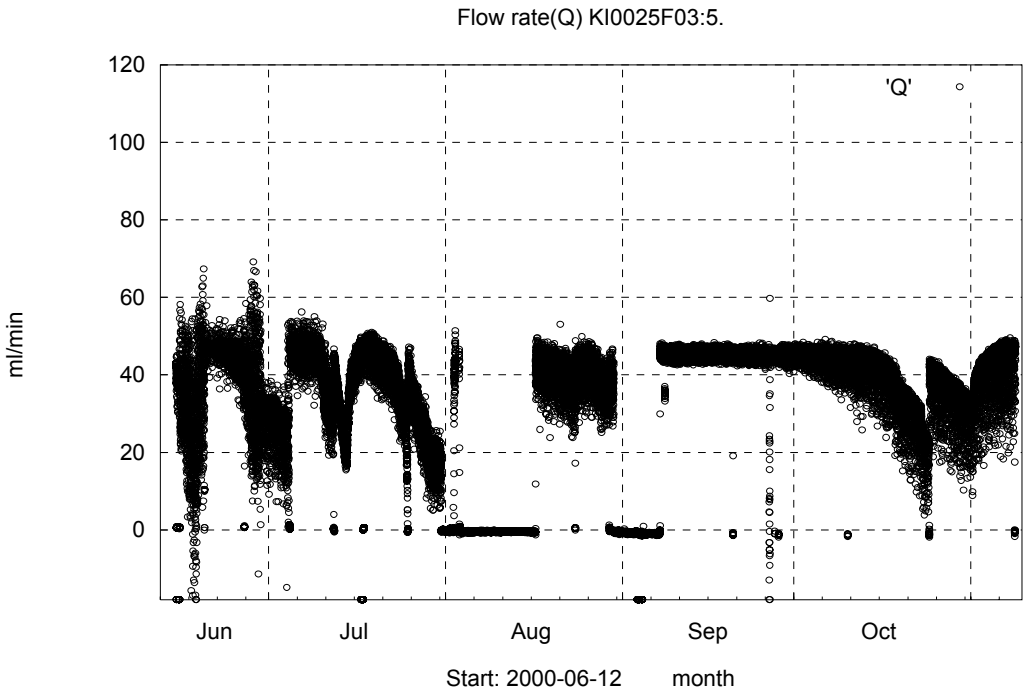

Figure 3-16. *Injection pump flow rate in KI0025F03:P5 during Phase C, June 12th, 2000 to November 8th, 2000.*

The electrical conductivity (EC) and redox potential (Eh) of the withdrawal water were measured continuously in-line during the pumping, see Figure 3-17. The electrical conductivity was stable at around 1500 mS/m during the entire test. The redox potential was decreasing somewhat during the test period, from about -250 mV in the end of June to about -300 mV in the beginning of November.

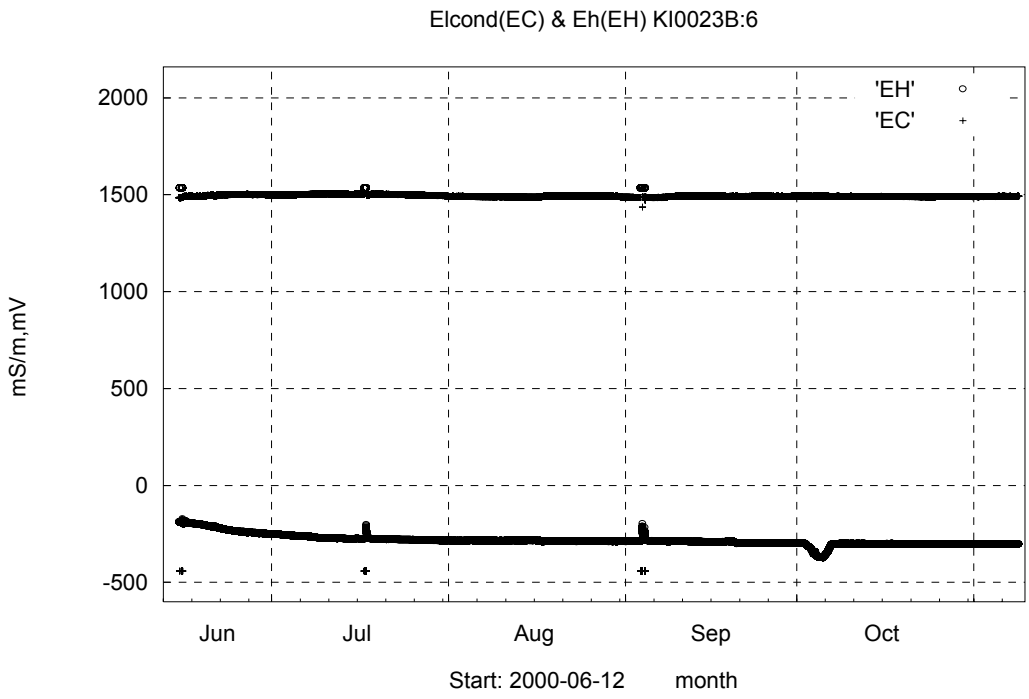

Figure 3-17. *Electrical conductivity, EC, (upper curve) and REDOX potential, EH, (lower curve) of the pumped water in KI0023B:P6 during Phase C, June 12th, 2000 to November 8th, 2000.*

The head variations in the pumping borehole KI0023B during the test period is shown in Figure 3-18. A slight decrease in head during the period can be seen in all sections in borehole KI0023B. The pumping rate in the withdrawal borehole section, KI0023B:P6, was constant during the entire test, 1950 ml/min.

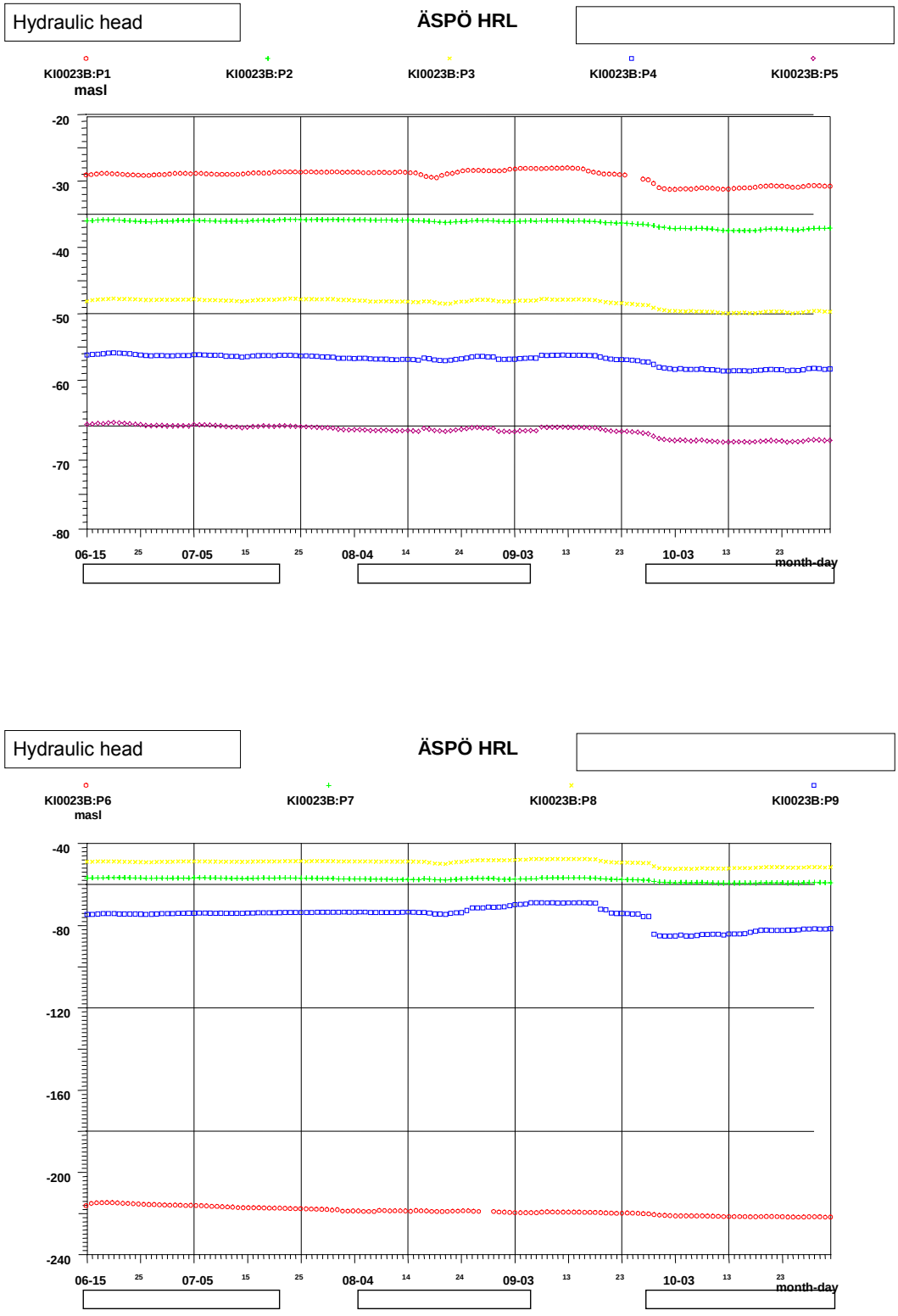

Figure 3-18 *Hydraulic heads in borehole KI0023B during Phase C, June 15th 2000, to November 1st, 2000 (upper graph, sections P1-P5 and lower graph, sections P6-P9).*

4 Conclusions

4.1 Equipment and performance

The TRUE Block Scale Phase C tracer tests have involved four tracer injections using radioactive sorbing tracers in three different source-sink pairs. The selected flow paths and the methodology used has earlier been successfully applied in the Phase B tracer tests (Andersson et al., 2000). The major difference is that radioactive sorbing tracers were introduced which made it necessary to modify some of the field procedures in order to keep the time of exposure for the personnel to the radioactive stock solution to a minimum. Also, tracer detection procedures were changed such that on-line detection of both injection concentration (activity) and breakthrough concentration (activity) was possible. This technique had also earlier been applied in the TRUE-1 experiments (Winberg et al., 2000) with the difference that three injection sections were monitored simultaneously during Phase C.

4.1.1 Selection and detection of tracers

The fact that three source-sink pairs were to be tested more or less simultaneously made it necessary to carefully select tracers to ensure that interference between different tracers were minimised. Optimisation of the radioactive tracers with respect to their half-lives also had to be done; i.e., the most short-lived tracers could only be used for injection in the shortest flow path. Another important criterion for tracer selection was that the retention characteristics should be comparable between the three flow paths. A careful optimisation using different isotopes of the same species and shorter half-lives for the faster flow paths was successfully employed.

One problem occurring in the TRUE-1 experiments was that precipitates were formed on the inner surfaces of the tubing around the HpGe detector, especially on the sampling side, and tracers were sorbed on them, creating a background activity. This problem was solved in TRUE Block Scale Phase C by continuously injecting nitric acid in the sampled water just before its passing of the detector.

The use of longer flow paths and thus, more dilution, and a variety of different tracers also made it necessary to develop special techniques to separate different tracers and to be able to measure very low activities. One method employed was the $CaCO_3$ co-precipitation method used to separate $^{133}Ba^{2+}$ in 12 samples from the C3 injection. The results gave measurements with much lower uncertainty than both the samples and the on-line measurements.

4.1.2 Equipment and procedures

During Phase B it was identified that problems associated with the forced injection procedure could occur. The weak point in the instrumentation was the HPLC plunger pump used to create the injection flow. However, due to a tight time schedule it was not possible to exchange these pumps between the two tests. Consequently, also during the Phase C tests quite a few pump stops occurred although a thorough service schedule was applied (see Appendix 3). During an extended pumping period, after the official ending of the Phase C tests, a new, industrial type of plunger-membrane pump was used. This pump has operated more than 6 months without any problems and will therefore be used in future experiments involving long-term injection.

The use of relatively high injection flow rates in the C1 and C4 injections also created some problems encountered during the evaluation. It was found that flow rates calculated based on tracer dilution were significantly lower than the ones measured by very accurate mass flow meters. The reason for this is that the injection flow rate is relatively large in comparison to the circulation flow rate in the injection loop. This implies that the water injected is not mixed with the whole circulating volume and thus, a lower mass flux of tracer is obtained. This points to the importance of actually measuring the input concentration (which also was done) rather than assuming that the volume is well mixed. For future tests, a better mixing (higher circulation flow rate in the injection loop) is desirable.

4.2 Evaluation procedures

The evaluation of the Phase C tracer tests has involved several new components compared to the "standard" evaluation applied in earlier tracer tests within the TRUE Block Scale Project. The so-called "basic" evaluation has included a relatively simple one-dimensional transport modelling using analytical solutions to the advection-dispersion equation. Phase C has also included sorption and diffusion parameters by fitting the so-called A-parameter which is a lumped parameter including both matrix diffusion and sorption. This model has earlier been used e.g. by Moreno et al (1983) among others. The new approach used in this work was to simultaneously fit the conservative and sorbing tracer breakthrough and thereby decrease the number of free parameters in the fit. The fitting procedure worked well although the number of free parameters and possibilities to vary parameters increased. An important tool in assessing the uniqueness of the model fit to the experimental data was the regression statistics (standard errors and correlation between derived parameters).

Another new evaluation procedure was an attempt to derive surface sorption coefficients by modelling of the measured injection functions. This could be done by assuming that the borehole volume acts like a closed tank and if there is a significant difference in slope of the injection function (concentration versus time) of the conservative reference tracer and the sorbing one. In addition, a non-linear sorption model as well as a model assuming first-order kinetics was used. These evaluation models seem to give reasonable values compared to laboratory data and could be a potential way of getting relatively fast data on sorption characteristics from a single borehole under ambient pressure and chemical conditions. An even better geometry would be to select a portion of the rock without fractures. The latter possibly more relevant to repository long term safety performance assessment.

4.3 Transport in the block scale

4.3.1 Character of flow paths

The three different flow paths tested, injection in KI0025F03:P5, P7 and KI0025F02:P3 are all quite different in character according to the structural model (Hermanson and Doe, 2000). Flow path KI0025F03:P5 – KI0023B:P6 (injection C1 and C4) is characterised as a fast and more or less single structure flow path in Structure #20 whereas KI0025F03:P7 – KI0023B:P6 (injection C2) is characterised as a "network flow path" including at least three structures (#23, 22 and 20). The third flow path KI0025F02:P3 – KI0023B:P6 (injection C3) is characterised as a long single flow path in Structure #21 but results from the Phase B tracer tests (Andersson et al, 2000b) indicate that the character is more like "network path". The geological characterisation of the interpreted structures shows a rather large variation between different intercepts in the boreholes of the array and thus, differences in the transport and retention characteristics could be expected between the different tested flow paths.

4.3.2 Conservative transport

The three flow paths tested in Phase C have also been tested in earlier tracer tests campaigns, in particular during Phase B of the project. The new runs with conservative tracers in Phase C have not changed any of the conclusions from Phase B given in Andersson et al. (2000b). In summary they are:

- Dispersivity varies between 2.1 m for the short flow path KI0025F03:P5 – KI0023B:P6 (16 m) to 9.0 m for the long "single" flow path KI0025F02:P3 – KI0023B:P6 (33 m). The latter high value may be an indirect indication that this flow path actually is longer and more complicated than deduced from the hydro-structural model.

- The transport parameters derived show a significant difference between the fast flow path KI0025F03:P5 – KI0023B:P6 and the two slower ones; about one order of magnitude higher hydraulic conductivity/fracture aperture and about one order of magnitude lower flow porosity.

- Tracer mass recovery is high for all tested flow paths (73-100%).

- The conservative tracer breakthrough curves cannot be fitted well with a simple one-dimensional transport model with advection-dispersion only. Adding matrix diffusion improves the fits significantly.

- The magnitude of the estimated A-parameter (incorporating matrix diffusion and matrix porosity) for conservative tracers is significantly lower (about a factor 1000, indicating stronger retardation) than a value based on laboratory data on matrix porosity and diffusivity. This may be an indication that matrix diffusion and/or matrix porosity is larger than derived from laboratory investigations. However, it should also be noted that similar effects on the shape of the breakthrough curves may be induced by effects of multiple flow paths and/or diffusion into stagnant parts of the flow field. A more elaborate modelling effort is needed to clarify this issue.

4.3.3 Retention

The results show both similarities and differences when compared to the TRUE-1 tracer tests. Firstly, the order of retention between the different species is the same as in TRUE-1 and in the laboratory tests, i.e. $Na^+ < Ca^{2+} < Sr^{2+} < Ba^{2+} < Rb^+ < Cs^+$. Another similarity is that the retardation, expressed as the ratio of time at which 50% of the sorbing tracer was recovered compared to the conservative tracer ($R_{50\%}$), is about the same for most species when comparing TRUE-1 to the results of injection C1 and C4 in Structure #20, c.f. Table 4-1. However, for the breakthroughs of sorbing tracers in C2 and C3 (Na^+ and Sr^{2+} in C3 and Ca^{2+} in flow path C2) a 20-60% stronger retardation (expressed as $R_{50\%}$) is obtained. The reasons for this enhanced retardation between the two fast single flow paths (in the same source-sink pair) and the two slower and more complicated flow paths may be several different such as:

- Presence of gouge material in the structures
- Presence of gouge material in fracture intersection zones
- Differences in the mineralogy
- Larger portions of stagnant water along the flow path to interact with
- Higher porosity in the fracture rim zone

A more elaborate modelling effort including various modelling concepts (fracture network, channel network, etc.) is ongoing as a part of the TRUE Block Scale Project and will be added to this initial "basic" evaluation. A special effort is also made to study if fracture intersection zones (FIZ) are critical for the transport in fracture networks.

The cations Mn^{2+}, Co^{2+}, and Zn^{2+} injected in the fastest flow path (injection C4) were injected to study possible effects of other retention mechanisms such as partial hydrolysis and surface complexation. The results show a very strong sorption of Zn already in the injection equipment and no breakthrough in the sampling borehole. Also Co is sorbed in the injection equipment but a delayed breakthrough could be monitored (retardation factor >100). The strong sorption on equipment and in the rock indicates that other retention mechanisms than ion exchange are active. Also Mn is strongly retarded although not as strong as Co. Only a minor portion of the injected mass of Co and Mn could be recovered at the end of the sampling period and it is difficult to draw conclusions regarding limited reversibility of the sorption mechanisms for these tracers.

Table 4-1. Retardation factors based on recovery, $R_{50\%}$, (unless other specification) for the different TRUE-1 tests (Winberg et al. 2000) and the TRUE Block Scale tests C1-C4. The notation t_{50ref} refers to the elapsed time when 50% recovery was obtained for the conservative tracers. In cases when the recovery of the sorbing tracer was less than 5%, a minimum mass recovery is estimated from the last sampling time. The notation n.b. means no breakthrough

	TRUE-1 Detailed scale			*TRUE Block Scale*		
	STT1	**STT1b**	**STT2**	**C1/C4**	**C2**	**C3**
Tracer	r=4.7m t_{50ref}=36h	r=5,1m t_{50ref}=11h	r=4.7m t_{50ref}=79h	r=14 (16)m t_{50ref}=20h	r=17 (97)m t_{50ref}=260h	r=33 (>33)m t_{50ref}=820h
Uranine	Ref [1)]	Ref [1)]	Ref [1)]			
Br^-		1.03 [2)]	1.1	Ref [1)]		
I^-		1.03 [2)]				
ReO_4^-					Ref [1)]	
HTO	1.1	1.04 [2)]	1.2			Ref [1)]
Na^+	1.4	1.5	1.5	1.4		1.8
K^+		1.9 [2)]		5.1		
Ca^{2+}	1.2 [2)]		1.9	2.3	4.1 [3)]	
Sr^{2+}	1.8	3.2	2.4			3.6
Rb^+	9	20	15	20		>23 [4)] n.b.
Ba^{2+}	5		12	13	>20 [4)] n.b.	>25 [4)] n.b.
Cs^+	230 [3)]		130 [4)]	250	>56 [4)] n.b.	
Mn^{2+}				50		
Co^{2+}		300 [3)]		>390 [4)]		
Zn^{2+}				>390 [4)] n.b.		

[1)] Used as reference tracer, i.e., the tracer in relation to which the retardation factors have been calculated.

[2)] R_{peak}

[3)] $R_{25\%}$

[4)] $R_{5\%}$

5 References

Andersson K., 1983: Transport of radionuclides in water/mineral systems. Diss. Chalmers University of Technology, Göteborg, Sweden.

Andersson P., 1996: TRUE 1st stage Tracer Test Programme. Experimental data and preliminary evaluation of the TRUE-1 radially converging tracer test (RC1). Äspö HRL Progress Report HRL-96-24.

Andersson P., Ludvigson J-E., Wass E., Holmqvist M., 2000a: TRUE Block Scale Project Tracer Tests Stage. Interference tests, dilution tests and tracer tests, Phase A. Äspö Hard Rock Laboratory International Progress Report IPR-00-28.

Andersson P., Wass E., Holmqvist M., **Fierz T., 2000b:** TRUE Block Scale Project Tracer Tests Stage. Tracer tests, Phase B. Äspö Hard Rock Laboratory International Progress Report IPR-00-29.

Andersson P., Ludvigson J-E., Wass E., Holmqvist M., 2001: Detailed Characterisation Stage – Interference tests and tracer tests PT-1 – PT-4. Swedish Nuclear Fuel and Waste Management Company, Äspö Hard Rock Laboratory. International Progress Report IPR-01-52.

Andersson P., Byegård J., Winberg A. 2002 : Final report of the TRUE Block Scale Project - 2, Tracer tests in the block scale. SKB Technical Report TR-02-14.

Byegård J., Widestrand H., Skålberg M., Tullborg E.L., Siitari-Kauppi M., 2001. First TRUE Stage – Complementary investigation of diffusivity, porosity and sorptivity of Feature A-site specific geologic material. SKB International Cooperation Report ICR-01-04

Byegård J., Johansson H., Skålberg M., Tullborg E-L., 1998: The interaction of sorbing and non-sorbing tracers with different Äspö rock types. SKB TR-98-18. ISSN 0284-3757.

Heer W., Hadermann J., 1994: Grimsel test site: Modelling radionuclide migration field experiments. NAGRA Technical Report 94-18, National Cooperative for the Disposal of Radioactive Waste, Wettingen, Switzerland.

Hermanson J., Doe T., 2000: TRUE Block Scale Project Tracer test stage. March'00 structural and hydraulic model based on borehole data from KI0025F03. SKB International Progress Report IPR-00-34.

Gustafsson E., Klockars C-E., 1981: Studies of groundwater transport in fractured crystalline rock under controlled conditions using non-radioactive tracers. Swedish Nuclear Fuel and Waste Management Company. SKBF/KBS Technical Report TR 81-07.

Li Y.H., Gregory S., 1974: Diffusion of ions in sea water and in deep sea sediments. Geochim. Cosmochim. Acta 38, 703-714.

Moreno L., Neretnieks I., Klockars C-E., 1983: Evaluation of some tracer tests in the granitic rock at Finnsjön. SKBF/KBS Teknisk Rapport 83-38.

Moye D.G., 1967: Diamond drilling for foundation exploration. Civil Eng. Trans., Inst. Eng. Australia (Apr. 1967), 95-100.

Nordqvist R., 1994: Documentation of some analytical flow and transport models implemented for use with PAREST - Users manual. GEOSIGMA GRAP 94 006, Uppsala.

Poteri A., Billaux D., Cvetkovic V., Dershowitz B., Gómez-Hernández J-J., Hautojärvi A., Holton D., Medina A., Winberg A., 2002. TRUE Block Scale Project Final Report -3. Modellig of flow and transport. SKB Technical Report TR-02-15 (in prep.).

Skagius K., Svedberg G., Neretnieks I., 1982: A study of strontium and cesium sorption on granite. Nucl. Techn. 59, 302-313.

Tang G.H., Frind E.O., Sudicky E.A., 1981: Contaminant transport in fractured porous media. An analytical solution for a single fracture. Water Resources Research, Vol 17, p. 555.

Winberg A., Andersson P., Hermanson J., Byegård J., Cvetkovic V., Birgersson L., 2000: Äspö Hard Rock Laboratory. Final report of the first stage of the tracer retention understanding experiments. SKB Technical Report TR-00-07.

Winberg A. (ed), 2000: TRUE Block Scale Project. Final report of the detailed characterisation stage. Compilation of premises and outline of programme for tracer tests in the Block Scale. SKB International Cooperation Report ICR 00-02.

Winberg A., 1997: Test plan for the TRUE Block Scale Experiment. Äspö HRL International Cooperation Report ICR 97-02.

APPENDIX 1: Production/deliveries of radioisotopes

Preparation of the stock solutions

Productions of radionuclides

The radioisotopes used as tracers are described in Table 1 in terms of the productions and the specific activities used. Several of the radioisotopes used were available from commercial suppliers e.g., Amersham, NEN and Los Alamos National Laboratory (LANL). The tracers that were not commercially available were produced by neutron irradiation at the research reactor at Studsvik Nuclear AB (neutron flux ≈ $2 \cdot 10^{14}$ n/cm/s, 24 h irradiation time followed by an immediate transport of the radioisotopes to Äspö). The only exception to this was $^{133}Ba^{2+}$ which was produced by irradiation at the Kjeller reactor, Norway (neutron flux ≈ $1 \cdot 10^{13}$ n/cm/s, 14 d irradiation time). In all the irradiations of Ba, isotope enrichments were used in order to obtain a sufficient specific activity of the tracers. For the irradiations of Ca, isotope enrichments were used in order to favour the production of the wanted isotope ^{47}Ca and to minimise the production of the not wanted isotope ^{45}Ca ($t_{½}$=163 d, no measurable γ-radiation).

Preparation of the stock solutions

The preparations of the stock solutions were performed in the following way:

1. The irradiated chemicals were dissolved in 2.7 ml 37 % HCl.

2. Additions of appropriate aliquots from the stock solutions of the commercially available radioisotopes were performed.

3. Salts (according to Table 3) were dissolved in a separate batch of 100 ml of deionised water. When the salts had dissolved, the solution was passed through a 0.45 μm syringe filter and was transferred to the acidified solution with the radioisotopes.

4. The fluorescent dye tracer (2 g Uranine in injection C1, 8 g Naphtionate in injection C2) was dissolved in a separate batch of 100 ml of deionised water. The solution was filtered (as described above) and was transferred to the acidified solution with the radioisotopes.

5. 1.2 g of NaOH were dissolved in a separate batch of 100 ml of deionised water and the solution was passed through a 0.45 μm syringe filter. The solution was slowly added to the acidified solution with the radioisotopes until a neutral pH (~7) was obtained.

6. Deionised water was added to reach a weight of 400 g of the total solution.

7. 4x0.2 ml aliquots were sampled from the stock solution and were used for the measurement of the total injected mass/activity.

During paragraph 4, precipitations were obtained in the solution, probably because of the formation of the protonated forms of Uranine and Naphtionate, respectively. In the case of Uranine, the precipitation dissolved completely during the addition of NaOH. The precipitation of Naphtionate did not completely dissolve, so a filtration of the whole stock solution was performed. Coarse measurements of the radiation dose rate of the filters after the filtration showed that only negligible parts of the added radioisotopes were found in the filter.

Table 1. Specifications of the radioactive tracers used in the experiment, i.e, information about the irradiated tracers and radionuclides delivered by commercial radioisotope suppliers.

Tracer	Produced/ *Delivered by*	Irradiated material/ Specific activity	Isotope enrichment	Chemical purity	Injected activity (MBq)
C1					
$^{82}Br^-$	Irr: $^{81}Br(n,\gamma)$	0.3 mg KBr (Aldrich)	-	99.5 %	138±1
$^{24}Na^+$	Irr: $^{23}Na(n,\gamma)$	0.1 mg NaCl (Aldrich)	-	99.5 %	15.6±0.6
$^{42}K^+$	Irr: $^{41}K(n,\gamma)$	13.3 mg K_2CO_3 (Aldrich)	-	99.999 %	229±10
$^{47}Ca^{2+}$	Irr: $^{46}Ca(n,\gamma)$	2.8 mg $CaCO_3$ (Isoflex)	4.1 % ^{46}Ca	-	10.7±0.3
$^{86}Rb^+$	Amersham	100 MBq/mg	-	-	13.3±0.7
$^{134}Cs^+$	Risö	*500 000 MBq/mg*	-	-	7.79±0.08
C2					
$^{186}ReO_4^-$	Irr: $^{185}Re(n,\gamma)$	0.05 mg $KReO_4$ (Aldrich)	-	99.99 %	171±2
$^{47}Ca^{2+}$	Irr: $^{46}Ca(n,\gamma)$	22 mg $CaCO_3$ (Isoflex)	4.1 % ^{46}Ca	-	56.4±0.5
$^{131}Ba^{2+}$	Irr: $^{130}Ba(n,\gamma)$	0.3mg $Ba(NO_3)_2$ (ORNL)	38 % ^{130}Ba	99.96 %	25.7±0.3
$^{137}Cs^+$	Amersham	1000 MBq/mg	-	-	23.5±0.1
C3					
HTO	Amersham	*Carrier free*	-	-	244±7
$^{22}Na^+$	*LANL*	*Carrier free*	-	-	21.6±0.2
$^{85}Sr^{2+}$	*NEN*	*170 MBq/mg*	-	-	22.1±0.2
$^{83}Rb^+$	*LANL*	*Carrier free*	-	-	45.9±0.3
$^{133}Ba^{2+}$	Irr: $^{132}Ba(n,\gamma)$	5 mg $Ba(NO_3)_2$ (ORNL)	22 % ^{132}Ba	99.96 %	0.55±0.03
C4					
$^{82}Br^-$	Irr: $^{81}Br(n,\gamma)$	0.3 mg KBr (Aldrich)	-	99.5 %	11.4±0.3
$^{131}I^-$	*Amersham*	*Carrier free*	-	-	9.8±0.3
$^{47}Ca^{2+}$	Irr: $^{46}Ca(n,\gamma)$	2.8 mg $CaCO_3$ (Isoflex)	4.1 % ^{46}Ca	-	1.9±0.2
$^{131}Ba^{2+}$	Irr: $^{130}Ba(n,\gamma)$	0.7mg $Ba(NO_3)_2$ (ORNL)	38 % ^{130}Ba	99.96 %	65.1±0.8
$^{54}Mn^{2+}$	*NEN*	*Carrier free*	-	-	71.1±0.5
$^{57}Co^{2+}$	*Amersham*	*Carrier free*	-	-	28.9±0.2
$^{65}Zn^{2+}$	*NEN*	>5 MBq/mg	-	-	20.0±0.5

Table 2 . Groundwater composition used in the preparation of the synthetic groundwater in the injections. The compositions are based on the measurement of a groundwater sampled in KI0023B 71-72m 990407 (Andersson and Säfvestad, 1999). The concentration of Rb^+, Cs^+ and Ba^{2+} were obtained from the measurements of the TRUE-1 groundwater (Nilsson 1997).

Cation	Conc. (mg/l)	Anion	Conc. (mg/l)
Li^+	0.77	Cl^-	5360
Na^+	1930	Br^-	29
Mg^{2+}	44.5	SO_4^{2-}	334
K^+	7.5	HCO_3^-	27
Ca^{2+}	1289	Si	6.4
Rb^+	0.055		
Sr^{2+}	16.9	pH	7.8
Cs^+	0.005		
Ba^{2+}	0.080		

Table 3 . The amounts of the different chemicals used in order to prepare the synthetic groundwater according to the composition given in Table 2.

Chemical	Amount added
HCl (37%)	2.7 ml
$CaCl_2 \cdot 2H_2O$	1.90 g
Na_2SO_4	0.197 g
$MgCl_2 \cdot 6H_2O$	0.149 g
Na_4SiO_4	0.017 g
$SrCl_2 \cdot 6H_2O$	0.021 g
NaBr	0.015 g
$NaHCO_3$	0.015 g
KCl[1)]	0.006 g
LiCl	0.002 g
$BaCl_2 \cdot 2H_2O$[2)]	0.02 mg
RbCl[3)]	0.03 mg
CsCl[4)]	0.002 mg
NaOH[5)]	1.2 g

[1)] In injection C1, replaced by the irradiated K_2CO_3.
[2)] In injections C2, C3 and C4, replaced by the irradiated $Ba(NO_3)_2$.
[3)] In injection C1, replaced by the ^{86}Rb radioisotope.
[4)] In injection C2, replaced by the ^{137}Cs radioisotope.
[5)] Added until a neutral pH was reached.

APPENDIX 2: Di-valent metal ions as tracers, adressing hydrolysis and surface complexation as sorption mechanism

Divalent transition metals

By the use of divalent transition metals as tracers in the TRUE Block Scale experiment, sorption mechanisms of partly hydrolysed cations and surface complexation is addressed.

Hydrolysis

Hydrolysis of a divalent cation can be described as:

$$M^{2+} + nH_2O \Leftrightarrow M(OH)_n^{(2-n)+} + nH^+ \quad (1)$$

where the stability constant, β_n^*, is defined as:

$$\beta_n^* = \frac{\left[M(OH)_n^{(2-n)+}\right]\left[H^+\right]^n}{\left[M^{2+}\right]} \quad (2)$$

It is known from the literature that cations influenced by hydrolysis are stronger sorbed in geological systems. James and Healy (1972) studied the pH-dependence on the sorption of some cations on SiO_2 and found a strong correlation between hydrolysis and sorption. They furthermore found that the sorption dominated already at pH´s 1-2 units before the hydrolysis was predominating. In a study of the sorption of Co^{2+} on TiO_2, Jakobsson and Albinsson (1998) found that the dominating sorption reaction of Co^{2+} was the surface complexation reaction of:

$$\equiv SOH + Co^{2+} + H_2O \leftrightarrow \equiv SOHCo(OH)^+ + H^+ \quad (3)$$

They furthermore found no influence of the ionic strength on the sorption, which indicated that the surface complexation was an inner sphere complexation. Cui and Eriksen (1997) studied the influence of pH on the sorption of Co^{2+} on fracture filling materials extracted from the Stripa mine. In batch sorption experiments, they found strongly increasing sorption with increasing pH. In pH corresponding to a natural groundwater, it was found that the sorption of the presumed surface complexation sorbing Co^{2+} was much stronger than the sorption of the presumed cation exchange sorbing tracers, as Cs^+ and Sr^{2+}.

The divalent transition metals are somewhat different influenced by hydrolysis, see Table 1. It would therefore be interesting to see if retardation of these tracers could be observed as a function of their respective order of hydrolysis.

Another interesting issue is the limited reversibility in the sorption. This has been observed in the TRUE field and laboratory experiment, mainly for the relatively strongly sorbing tracer Cs^+. In the STT1b experiment (Johansson et al., 2000) it was shown that a limited reversibility had to be applied for Co^{2+} in order to fit the breakthrough results. In the STT1 and STT2 experiments, limited reversibility of approximately the same magnitude had to be used by Johansson et al. (2000) for fitting the Cs^+ results. However, in the laboratory studies of sorption of Cs^+ and Co^{2+}, Cui and Eriksen (1997) observed a much more pronounced limited reversibility of Cs^+ than of Co^{2+}.

In a NMR investigation of the sorption of Cs^+ on illite (Kim et al 1996), the authors concluded that the part of Cs^+ that sorbed with reversibility corresponded to sorption mechanism of inner sphere complexation. It would thus be interesting to use the divalent transition metals as tracers in the TRUE Block Scale Experiment and see if the results of any breakthrough of these tracers could provide general information of the relationship between inner sphere complexation and limited sorption reversibility.

The hydrolysis constants for some divalent transition metals, given for zero ionic strength (Smith and Martell, 1989). Only cations which have suitable γ-emitting isotopes are included. The (-log β_1^*) corresponds roughly to the pH-value where the concentration of the M^{2+} and the $M(OH)^+$ are equal.

Cation	-log β_1^*
Mn^{2+}	10.6
Co^{2+}	9.7
Zn^{2+}	9.0

References

Cui, D., Eriksen, T.E., 1997: "On the sorption of Co and Cs on Stripa granite fracture filling material", Radiochim. Acta **79** 29-35

Kim, Y., Kirkpatrick, R.J., Cygan, R.T., 1996: "133-Cs NMR study of cesium on the surfaces of kaolinite and illite" Geochim. et Cosmochim. Acta, **60**(21) 4059-4074

Jakobsson, A.M., Albinsson, Y., 1998: "Sorption of NpO_2^+ and Co^{2+} onto TiO_2", Radiochim. Acta **82** 257-262

James R.O., Healy, T.W., 1972: "Adsorption of hydrolyzable metal ions in the oxide-water interface" J. Colloid Interface Sci. **40** 42-52

Johansson, H., Haggerty, R., Byegård, J., Skålberg, M. (submitted): In situ migration experiments at Äspö Hard Rock Laboratory, Sweden: Applicatio of laboratory-derived retardation and diffusivity data in modeling of sorbing tracer tests, submitted to J. Cont. Hydrol.

Smith, R.M., Martell, A.E., 1989: "Critical Stabilty Constants", Vol 3, 5 and 6 (latest update 1989), Plenum Press, New York.

APPENDIX 3: Log of Events during TRUE Block Scale Tracer tests Phase C.

Log of events (borehole notations are shortened by removing the prefix "KI00-" from the borehole labels).

Date	Event
000310	Start pumping 23B:P6. Q=1200 ml/min
000406	Increased pumping in 23B:P6, Q=2090 ml/min
000418	Removed flow regulator in 23B:P6, Q increased to 2100 ml/min
000614	Start injection of water for dipole in 25F03:P5
000614	Stop injection of water in F03:P5, power failure
000614	Re-start water injection in F03:P5
000615	Stop injection of water in F03:P5, power failure
000615	Re-start water injection in F03:P5
000615	Start tracer injection in F03:P5, test **C1**
000619	Stop injection of water in F03:P5, pump repair/maintenance
000619	Re-start water injection in F03:P5
000620	Start tracer injection in F02:P3, test **C3**
000620	Start injection of water for dipole in 25F03:P7
000621	Start tracer injection in F03:P7, test **C2**
000622	Decreasing water injection pump capacity in F03:P7
000624	Increasing water injection pump capacity in F03:P7
000625	Decreasing water injection pump capacity in F03:P7
000625	Increasing water injection pump capacity in F03:P7
000625	Stop injection of water in F03:P7, pump failure
000626	Re-start water injection in F03:P7
000626	Stop injection of water in F03:P5, pump maintenance
000626	Re-start water injection in F03:P5
000629	Stop injection of water in F03:P5, pump maintenance
000629	Re-start water injection in F03:P5
000704	Stop injection of water in F03:P5, pump repair/maintenance
000704	Stop injection of water in F03:P7, pump maintenance
000704	Re-start water injection in F03:P7
000704	Re-start water injection in F03:P5
000710	Decreasing water injection pump capacity in F03:P5
000712	Stop injection of water in F03:P5, pump maintenance
000712	Re-start water injection in F03:P5
000712	Stop injection of water in F03:P7, pump maintenance
000712	Re-start water injection in F03:P7
000712	Decreasing water injection pump capacity in F03:P5
000714	Increasing water injection pump capacity F03:P5
000715	Stop injection of water in F03:P7, pump failure
000717	Stop injection of water in F03:P5, power failure
000717	Re-start water injection in F03:P5
000717	Re-start water injection in F03:P7
000722	Decreasing water injection pump capacity in F03:P5
000725	Stop injection of water in F03:P5, pump failure
000725	Re-start water injection in F03:P5
000725	Decreasing water injection pump capacity in F03:P5
000731	Stop injection of water in F03:P5, pump failure
000802	Stop injection of water in F03:P7, pump maintenance
000802	Re-start water injection in F03:P7
000802	Re-start water injection in F03:P5
000802	Stop injection of water in F03:P5, pump failure
000803	Re-start water injection in F03:P5
000803	Stop injection of water in F03:P5, pump failure
000810	Stop injection of water in F03:P7, pump failure
000816	Re-start water injection in F03:P7
000816	Re-start water injection in F03:P5
000817	Decreasing water injection pump capacity in F03:P5
000818	Stop injection of water in F03:P7, pump failure
000823	Stop injection of water in F03:P5, pump repair/maintenance
000823	Re-start water injection in F03:P5
000823	Re-start water injection in F03:P7
000829	Stop injection of water in F03:P5, pump maintenance

000829	Re-start water injection in F03:P5
000830	Stop injection of water in F03:P5, pump repair
000901	Decreasing water injection pump capacity in F03:P7
000901	Stop injection of water in F03:P7, pump failure
000903	Re-start water injection in F03:P7
000904	Stop injection of water in F03:P7, power failure
000904	Re-start water injection in F03:P7
000904	Stop injection of water in F03:P7, power failure
000907	Re-start water injection in F03:P7
000907	Re-start water injection in F03:P5
000907	Stop injection of water in F03:P7, pump failure
000907	Re-start water injection in F03:P7
000908	Start tracer injection in F03:P5, test **C4**
000908	Stop injection of water in F03:P7, pump repair/change
000908	Re-start water injection in F03:P7
000920	Stop injection of water in F03:P7, pump maintenance
000920	Re-start water injection in F03:P7
000920	Stop injection of water in F03:P5, pump maintenance
000920	Re-start water injection in F03:P5
000926	Stop injection of water in F03:P5 and F03:P7 due to empty water storage tanks
000926	Re-start water injection in F03:P5
000927	Re-start water injection in F03:P7
000927	Stop injection of water in F03:P5 and F03:P7, change of filter
000927	Re-start water injection in F03:P5 and F03:P7
000928	Stop injection of water in F03:P5, pump maintenance
000928	Re-start water injection in F03:P5
001006	Decreasing water injection pump capacity in F03:P7
001009	Stop injection of water in F03:P7, pump failure
001010	Stop injection of water in F03:P5, pump maintenance
001010	Re-start water injection in F03:P5
001010	Re-start water injection in F03:P7
001023	Decreasing water injection pump capacity in F03:P5, leakage
001024	Stop injection of water in F03:P5, pump maintenance
001024	Re-start water injection in F03:P5
001024	Stop injection of water in F03:P7, pump maintenance
001024	Re-start water injection in F03:P7
001025	Stop injection of water in F03:P7
001025	Re-start water injection in F03:P7
001030	Stop injection of water in F03:P7

APPENDIX 4: Model fits, simultaneous run conservative tracer - sorbing tracer. TRUE Block Scale Tracer tests Phase C.

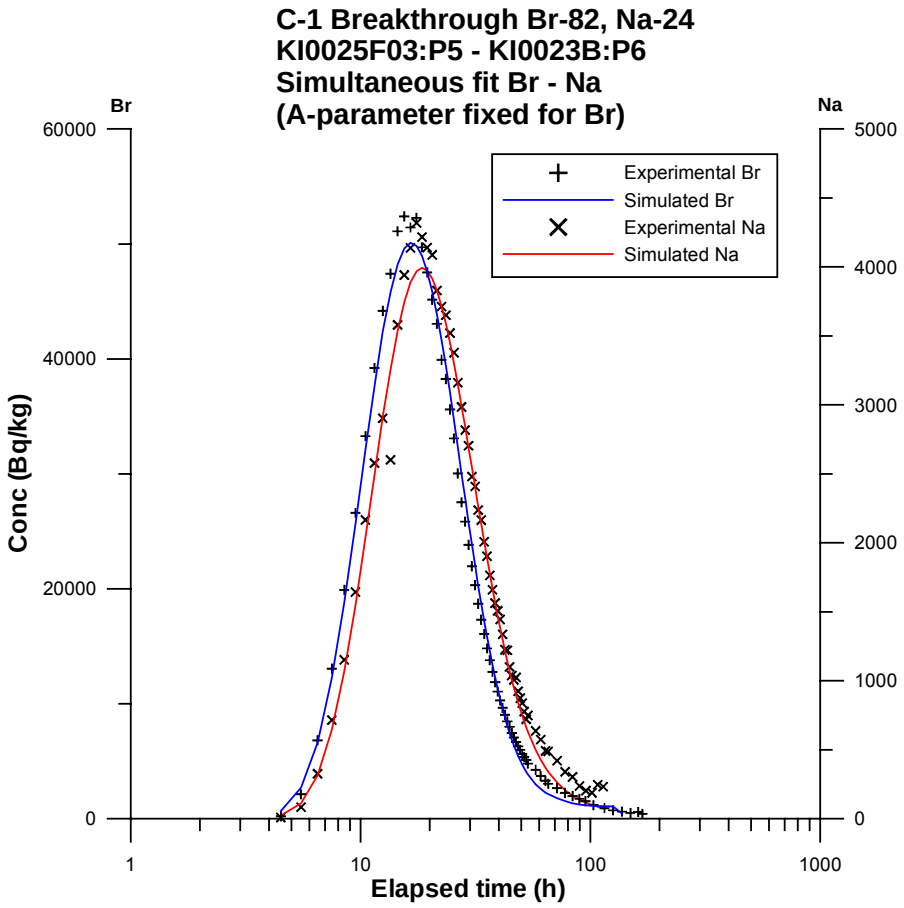
C-1 Breakthrough Br-82, Na-24
KI0025F03:P5 - KI0023B:P6
Simultaneous fit Br - Na
(A-parameter fixed for Br)
Br
Na
Experimental Br
Simulated Br
Experimental Na
Simulated Na
Conc (Bq/kg)
Elapsed time (h)
60000
40000
20000
0
5000
4000
3000
2000
1000
1
10
100
1000

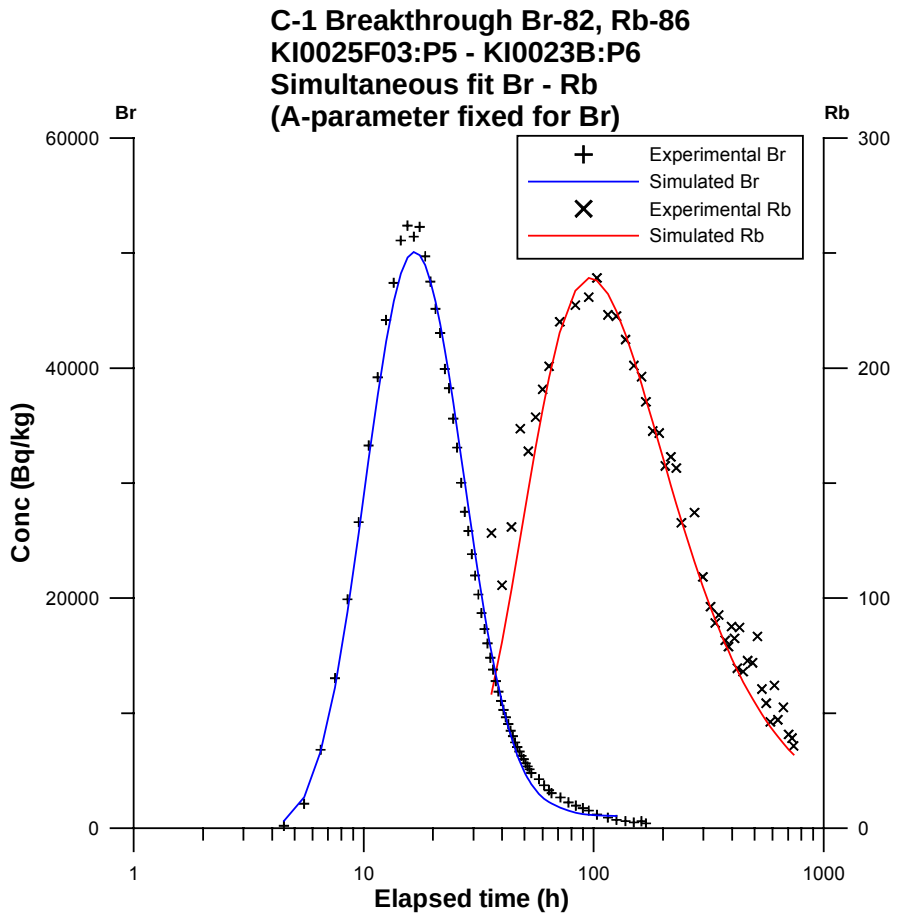
C-1 Breakthrough Br-82, Rb-86
KI0025F03:P5 - KI0023B:P6
Simultaneous fit Br - Rb
(A-parameter fixed for Br)
Br
Rb
Experimental Br
Simulated Br
Experimental Rb
Simulated Rb
Conc (Bq/kg)
Elapsed time (h)
60000
40000
20000
0
300
200
100
1
10
100
1000

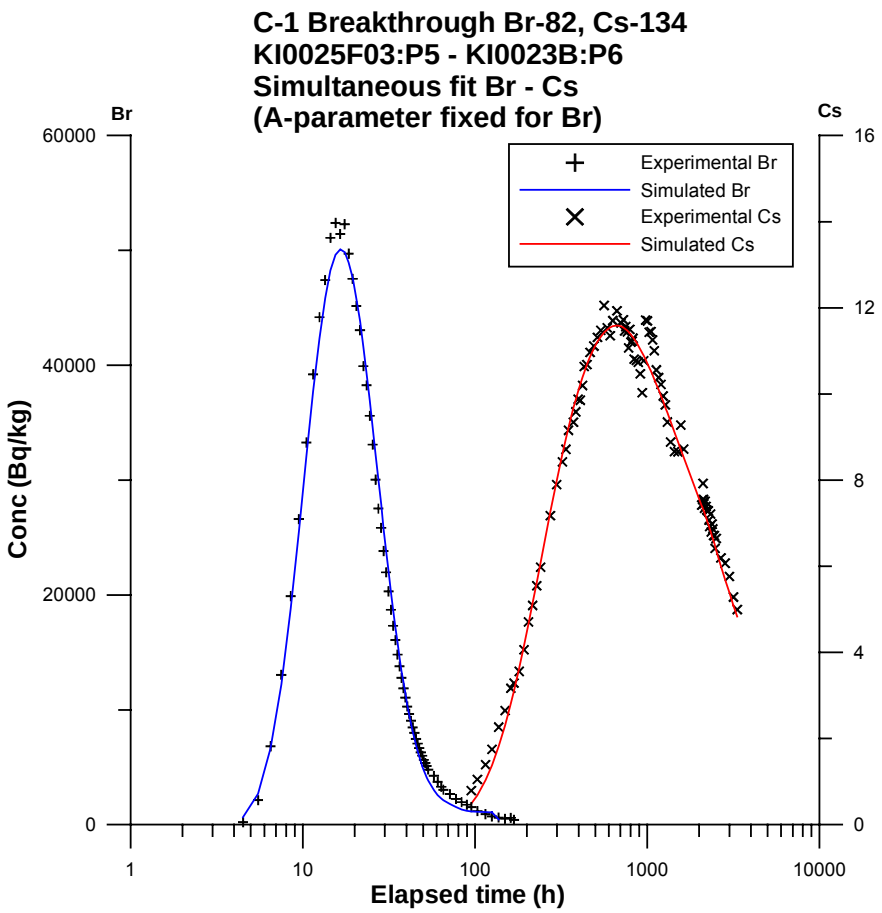
C-1 Breakthrough Br-82, Cs-134
KI0025F03:P5 - KI0023B:P6
Simultaneous fit Br - Cs
(A-parameter fixed for Br)
Br
Cs
Experimental Br
Simulated Br
Experimental Cs
Simulated Cs
Conc (Bq/kg)
Elapsed time (h)
60000
40000
20000
0
16
12
8
4
0
1
10
100
1000
10000

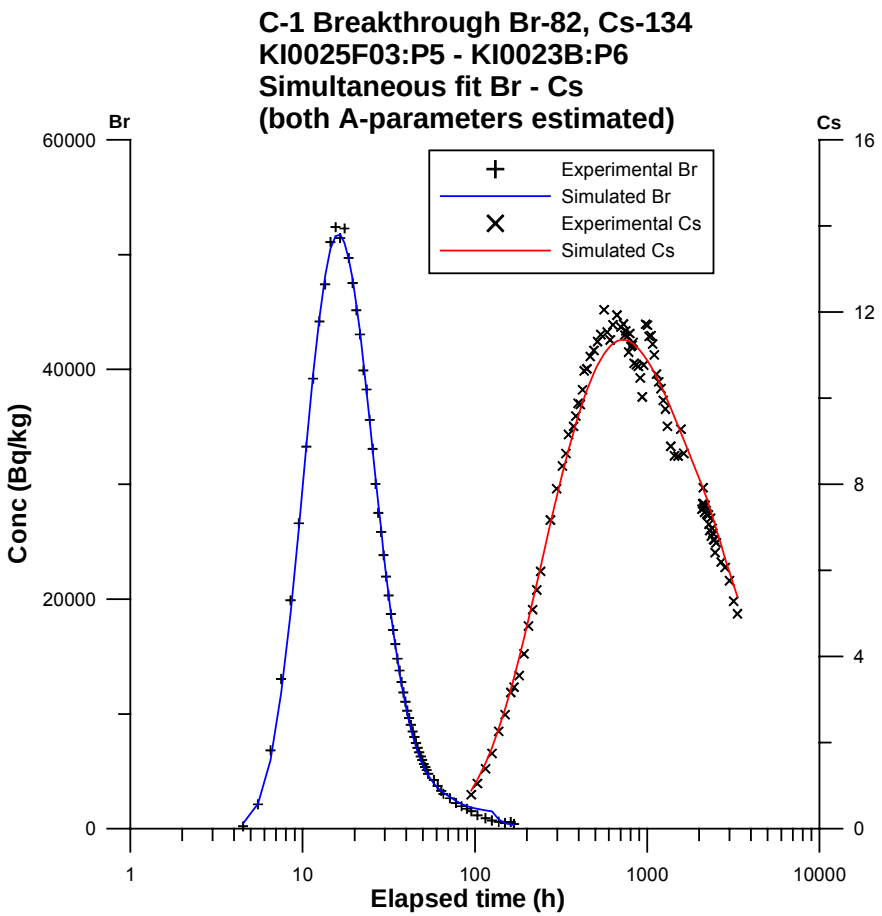
C-1 Breakthrough Br-82, Cs-134
KI0025F03:P5 - KI0023B:P6
Simultaneous fit Br - Cs
(both A-parameters estimated)
Br
Cs
Experimental Br
Simulated Br
Experimental Cs
Simulated Cs
Conc (Bq/kg)
Elapsed time (h)
60000
40000
20000
0
16
12
8
4
0
1
10
100
1000
10000

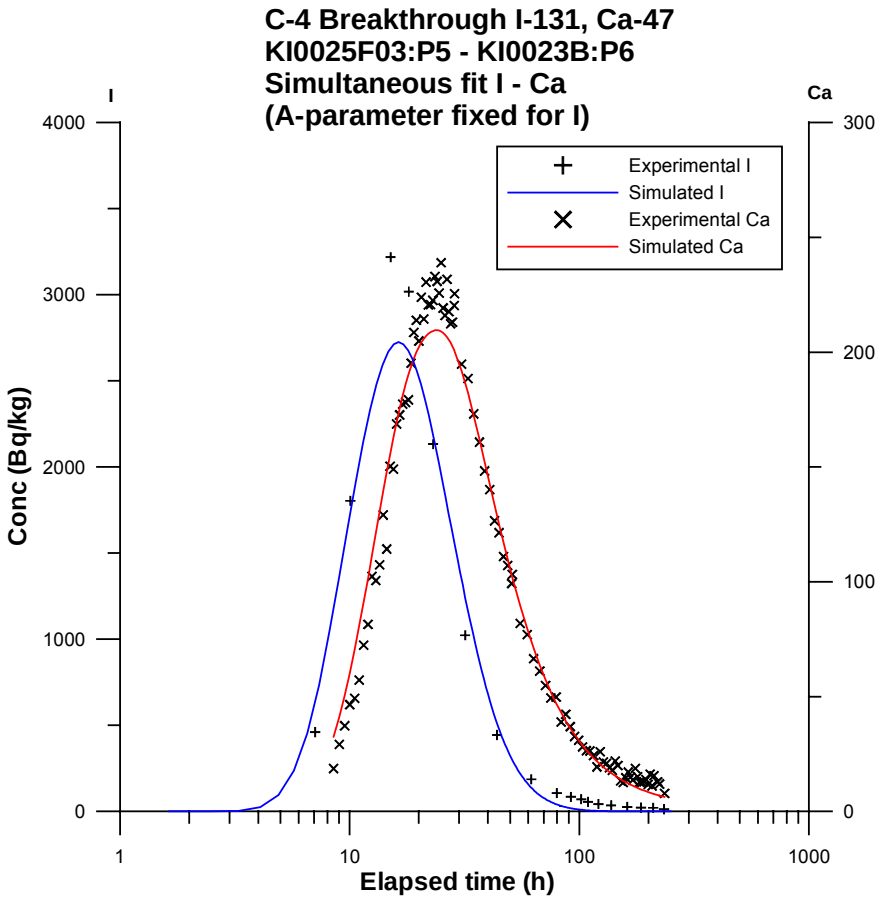
C-4 Breakthrough I-131, Ca-47
KI0025F03:P5 - KI0023B:P6
Simultaneous fit I - Ca
(A-parameter fixed for I)
I
Ca
Experimental I
Simulated I
Experimental Ca
Simulated Ca
Conc (Bq/kg)
Elapsed time (h)
4000
3000
2000
1000
0
300
200
100
0
1
10
100
1000

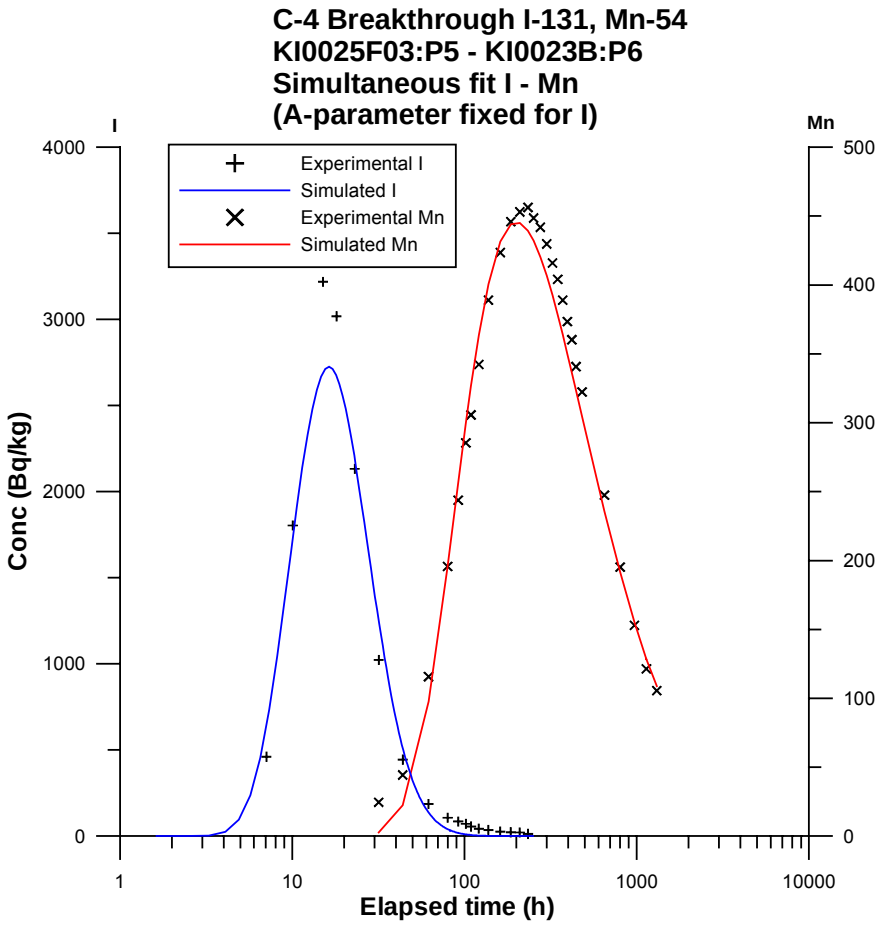
C-4 Breakthrough I-131, Mn-54
KI0025F03:P5 - KI0023B:P6
Simultaneous fit I - Mn
(A-parameter fixed for I)
I
Mn
Experimental I
Simulated I
Experimental Mn
Simulated Mn
Conc (Bq/kg)
Elapsed time (h)
4000
3000
2000
1000
0
500
400
300
200
100
0
1
10
100
1000
10000

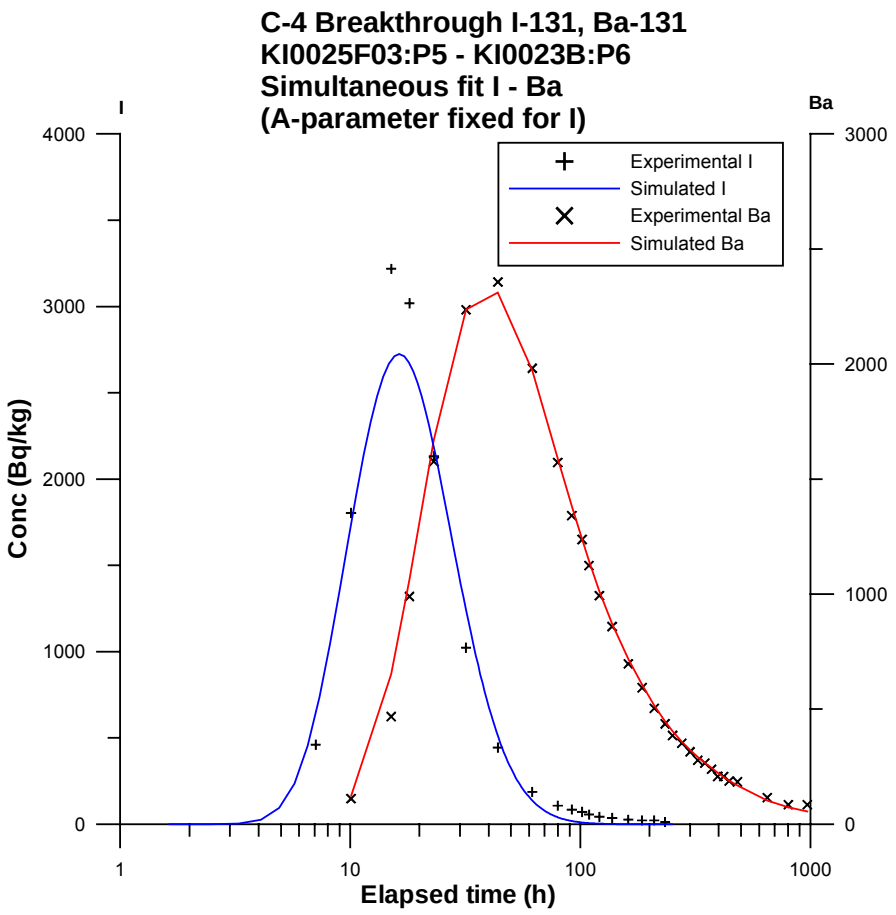
C-4 Breakthrough I-131, Ba-131
KI0025F03:P5 - KI0023B:P6
Simultaneous fit I - Ba
(A-parameter fixed for I)
I
Ba
Experimental I
Simulated I
Experimental Ba
Simulated Ba
Conc (Bq/kg)
Elapsed time (h)
4000
3000
2000
1000
0
3000
2000
1000
0
1
10
100
1000

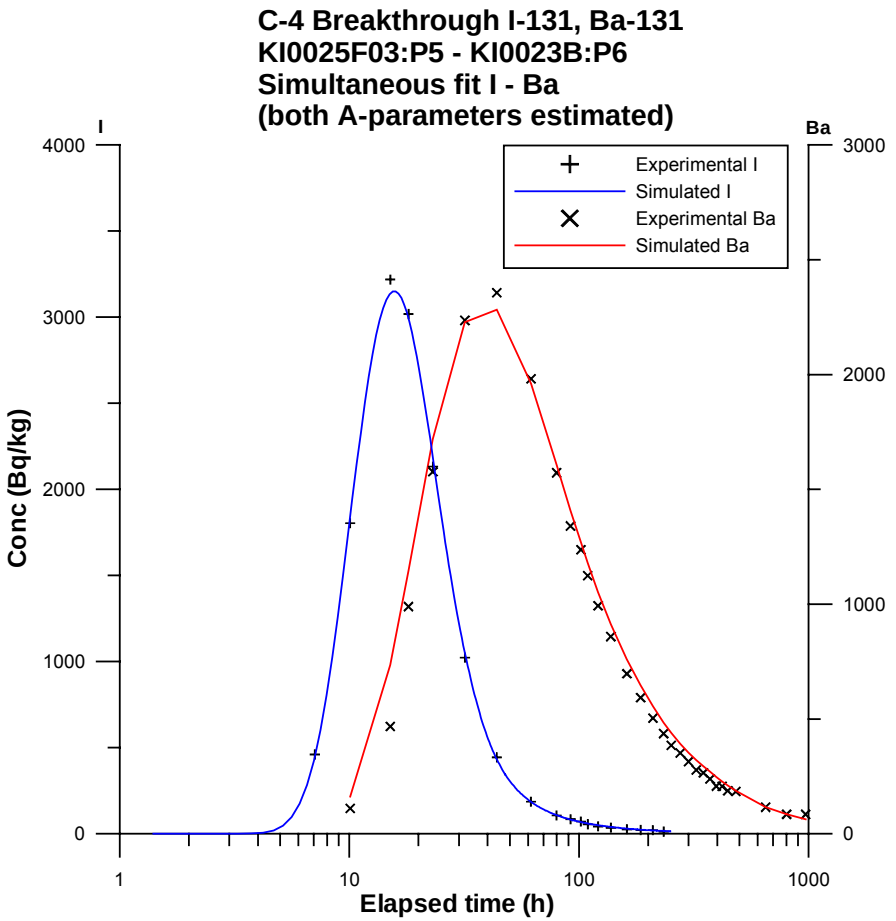
C-4 Breakthrough I-131, Ba-131
KI0025F03:P5 - KI0023B:P6
Simultaneous fit I - Ba
(both A-parameters estimated)
I
Ba
Experimental I
Simulated I
Experimental Ba
Simulated Ba
Conc (Bq/kg)
Elapsed time (h)
4000
3000
2000
1000
0
3000
2000
1000
0
1
10
100
1000

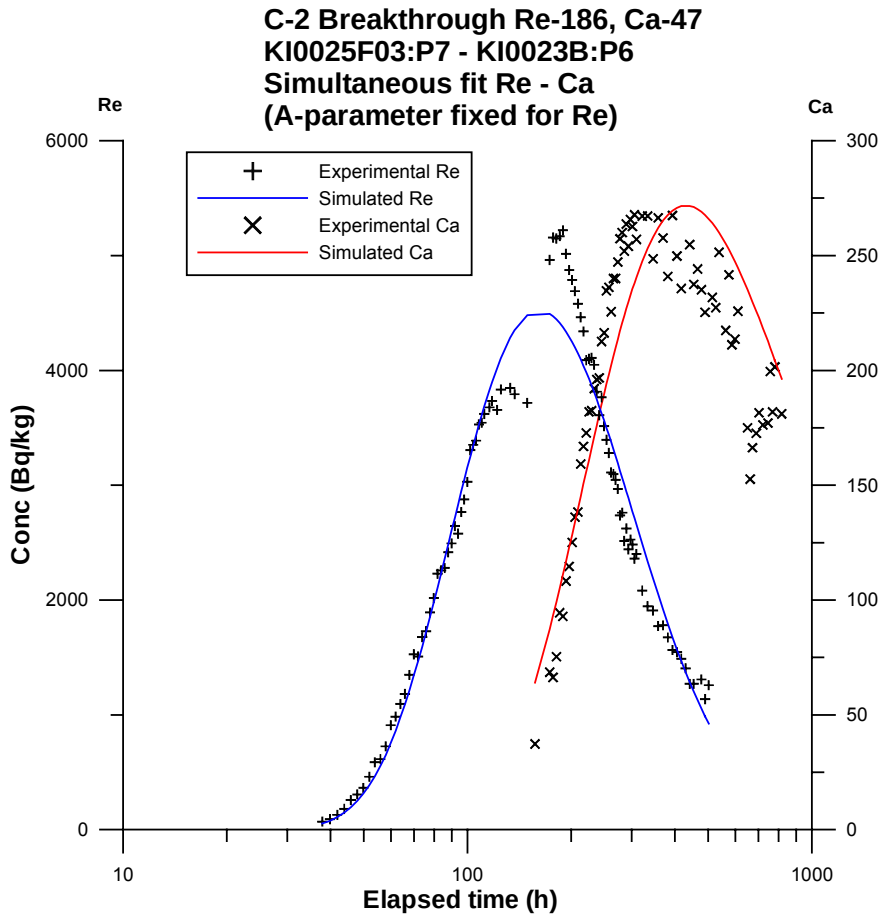
C-2 Breakthrough Re-186, Ca-47
KI0025F03:P7 - KI0023B:P6
Simultaneous fit Re - Ca
(A-parameter fixed for Re)
Re
Ca
Experimental Re
Simulated Re
Experimental Ca
Simulated Ca
Conc (Bq/kg)
Elapsed time (h)
6000
4000
2000
0
300
250
200
150
100
50
0
10
100
1000

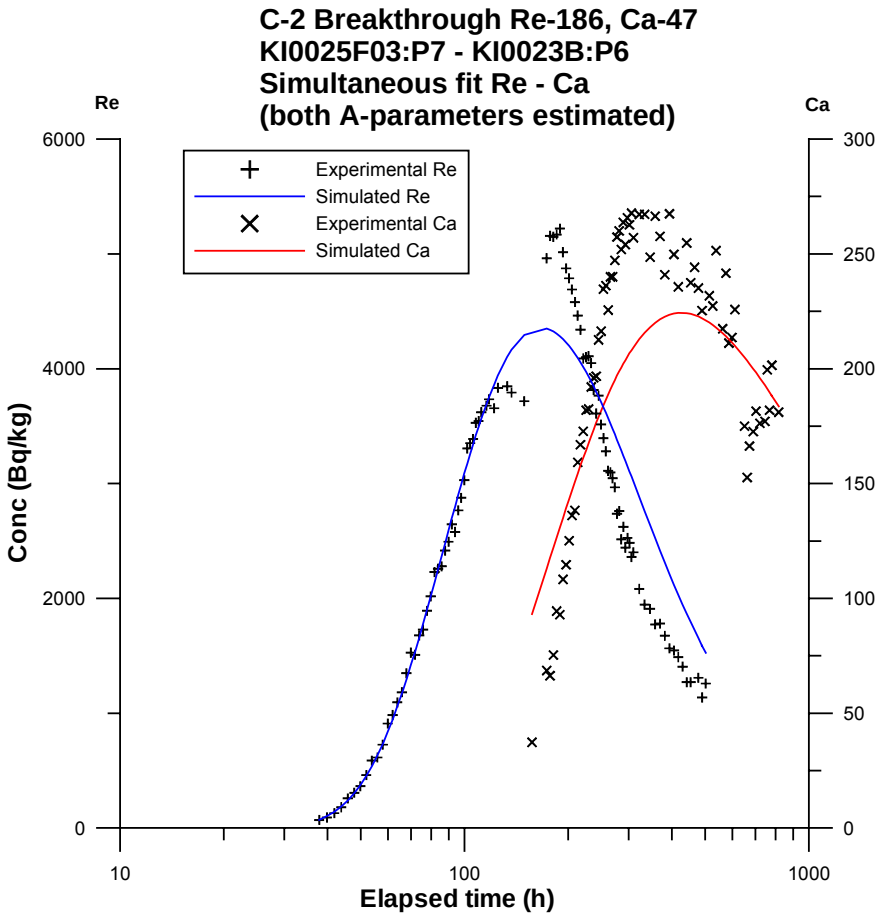
C-2 Breakthrough Re-186, Ca-47
KI0025F03:P7 - KI0023B:P6
Simultaneous fit Re - Ca
(both A-parameters estimated)
Re
Ca
Experimental Re
Simulated Re
Experimental Ca
Simulated Ca
Conc (Bq/kg)
Elapsed time (h)
6000
4000
2000
0
300
250
200
150
100
50
0
10
100
1000

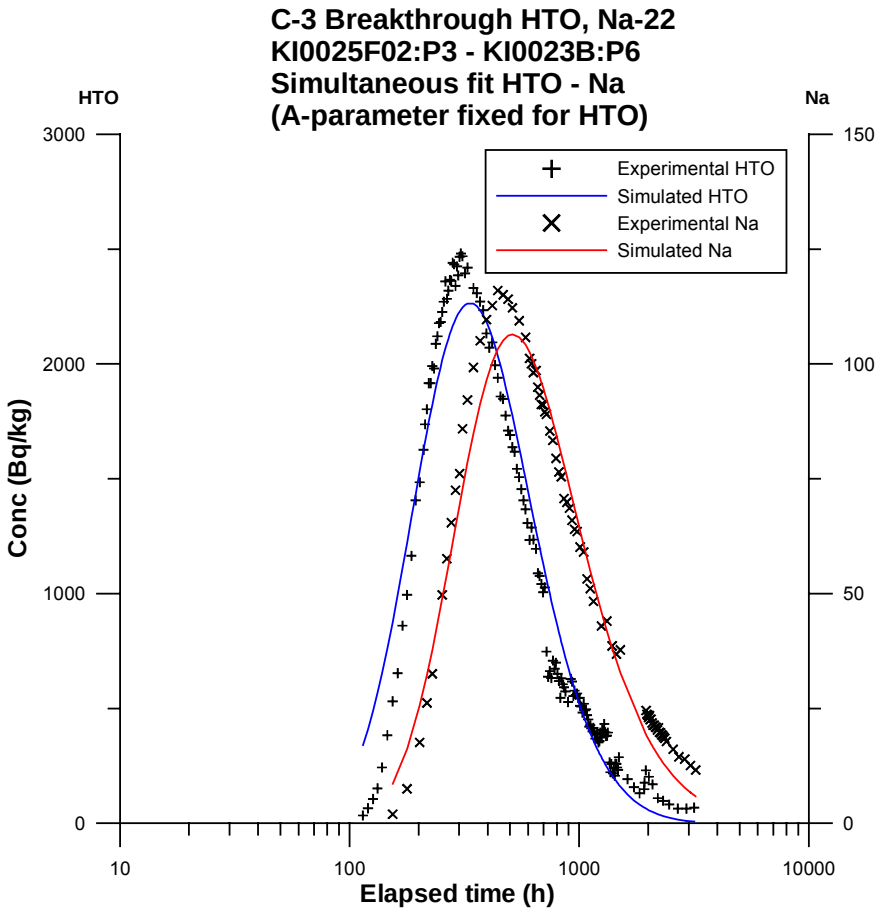
C-3 Breakthrough HTO, Na-22
KI0025F02:P3 - KI0023B:P6
Simultaneous fit HTO - Na
(A-parameter fixed for HTO)
HTO
Na
Experimental HTO
Simulated HTO
Experimental Na
Simulated Na
Conc (Bq/kg)
Elapsed time (h)
3000
2000
1000
0
150
100
50
0
10
100
1000
10000

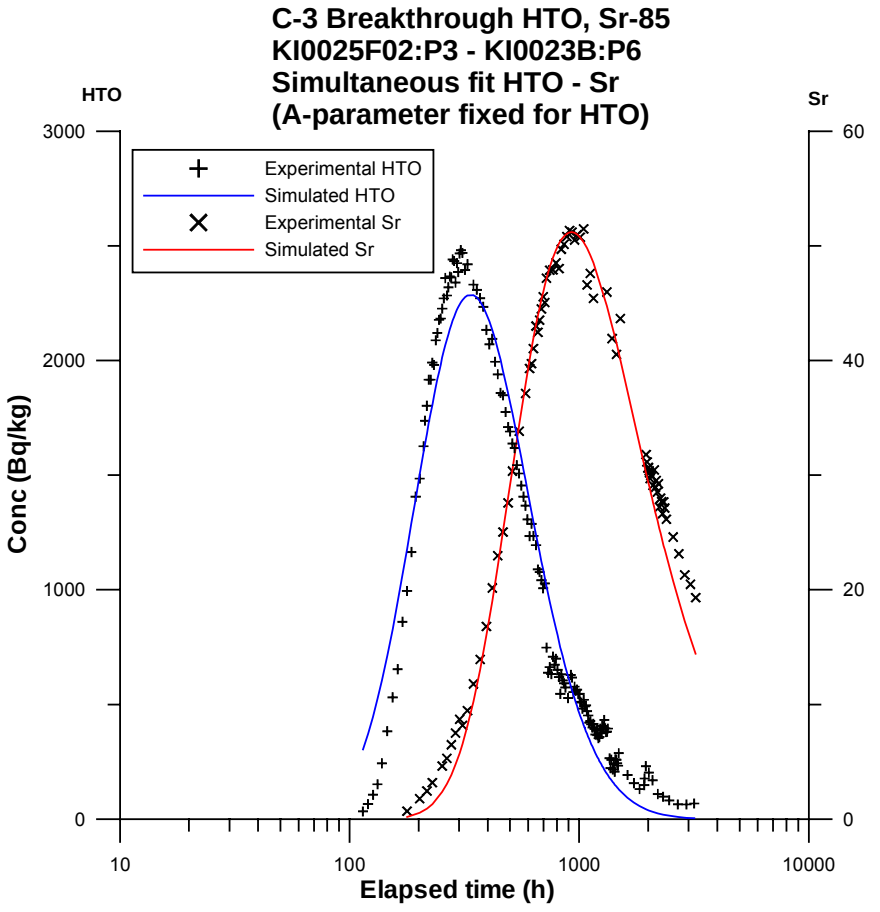
C-3 Breakthrough HTO, Sr-85
KI0025F02:P3 - KI0023B:P6
Simultaneous fit HTO - Sr
(A-parameter fixed for HTO)
HTO
Sr
Experimental HTO
Simulated HTO
Experimental Sr
Simulated Sr
Conc (Bq/kg)
Elapsed time (h)
3000
2000
1000
0
60
40
20
0
10
100
1000
10000